MODELING THE CHEMICAL VAPOR DEPOSITION

OF DIAMOND

By

RUSTOM BANDORAWALLA

Bachelor of Engineering

Manipal Institute of Technology
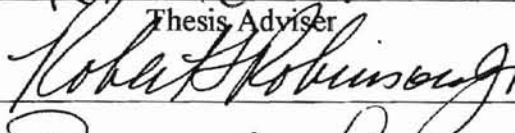
Manglore University

Manipal, India

1993

Submitted to the Faculty of the
Graduate College of the
Oklahoma State University
in partial fulfillment of
the requirements for
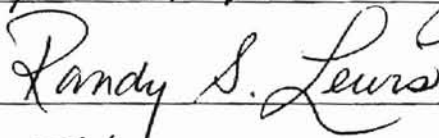the Degree of
MASTER OF SCIENCE
July, 1994

MODELING THE CHEMICAL VAPOR DEPOSITION

OF DIAMOND

Thesis Approved:

K.AM.GASON
_____
Thesis Adviser

Robert Robinson
_____

Randy S. Lewis
_____

Thomas C. Collins
_____
Dean of the Graduate College

PREFACE

Diamond has been the focus of much attention through the years, largely due to its potential usefulness in a wide variety of industrial applications. Diamond research has centered around the development of alternative, commercially viable methods of synthesis, and in recent years considerable progress has been achieved in approaches involving the low pressure chemical vapor deposition of diamond. Nevertheless, a thorough understanding of this phenomenon remains illusive despite the number of ongoing studies in this area.

The purpose of this study was to develop a simple model to predict accurately the chemical vapor deposition of diamond using low pressure combustion synthesis. An effort was made to formulate a plausible growth mechanism based on a review of previous studies in the literature elucidating the process of diamond chemical vapor deposition. A thermodynamic approach was then utilized to analyze the growth of carbon in $C_2H_2 + O_2$, $C_2H_4 + O_2$, and $CH_4 + O_2$ systems with the purpose of estimating an approximate growth domain for diamond. Finally, a coupled thermodynamic-kinetic model was developed to predict steady-state diamond growth rates in atmospheric $C_2H_2 + O_2$ combustion systems. Results obtained agreed reasonably well with experimental data. Although the proposed model was still in its preliminary stages of development, it proved to be a useful predictive tool for qualitative analysis.

I would like to take this opportunity to express my gratitude to my adviser, Dr. Khaled A. M. Gasem for his invaluable guidance and patience. He helped make this

study an enjoyable and memorable experience. I extend my sincere appreciation to the other members of my committee Dr. Robert L. Robinson, Jr. (Amoco Chair and Head), and Dr. Randy S. Lewis, for their valuable suggestions, which helped make this a successful presentation, and who often accommodated me on the shortest of notice in spite of their busy schedules.

Most of all, I would like to thank my parents for their inexhaustible encouragement and support through the course of my studies. They have been a constant source of love and understanding over the years.

Also, I wish to thank Kyoungho Row for his help in compiling data for a substantial portion of Section 2 of this study. Finally, support provided by the Energy Center and the School of Chemical Engineering, Oklahoma State University is gratefully acknowledged.

<div align="right">

Rustom Bandorawalla

July, 1995

</div>

TABLE OF CONTENTS

LIST OF TABLES

LIST OF FIGURES

NOMENCLATURE

a_i	Polynomial coefficients (for the heat capacity of species, i=1 to 5)
C	Molar concentration
C_p	Heat capacity
E	Activation energy
F	Molar flow rate
G	Gibbs free energy of the system
ΔH^o_f	Heat of formation at standard conditions
k	Pre-exponential factor
m	Sum of stoichiometric coefficients
n	Number of moles
$_n(m)$	Estimate for number of moles
p	Partial pressure
R	Universal gas constant
(R)	Radical species capable of forming a chemical bond
(S)	Surface species
T	Absolute temperature
V	Volume of the reactor
W	Molecular weight of the gas-phase species (for gas-surface interface reactions)

Greek Symbols

α	Concentration exponent

δ	Change in (e.g., number of moles)
γ	Reaction probability
Γ	Number of surface sites available for reaction
μ	Chemical potential
ξ	Reaction extent variable

Subscripts

f	Forward reaction
i, j	Component identification numbers
r	Reverse reaction
t, T	Total number of (e.g., moles)

Superscripts

o	Standard state

CHAPTER I

INTRODUCTION

Background

Diamond has been the center of much attention throughout the history of mankind. Its name is derived from the Greek word *adamas*, meaning 'unconquerable, invincible.' Researchers have attempted to synthesize diamond ever since Lavoisier and Tennant [1] established in 1772 that it was the crystalline form of carbon. Since then, diamond synthesis has evolved significantly, with diamonds being sought as more than just lustrous ornaments.

Developments in chemical thermodynamics through the 19th and 20th centuries culminated in the synthesis of diamond in 1955 [2] under conditions at which diamond is thermodynamically stable with respect to graphite. A team at Allemana Svenska Elektriska Aktiebolaget [2] had succeeded even earlier in 1953 but elected not to announce their discovery. Both teams crystallized diamond from a molten transition metal solvent-catalyst at pressures and temperatures of about 55 Kbar and 1600 K. The synthesis of diamond using high pressure methods is commonplace today, producing approximately 80 tons of diamond each year to cater to an ever expanding world market.

While feasible, high pressure synthesis methods are expensive and elaborate. In an effort to simplify and make the diamond synthesis process less costly, researchers

explored the possibility of diamond growth at low pressures, where it is the metastable phase. Eversole [2], a pioneer in this field, was successful in synthesizing diamond at low pressures in the early 1950's. Eversole's work was later confirmed by Angus [2] and Deryagin [2] in separate studies.

Initially, the low pressure methods were plagued by extremely low growth rates on the order of about 0.1 μm hour^{-1}. During the last two decades, the low pressure techniques have been extensively studied, and considerable advances have been made. By the early 1980's, Japanese scientists announced the successful synthesis of diamond using chemical vapor deposition (CVD). Since then, growth rates approaching a millimeter per hour have been achieved. The chemical vapor deposition methods have proven to be more versatile, less expensive, and much simpler. Further, these results have been reproduced within a reasonable degree of accuracy, which is critical if the process is to be commercially viable.
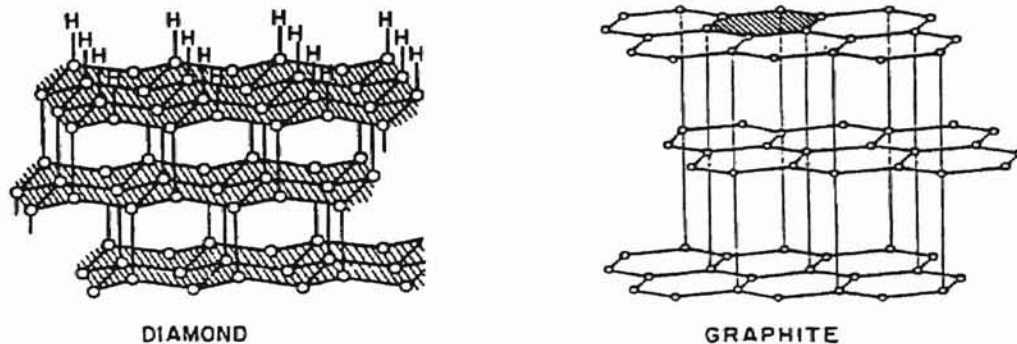
DIAMOND   GRAPHITE

Figure 1. Crystal Structure of diamond and graphite [4].

Structurally, the diamond-cubic lattice is derived from a face-centered cubic lattice with two atoms per lattice site, displaced by one quarter of the cube diagonal. A fragment of the general crystal structure of diamond in comparison with that of graphite is illustrated in Fig. 1 [4].

2

Table 1. Properties of diamond [2].

Hardness	GPa	~90[a]
Mass density	g/cm^3	3.515
Molar density	g atom/cm^3	0.293[a]
Thermal conductivity at 298 K	w/cm K	~20[a]
Bulk modulus	N/m^2	4.4-5.9 ×10^{11}
Compressibility	cm^2/kg	1.7 ×10-7[b]
Thermal expansion coefficient at 293 K	K^{-1}	0.8 ×10-6[c]
Refractive index at 589.29 nm		2.41726
Dielectric constant at 300 K		5.7±0.05
Specific heat at 300 K	J/g K	6.195
Optical band gap	eV	5.5
Enthalpy of formation, ΔH_f^o, from graphite at 298 K		1.895 kJ/mole
Free energy of formation, ΔG_f^o, from graphite at 298 K		2.900 kJ/mole
Entropy of formation, ΔS^o, from graphite at 298 K		-3.363 J/mole K

[a] Higher than any other known material.
[b] Lower than any other known material.
[c] Lower than Invar.

Diamond possesses a unique combination of properties. It is the hardest known material, has the highest elastic modulus, and consequently, the lowest compressibility. It has the best thermal conductivity, and a thermal coefficient lower than that of Invar. It has a high refractive index and is transparent to most wavelengths through the ultraviolet to infrared bands. It has the same crystal structure as silicon. Its electronic structure is similar too, except that it has a much higher energy band gap, and can be readily doped with boron to obtain p-type semi-conductivity. It has a high resistivity against acids too. Some of the noteworthy properties of diamond are summarized in Table 1 [2].

Synthetic diamonds possess most of the unique properties described above. As such, they represent an attractive alternative for use in a wide range of important

industrial applications. Efforts to develop an industrially viable process are spurred by this vast potential that diamond has to offer as a material.

Vapor-grown diamonds are largely used as abrasive grit on drilling, cutting, and polishing tools. Diamond has a heat conductivity five times that of silver, but it is an electrical insulator [3]. Thus, it can be used as a heat sink in many electronic applications, paving the way for more powerful, rugged, and faster electronic hardware. Also, diamond is a semiconductor, with a high frequency limit 32 times that of silicon and a power dissipation 8200 times better than silicon [3]. This makes it an attractive option for high-temperature semi-conducting devices. Other potential applications include laser and x-ray windows, lenses, bearing surfaces, and tribological coatings [1]. Its resistance to chemical attack and radiation damage appear to further lengthen its list of wide applications.

Rationale for the Study

A unique combination of properties make diamond an extremely useful product for a wide variety of industrial applications. Current high pressure methods for the synthesis of diamond are costly and inconvenient. As a result, within the last two decades an entire realm of low pressure methods have been developed with the chemical vapor deposition low pressure methods proving to be the simplest and least expensive technique. However, these methods are presently not capable of reproducibly generating diamond of particular mechanical and chemical specifications at commercially feasible rates of production.

Currently, there still exists considerable debate as to the exact nature of the reactions involved and the various factors influencing the growth of diamond under

conditions prevalent during these low pressure methods. A clear understanding of the physical and chemical phenomena involved is essential in the development of a commercially viable process.

Further, the low pressure synthesis of diamond involves a large number of variables and a wide range of operating conditions. Consequently, the development of a process solely based on experimental trial-and-error would prove to be extremely time consuming and ineffective. It is with this in view, that this study attempts to contribute to the development of an *a priori* predictive capability for the growth of diamond during low pressure chemical vapor deposition techniques. This study employs chemical equilibrium thermodynamics and kinetics to identify the most favorable conditions for diamond growth.

Objectives

The goal of this study is to address the low pressure chemical vapor deposition techniques for the synthesis of diamond from a thermodynamic/kinetic point of view and to determine the optimum operating conditions for the growth of diamond.

More specifically, the study attempts to develop a simple model for the low pressure chemical vapor deposition of diamond. It begins with the presentation of a plausible growth mechanism for the low pressure synthesis of diamond compiled on the basis of studies conducted by various researchers. It includes an overview of the probable gas phase reactions, the nucleation process, and the subsequent growth of diamond on the substrate. An attempt was made to illustrate the nucleation and surface reaction mechanisms on an elementary level, taking into account the energetics of the various species involved.

A thermodynamic approach was used to model the growth of carbon after having developed the overall scenario of the diamond deposition process. The presence of carbon is a prerequisite for the growth process, since diamond itself is an allotrope of carbon. Such an approach illustrated the effect of various parameters such as pressure, temperature, and composition of the feed gases on the growth rate of carbon. More importantly, it helped estimate the domain in which the growth of diamond may be best expected.

The thermodynamic approach was then extended a step further in an effort to kinetically model the growth of diamond itself. A simple one-dimensional kinetic model was developed to predict the growth rate of diamond and to study the influence of temperature, feed gas compositions, and atomic hydrogen concentrations on the diamond deposition rates.

SECTION 1

FORMULATION OF A GROWTH MECHANISM

CHAPTER II

INTRODUCTION

The low pressure chemical vapor deposition of diamond has progressed measurably in the last few decades. Significant advances have been made in improving the synthesis methods and in understanding the phenomenon of diamond growth. However, despite these advances much is yet to be learned of the mechanism, the chemical reactions taking place in the gas phase and on the surface, and the nucleation process. Both the thermodynamics and the kinetics of the process are presently a source of controversy.

A clear understanding of the deposition process on an elementary level is essential. Such a fundamental approach is extremely useful if one is to develop an accurate predictive model and determine the parameters which play a role in the deposition process. Towards this goal, this section of the study aims to present a mechanism for the low pressure chemical vapor deposition of diamond. The following work is based on a review of various studies conducted in the past attempting to elucidate the complex phenomena of low pressure diamond growth.

A simplified schematic for the deposition of diamond is depicted in Fig. 2 [5]. This illustrative overview outlines the main steps of the growth process. Accordingly, the chemical vapor deposition of diamond film at low pressures on a substrate may be looked upon as a sequence of three major steps.

7

[i] The activation of the hydrocarbon source gases and the subsequent *gas-phase reactions*

[ii] The *nucleation process* occurring on the surface of the substrate

[iii] The subsequent *surface reactions* resulting in the growth of diamond

Each of the above mentioned steps will be explored individually while attempting to describe the overall growth mechanism.
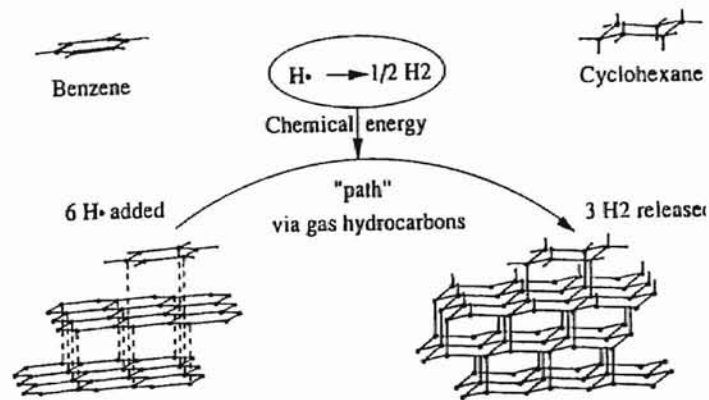
Figure 2. An idealized schematic of the diamond deposition mechanism [5].

However, it should be noted that the success of a mechanism to predict diamond growth rates accurately does not necessarily indicate that it is entirely accurate in representing the actual physical situation. Also, such studies do not rule out the possibility of other species and/or factors that may contribute towards the growth process.

8

CHAPTER III

THERMODYNAMIC AND KINETIC ASPECTS

Diamond is slightly unstable with respect to crystalline graphite at standard conditions of 1 atm and 298 K. Thus, during the low pressure chemical vapor deposition techniques, diamond is metastable with respect to graphite. As a result, pioneers in this field faced much skepticism for trying to achieve the 'thermodynamically impossible.' However, once the chemical vapor deposition of diamond at low pressure was established experimentally, there arose a host of queries regarding the observed phenomena. The existence of a single theory to rationalize the deposition process is frequently debated; however, most efforts are hampered by the absence of sufficiently detailed information to delineate the various factors contributing towards the process.

Researchers have attempted to explain the low pressure chemical vapor deposition of diamond based on Ostwald's rule of steps, which states that in the course of going from a non-equilibrium state to a final equilibrium state, a system will pass step-wise through a sequence of states of lesser intermediate stability [53, 94]. At certain temperatures, the free energy of carbon atoms in some hydrocarbons may be higher than that of carbon in the diamond form. During the decomposition of such hydrocarbons, while the carbon atoms descend from a state of higher free energy, they could pause at the level of diamond instead of assuming the lower free energy state of graphite. Such phenomena wherein pauses at metastable phases occur have been documented and are economically important in many other physical and chemical systems [94].

9

Subsequently, the spontaneous transformation of diamond to the more stable phase is prevented by a substantial activation or kinetic-barrier which forces the two phases to co-exist [94, 95]. This could well be the mechanism involved in the low pressure deposition of diamond.
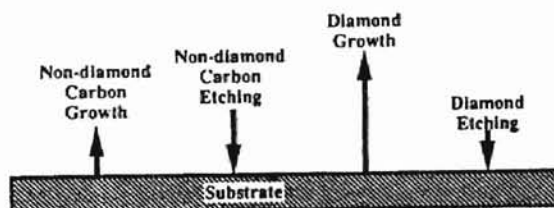
Figure 3. Schematic of the kinetics of an idealized diamond growth mechanism. The net reaction rate is the sum of all the individual rates [91].

Since the growth of diamond is believed to be thermodynamically unfavorable at low pressures, some researchers suggest that the mechanism must be controlled by mass transfer or kinetics. Early Soviet researchers [1] were of the opinion that atomic hydrogen etches graphite preferentially, thereby inhibiting the nucleation of graphite or graphitic carbon. The rationale behind such a concept is that the preferential etching of graphite or graphitic species results in diamond becoming kinetically stable relative to graphite. A schematic illustrating the kinetics of a simplified diamond growth mechanism is depicted in Fig. 3 [91]. As shown, both diamond and non-diamond carbon grow simultaneously on the surface. The non-diamond carbon is etched by gas-phase species, thought to be atomic H and OH. As long as non-diamond carbon is etched faster than its growth rate and diamond grows at a rate larger than its etching rate, the net result will be a diamond dominant phase.

The growth of diamond is known to be controlled by the nature of the substrate. Some theorize that the structure of diamond is pseudomorphically stabilized by the

10

underlying structure [90]. Still others suggest that the growth of diamond is rendered thermodynamically possible due to the presence of defects on the growth surface [90].

Another view adopted by a number of researchers explains that the formation of diamond in preference to other non-diamond forms of carbon is surface controlled not by defects, but by the reversible chemisorption of other species [90]. Experiments support such an observation in that the graphitization of diamond is essentially surface controlled and highly dependent on the pressure and composition of the gases present [90]. Proponents of this theory further argue that diamond growth is possible at low pressures and temperatures because the hydrogenated diamond structure surface is the lowest free-energy surface, and once this surface is covered by a layer of carbon, graphitization is inhibited. Calculations performed by a number of researchers, comparing the stability of various hybridized carbon clusters, indicate that if the surface to volume ratio was sufficiently large, the diamond structure cluster was the more stable [91, 92].

Similar arguments are used to explain the nucleation process of diamond [38, 92]. Some researchers suggest that the formation of a stable nucleus of critical size emerges as a result of a balance between the contributions of the volume and surface energies. Thus, a diamond nucleus may be more stable at normal pressure than a graphite nucleus containing the same number of atoms [92], allowing for the subsequent growth of crystalline diamond.

Numerous researchers have modeled the growth of diamond based on kinetic and thermodynamic principles attempting to explain the diamond growth process [5]. The earliest models utilized the kinetic approach to explain the formation of the metastable diamond phase [5]. Later approaches involved thermodynamic quasi-equilibrium models [93, 96, 97], surface reaction models [5], and defect-induced models [5]. In still another

approach, Wang and Carlsson [5] proposed a chemical pump model (or the thermodynamic coupling model) utilizing thermodynamically favorable reactions to drive a thermodynamically unfavorable reaction. Thus, ions or molecules can be 'pumped' in a direction against their concentration gradients.

Still others have utilized a thermodynamic approach to model the gas phase composition [98], or perform chemical equilibrium calculations to determine the nature of the diamond growth domain [85, 99]. In spite of the variety of models proposed, a generally acceptable explanation for the chemical vapor deposition process of diamond is still lacking.

CHAPTER IV

GAS-PHASE REACTION MECHANISM

Introduction

The synthesis of diamond films or crystals at low pressure has been carried out by a strikingly large number of deposition techniques using a variety of different hydrocarbon gases as feed. Some of the common low pressure methods for the synthesis of diamond are listed in Table 2 [6]. Depending on the means of activation, the temperature of the gas phase may vary from anywhere as low as 1500 K, in the case of thermal decomposition methods, to above 5000 K, in the case of thermal radio frequency and direct current plasmas, arc discharges, and plasma jets.

The subsequent deposition of diamond from the gas-phase species involves the processes of nucleation and surface growth. During both these stages, chemical reactions in the gas phase and transport phenomena predetermine which chemical species will be supplied to the growth field as well as their concentrations and fluxes. Data on the processes taking place in the gas phase is therefore indispensable in order to study the nucleation and growth of nuclei on the surface.

A variety of techniques have been used, including *in-situ* mass spectrometry [7, 8], *in-situ* infrared adsorption [9], resonance ionization [10], planar laser-induced photo-dissociation [11], laser-induced fluorescence [8], plasma emission spectrometry [12], and

in-situ Fourier transform infrared spectroscopy [13], in an effort to analyze the composition of the gas-phase species present.

Table 2. Low pressure methods for the preparation of diamond [6].

Thermal CVD
    Thermal decomposition
    Chemical transport reaction (CTR)
    Hot filament technique
    Oxyacetylene torch
    Halogen-assisted CVD

DC plasma CVD
    Low pressure DC plasma
    Medium pressure DC plasma
    Hollow cathode discharge
    DC arc plasmas and plasma jets

RF plasma CVD
    Low pressure RF glow discharge
    Thermal RF plasma CVD

Microwave plasma CVD
    915 MHz plasma
    Low pressure 2.45 GHz plasma
    Atmospheric pressure 2.45 GHz plasma torch
    2.45 GHz magnetized (ECR) plasma
    8.2 GHz plasma

Other (non-CVD) methods
    C-implantation/laser treatment

Based on analyses of experimental data, some researchers have kinetically modeled the gas-phase reactions [14-16, 17-21]. Such studies give an interesting insight into the possible species that may serve as precursors for the subsequent growth of diamond [16], the effect of individual species [22], the effect of various operating

conditions [18, 21], and the quality and/or morphology of the resultant diamond deposited [12, 23, 24].

The identification of a gas-phase precursor primarily responsible for diamond growth during low pressure chemical vapor deposition methods has been extensively studied. An increasing amount of evidence supports the possibility of multiple primary growth precursors, with the predominant species depending on the method of activation and the conditions prevalent at the time. Stephen and Weiner [16] agree with this view-point in that no single species need always be the primary growth species for diamond formation, believing that a variety of hydrocarbons could act as precursors during the growth mechanism.

Another interesting feature is that in spite of the variety of deposition processes and source hydrocarbon gases used, diamond growth is observed to be relatively independent of the nature of the input hydrocarbon species. This fact seems to suggest that most hydrocarbon sources tend to chemically transform to some common product species. Gas-phase analyses indicate this to be true [22, 93]. Such an argument would also support the theory of multiple gas-phase primary growth precursors, with the dominant species being subject to the environmental and compositional constraints of the method being used.

Studies of gas-phase compositions prevalent during the low pressure chemical vapor deposition of diamond indicate that only C_2H_2, C_2H, C_2, CH_4, CH_3, CH, and C radicals exist in high enough concentrations to be able to contribute significantly to the growth mechanism [8, 11, 14-17].

Matsui et al. [8] concluded on the basis of a relational study between experimentally-obtained diamond growth rates and species concentrations that C_2 and CH radicals were important growth precursors. A similar approach lead Harris [15] to discount C_2H_2 and CH_3 radicals as possible growth precursors, and propose CH_4 as the primary growth species on the diamond surface. In a later work, Harris and Weiner [16] concluded that CH_3 radicals were the principal growth species. D'Evelyn et al. [19] arrived at a similar conclusion on the basis of carbon-13 studies. Kondoh et al. [25] performed two-dimensional reactive flow simulations of the hot-filament chemical vapor deposition system. Based on their findings, they support CH_3 being a growth species in such systems. More recently, Pinter et al. [26] obtained a good correlation between the concentration of CH_5^+ radicals and the deposition rates of diamond. They presented a basic reaction pathway with CH_5^+ as the primary growth species. Such findings only further support the argument of more than a single predominant gas-phase species as the primary growth precursor.

Nevertheless, gas-phase analyses do clarify certain facts. Acetylene/acetylenic species are present in abundance during high temperature activation methods. C_2H_2 is considered a very probable growth species due to its stability under harsh environments such as those found in high temperature pyrolysis, combustion methods, and plasma techniques of synthesis. On the other hand, methyl radicals are present in high concentrations in the lower temperature environments of microwave and hot filament synthesis. Such observations indicate the possibility of either acetylene/acetylenic radicals and/or methyl radicals playing a dominant role in the growth process.

Gas-Phase Reactions

The gas-phase reaction mechanism has been studied by a number of researchers. Kondoh et al. [17] modeled the gas-phase chemical reactions in an effort to assess the role played by chemical species such as hydrogen atoms and methyl radicals in the growth of diamond. Their mechanism included 10 chemical species and 25 gas-phase reactions for the analysis of the gas species present during the advanced hot filament chemical vapor deposition method. The reaction mechanism is illustrated in Table 3 [17].

Table 3. †Gas-phase reaction mechanism proposed by Kondoh et al. [17].

$$H_2 + M \Leftrightarrow H\bullet + H\bullet + M$$
$$CH_4 + H\bullet \Leftrightarrow CH_3\bullet + H_2$$
$$CH_3\bullet + H\bullet \rightarrow CH_4$$
$$CH_3\bullet + CH_3\bullet \Leftrightarrow C_2H_6$$
$$C_2H_6 + H\bullet \Leftrightarrow C_2H_5\bullet + H_2$$
$$C_2H_5\bullet + H\bullet \Leftrightarrow C_2H_4 + H_2$$
$$C_2H_4 + H\bullet \Leftrightarrow C_2H_3\bullet + H_2$$
$$C_2H_3\bullet + H\bullet \Leftrightarrow C_2H_2 + H_2$$
$$C_2H_2 + H\bullet \Leftrightarrow C_2H\bullet + H_2$$
$$CH_3\bullet + CH\bullet \rightarrow CH_4 + C_2H_5\bullet$$
$$C_2H_5\bullet + CH_4 \rightarrow C_2H_6 + CH_3\bullet$$
$$C_2H_5\bullet + M \rightarrow C_2H_4 + H\bullet + M$$
$$C_2H_4 + H\bullet \rightarrow C_2H_5\bullet$$
$$C_2H_4 \Leftrightarrow C_2H_2 + H_2$$
$$C_2H_2 \Leftrightarrow C_2H\bullet + H\bullet$$
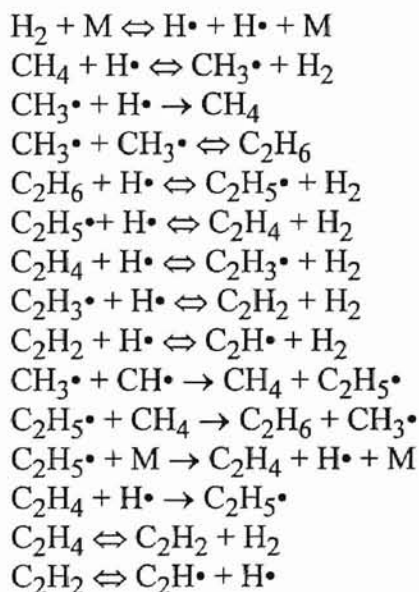
†Conventions, usage and formalism given in Ref. 17

Reeve et al. [20] modeled the gas-phase reaction mechanism occurring in the flame of the DC plasma jet reactor system. They considered 14 possible chemical species and a total of 29 reactions in their model. They concluded that CH_3 was a very likely

gas-phase diamond growth precursor, with H atoms playing a crucial role in the growth mechanism. The reaction mechanism is illustrated in Table 4 [20].

Table 4. †Gas-phase reaction mechanism proposed by Reeve et al. [20].

$CH_3• + CH_3•$ (+M) $\Leftrightarrow C_2H_6$ (+M)
$CH_3• + H• \Leftrightarrow CH_4$ (+M)
$CH_4 + H• \Leftrightarrow CH_3• + H_2$
$CH_3• + H• \Leftrightarrow CH_2• + H_2$
$CH_2• + H• \Leftrightarrow CH• + H_2$
$CH• + H• \Leftrightarrow C• + H_2$
$CH• + CH_2• \Leftrightarrow C_2H_2 + H•$
$CH• + CH_3• \Leftrightarrow C_2H_3• + H•$
$CH• + CH_4 \Leftrightarrow C_2H_4 + H•$
$C• + CH_3• \Leftrightarrow C_2H_2 + H•$
$C• + CH_2• \Leftrightarrow C_2H• + H•$
$C_2H_6 + CH_3• \Leftrightarrow C_2H_5• + H_2$
$C_2H_6 + H• \Leftrightarrow C_2H_5• + H_2$
$C_2H_4 + H• \Leftrightarrow C_2H_3• + H_2$
$CH_2• + CH_3• \Leftrightarrow C_2H_4 + H•$
$H• + C_2H_4$ (+M) $\Leftrightarrow C_2H_5•$ (+M)
$C_2H_5• + H• \Leftrightarrow CH_3• + CH_3•$
$H_2 + C_2H• \Leftrightarrow C_2H_2 + H•$
$H• + C_2H_2$ (+M) $\Leftrightarrow C_2H_3•$ (+M)
$C_2H_3• + H• \Leftrightarrow C_2H_2 + H_2$
$C_2H_3• + CH_2• \Leftrightarrow C_2H_2 + CH_3•$
$C_2H_3• + C_2H• \Leftrightarrow C_2H_2 + C_2H_2$
$C_2H_3• + CH• \Leftrightarrow CH_2• + C_2H_2 + CH_2•$
$CH_2• + CH_2• \Leftrightarrow C_2H_2 + H_2$
$C_2H_2 + M \Leftrightarrow C_2H• + H• + M$
$C_2H_4 + M \Leftrightarrow C_2H_2 + H_2 + M$
$C_2H_4 + M \Leftrightarrow C_2H_3• + H• + M$
$H• + H• + M \Leftrightarrow H_2 + M$
$H• + H• + H_2 \Leftrightarrow H_2 + H_2$
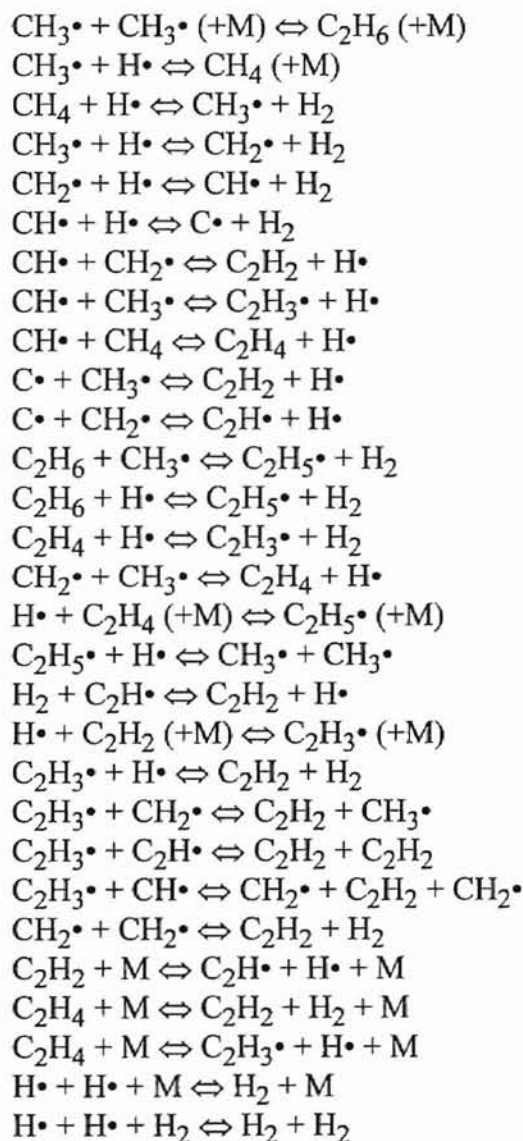
† Conventions, usage and formalism given in Ref. 20.

18

Genchi et al. [22] performed a more simple model calculation in an attempt to obtain data on the processes taking place in the gas phase during the deposition of diamond. The reaction mechanism they presented is illustrated in Table 5 [22].

Table 5. †Gas-phase reaction mechanism proposed by Genchi et al. [22].

$$CH_4 + M \Leftrightarrow CH_3\bullet + H\bullet + M$$
$$CH_4 + H\bullet \Leftrightarrow CH_3\bullet + H_2$$
$$CH_3\bullet + CH_3\bullet \Leftrightarrow C_2H_4 + H_2$$
$$C_2H_6 + M \Leftrightarrow CH_3\bullet + CH_3\bullet + M$$
$$C_2H_6 + H\bullet \Leftrightarrow C_2H_5\bullet + H_2$$
$$C_2H_6 + CH_3\bullet \Leftrightarrow C_2H_5\bullet + CH_4$$
$$C_2H_5\bullet + M^* \Leftrightarrow C_2H_4 + H\bullet + M$$
$$C_2H_5\bullet + H\bullet \Leftrightarrow CH_3\bullet + CH_3\bullet$$
$$C_2H_5\bullet + H\bullet \Leftrightarrow C_2H_4 + H_2$$
$$C_2H_4 + H\bullet \Leftrightarrow C_2H_3\bullet + H_2$$
$$C_2H_4 + CH_3\bullet \Leftrightarrow C_2H_3\bullet + CH_4$$
$$C_2H_3\bullet + M \Leftrightarrow C_2H_2 + H\bullet + M$$
$$C_2H_3\bullet + H\bullet \Leftrightarrow C_2H_2 + H_2$$
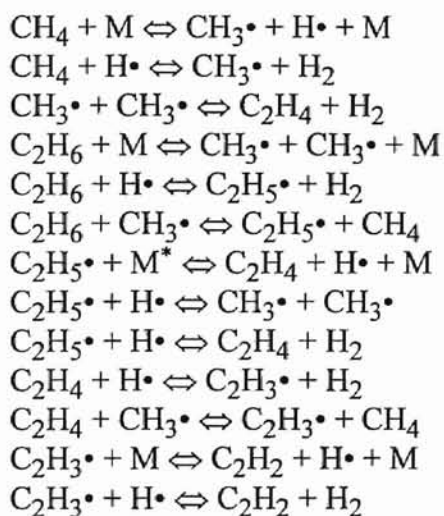
† Conventions, usage and formalism given in Ref. 22

Meeks et al. [28] modeled the gas-phase chemistry in a computational study of the growth of diamond in premixed flames. They utilized the gas-phase chemistry model of Miller and Melius in a reaction mechanism consisting of up to 221 reactions. Coltrin and Dandy [29] modeled the gas-phase reaction mechanism while analyzing the growth of diamond in sub-atmospheric direct current arc plasma jet reactors. In an exhaustive study of the gas-phase reaction mechanism, they included 190 species and 853 reactions. A simplified version of that reaction mechanism consisting of 34 reactions is illustrated in Table 6 [29].

Table 6. [†] Gas-phase reaction mechanism proposed by Coltrin and Dandy [29].

$$CH_3\bullet + CH_3\bullet + M \Leftrightarrow C_2H_6 + M$$
$$CH_3\bullet + H\bullet + M \Leftrightarrow CH_4 + M$$
$$CH_4 + H\bullet \Leftrightarrow CH_3\bullet + H_2$$
$$CH_3\bullet + H\bullet \Leftrightarrow CH_2\bullet + H_2$$
$$CH_2\bullet + H\bullet \Leftrightarrow CH\bullet + H_2$$
$$CH\bullet + H\bullet \Leftrightarrow C\bullet + H_2$$
$$CH\bullet + CH_2\bullet \Leftrightarrow C_2H_2 + H\bullet$$
$$CH\bullet + CH_3\bullet \Leftrightarrow C_2H_3\bullet + H\bullet$$
$$CH\bullet + CH_4 \Leftrightarrow C_2H_4 + H\bullet$$
$$C\bullet + CH_3\bullet \Leftrightarrow C_2H_2 + H\bullet$$
$$C\bullet + CH_2\bullet \Leftrightarrow C_2H\bullet + H\bullet$$
$$C_2H_6 + CH_3\bullet \Leftrightarrow C_2H_5\bullet + CH_4$$
$$C_2H_6 + H\bullet \Leftrightarrow C_2H_5\bullet + H_2$$
$$C_2H_4 + H\bullet \Leftrightarrow C_2H_3\bullet + H_2$$
$$CH_2\bullet + CH_3\bullet \Leftrightarrow C_2H_4 + H\bullet$$
$$H\bullet + C_2H_4 + M \Leftrightarrow C_2H_5\bullet + M$$
$$C_2H_5\bullet + H\bullet \Leftrightarrow CH_3\bullet + CH_3\bullet$$
$$C_2H\bullet + H_2 \Leftrightarrow C_2H_2 + H\bullet$$
$$C_2H_2 + H\bullet + M \Leftrightarrow C_2H_3\bullet + M$$
$$C_2H_3\bullet + H\bullet \Leftrightarrow C_2H_2 + H_2$$
$$C_2H_3\bullet + CH_2\bullet \Leftrightarrow C_2H_2 + CH_3\bullet$$
$$C_2H_3\bullet + C_2H\bullet \Leftrightarrow C_2H_2 + C_2H_2$$
$$C_2H_3\bullet + CH\bullet \Leftrightarrow CH_2\bullet + C_2H_2$$
$$CH_2\bullet(singlet) + M \Leftrightarrow CH_2\bullet + M$$
$$CH_2\bullet(singlet) + CH_4 \Leftrightarrow CH_3\bullet + CH_3\bullet$$
$$CH_2\bullet(singlet) + C_2H_6 \Leftrightarrow C_2H_5\bullet + CH_3\bullet$$
$$CH_2\bullet(singlet) + H_2 \Leftrightarrow CH_3\bullet + H\bullet$$
$$CH_2\bullet(singlet) + H\bullet \Leftrightarrow CH_2\bullet + H\bullet$$
$$CH_2\bullet + CH_2\bullet \Leftrightarrow C_2H_2 + H_2$$
$$C_2H_2 + M \Leftrightarrow C_2H\bullet + H\bullet + M$$
$$C_2H_4 + M \Leftrightarrow C_2H_2 + H_2 + M$$
$$C_2H_4 + M \Leftrightarrow C_2H_3\bullet + H\bullet + M$$
$$H\bullet + H\bullet + M \Leftrightarrow H_2 + M$$
$$H\bullet + H\bullet + H_2 \Leftrightarrow H_2 + H_2$$

[†] Conventions, usage and formalism given in Ref. 29

Table 7 Reduced gas-phase reaction mechanism [27].

$$H_2 + H\bullet + H\bullet \Leftrightarrow H_2 + H_2$$
$$CH_4 \Leftrightarrow CH_3\bullet + H\bullet$$
$$CH_4 + H\bullet \Leftrightarrow CH_3\bullet + H_2$$
$$CH_3\bullet + H\bullet \Leftrightarrow CH_2\bullet + H_2$$
$$CH_3\bullet + CH_3\bullet \Leftrightarrow C_2H_5\bullet + H\bullet$$
$$CH_3\bullet + CH_2\bullet \Leftrightarrow C_2H_5\bullet + H\bullet$$
$$C_2H_5\bullet \Leftrightarrow C_2H_4 + H\bullet$$
$$C_2H_4 + H\bullet \Leftrightarrow C_2H_3\bullet + H_2$$
$$C_2H_3\bullet \Leftrightarrow C_2H_2 + H\bullet$$
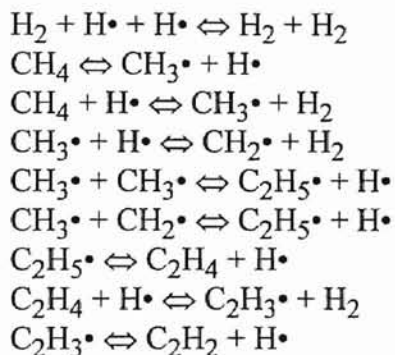
Readers are referred to the works of Meeks et al. [28], Coltrin and Dandy [29], and Miller and Melius [30] for a more complete stepwise analysis of gas-phase reaction mechanisms.

Summary

As is evident, a number of studies have been conducted by various researchers on the probable gas-phase reaction mechanisms. Such theoretical studies, in parallel with experimental evidence, help determine the species present within the high temperature environments of the low pressure chemical vapor deposition techniques, and the possible compositional role they may play in the subsequent nucleation and surface reactions. On the basis of this review, about twenty different predominant gas-phase species were identified. These species were included in the analysis of the gas-phase conducted at a later stage of this study.

CHAPTER V

NUCLEATION PROCESS

Introduction

The creation of a diamond seed or nucleus precedes any subsequent growth of diamond that may later take place on the surface. This initial nucleation of a diamond 'kernel' is a distinct and critical stage in the growth process of a diamond lattice. Moreover, the quality of diamond films deposited is determined by both the nucleation and growth processes. These processes are believed to be driven by the surface excess free energies and surface tensions at the substrate-gas, substrate-coating, and coatings-gas interfaces, respectively. An understanding of the fundamental processes leading to the formation of stable nuclei would allow one to control the nucleation behavior of the new phase and to vary the micro structure/morphology of the deposited film.

In recent years, researchers have synthesized diamond under a variety of conditions in an effort to understand the nucleation mechanism that occurs during the low pressure chemical vapor deposition of diamond. As mentioned previously, diamonds have been grown by a variety of different methods using a number of different hydrocarbon gas mixtures as sources [31-35].

The nucleation of diamond at low pressures involves growth under conditions in which diamond is the metastable phase. The chemical vapor deposition conditions

facilitate the kinetic growth of diamond; however, this process is extremely sensitive to a host of process parameters, and there always exists the possibility of the co-deposition of graphite or other allotropes of carbon. Thus, during the nucleation process both forms of carbon are constantly competing for existence.

The heterogeneous nucleation process accompanying the phase change at surfaces has been widely studied on the basis of both thermodynamic and kinetic arguments [36, 37]. Thermodynamic studies help identify the growth mechanism and characterize the nucleus including its chemical composition, shape, and dimension. In comparison, kinetic studies allow for the evaluation of the rate at which the new phase transforms, and the rates at which both nucleation and surface coverage occur [36]. Hwang et al. [38] modeled the nucleation of diamond based on the classical nucleation theory. Such studies clearly indicate the extreme sensitivity of the nucleation process, and how slight modifications in the values of parameters like the molar surface energy ratios of the two phases can easily reverse the dominance of nucleation to the non-diamond phase.

Nature of the Nucleation Site

The initial nucleation mechanism of a diamond crystallite is distinct from the subsequent growth mechanism for the extension of pre-existing diamond lattices. The mechanism whereby new, independent diamond crystals are nucleated in the harsh growth environments of the low pressure chemical vapor deposition methods remains unclear. Also, in spite of diamond nuclei being formed on a variety of substrates, the atomic arrangement of the nucleation sites is questionable.

Kawarada et al. [1] on the basis of their study of the silicon-diamond interface showed that diamond crystals grew from a single nucleation site, but did not determine

the nature of the site. Matsumoto and Matsui [1, 2] proposed that certain hydrocarbon cage compounds could serve as nuclei for vapor-grown diamond. Three of these cage compounds are illustrated in Fig. 4 [2]. Such molecules have the same symmetry and twinning found in vapor-grown diamond crystals. Angus and Hayman [1] suggest that analogous nuclei containing Si or various metals would be more thermally stable at the growth temperatures and consequently would be more likely candidates for diamond embryos. Such metal-containing clusters would also explain the observed sensitivity of nucleation rates to impurity levels.

adamantane   tetracyclododecane   hexacyclopentadecane

Figure 4. Structure of proposed nuclei [2].

Angus [2] suggested that multiple twinned saturated ring compounds were kinetically more favorable, as illustrated in Fig. 5 [2]. These molecules have easy sites for the addition of atoms. Some of the various possible formations for nuclei are illustrated in Figs. 6 [2] and 7 [1]. Moreover, it is believed that these ring structures will be found in greater abundance in the reaction environment.

cis boat-boat bicyclodecane   trans boat-boat bicyclodecane
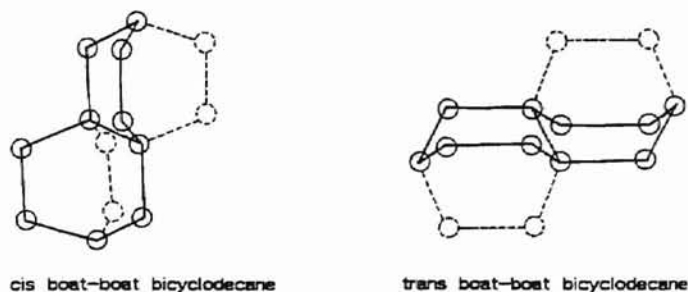
Figure 5. Formation of proposed nuclei. Formation of nucleus shown with dashed lines and circles [2].

Figure 6. The unreconstructed (111) and (100) surfaces showing addition of adatoms [2].
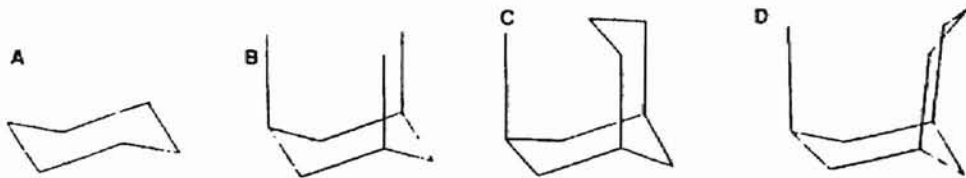
Figure 7. Formation of nuclei. (A) denotes an element of the (111) surface; (B) an element of the surface with three carbon atoms attached; (C) the start of a cubic nuclei and (D) the start of a hexagonal nuclei [1].

Nature of Substrates and Effect on Nucleation

The nucleation of diamond crystals on a substrate is known to be strongly dependent on the nature of the substrate and the substrate conditions. Diamonds have been deposited on many diverse substrates in an effort to understand the process of nucleation. The substrates on which deposition has been obtained may be classified into three categories.

[i] *Lattice matched* or *chemically compatible* materials such as diamond and cubic boron nitride

[ii] *Non-carbide forming* substrates such as Cu, Ni, Pt and Au

[iii] *Carbides and carbide forming* materials such as Si, Mo, SiC, Al_2O_3 and refractory-metals and metal carbides

A variety of surface treatments have been reported to increase nucleation density and improve diamond quality. The most common technique employed to enhance

diamond nucleation density on many different materials is to polish or abrade the surface with a fine diamond powder [12, 39, 40] or other abrasives [41]. Presently, there exist two possible explanations for the observed increase in nucleation rates. Some believe that scratching or polishing the surface results in diamond residual particles and/or other carbonaceous residues which provide seeds for diamond growth [42]. Subsequent nucleation is simply the result of diamond growing on diamond. However, since other abrasives give a similar, albeit a less pronounced effect, it is concluded that this cannot be the only process involved. Others believe that the mechanical and crystallographic damage done by abrading the surface enhances nucleation by creating high-energy damage sites on the surface. This view is supported by Dennig and Stevenson [43] who feel that the presence of residual abrasive is not a sufficient condition to initiate nucleation. Their results indicate that topographical features alone promote nucleation. In another study, Polini [44] concluded that the occurrences of edges is a necessary but not sufficient condition for nucleation. He suggests that particular atomic arrangements are required for diamond nucleus formation; one of the very few studies that recognizes the requirements of some nucleic site or atomic cluster (such as those presented in the previous section of this study on the 'Nature of the Nucleation Site').

Some of the other surface pre-treatment methods to enhance diamond nucleation rates include the addition of hydrocarbon oils to the surface [45], overlaying the Si substrate with carbon fibers [46], the use of a cleaved Si substrate [44], bombarding the substrate with electrons [47], the use of substrates implanted with non-oxide ceramics [48], and irradiating the surface with Ar^+ beams [49].

Experimental studies have shown that nucleation is promoted at clean surfaces, which are not flat, particularly at surface imperfections like a dislocation or a kink, or at irregular atomic arrangement such as a point or line defect on the substrate surface. The

free energy of formation of the critical nucleus is lower at such sites. This leads one to believe that the number of probable sites for embryo formation is finite in such cases of defect initiated heterogeneous nucleation. Results obtained by Kim et al. [50] are in accordance with this view.

In general, diamond crystals nucleated on non-diamond substrates essentially reflect a random orientation. Hetero-epitaxial growth of diamond has been achieved only on c-BN, which has a lattice structure that closely matches that of diamond [51]. Maeda et al. [48] observed in their studies on the effect of substrates pretreated with non-oxide ceramic particles that there was a tendency for the deposited film to reflect the chemical properties of the implanted ceramic. Other advances, contrary to popular belief, resulted in the growth of well defined diamond crystals with large and uniform grain sizes using various selective nucleation processes [44, 49, 52].

Nucleation Mechanism

The nucleation process may be divided into essentially two main stages.

[i]   The formation of stable diamond seeds or nuclei

[ii] The subsequent growth of existing seeds of the new phase

The nucleation mechanism has been treated individually for each substrate type as classified in the previous section of this study on the 'Nature of Substrates and Effect on Nucleation.'

[i] Nucleation mechanism of diamond on *lattice matched* or *chemically compatible* materials.

The reader is referred to the next section of this study on the 'Surface Reaction Mechanism.' The surface reaction mechanism presented in that section deals directly with the growth of diamond on a diamond lattice, assuming the presence of a pre-existing diamond lattice. This is not true in the case of non-diamond substrates where some intermediate interface layer is created and in which the diamond seed crystals or nuclei are first formed.

[ii] Nucleation mechanism of diamond on *non-carbide forming* substrates.

The nucleation of diamond on non-carbide forming substrates such as Cu, Ni, Au and Pt proceeds with the formation of an amorphous or diamond-like carbon layer on the surface of the substrate. Subsequent growth of large diamond crystals is observed on diamond micro crystallites which are formed as a result of direct transformation of diamond-like carbon into diamond.

Belton and Schmieg studied the nucleation process of diamond on both scratched and unscratched Pt and Ni substrates [39]. They observed the pre-deposition of graphitic carbon precursors on the Ni and Pt substrates preceding the nucleation process. The presence of these graphitic species was found to be a necessary but insufficient condition for nucleation. Scratching the surface was observed to stabilize graphitic deposits on surfaces that were otherwise resistant to growth, and it introduced defects into the graphite layers. In keeping with these observations, nucleation was envisaged to take place on defect sites in these graphite deposits. However, nothing was mentioned about the nature of those nucleation sites or their origin.

Singh and Vellaikal [53] studied the nucleation mechanism of diamond on Cu grids during the hot filament chemical vapor deposition process using high resolution transmission electron microscopy. The different steps involved during the nucleation and growth process of diamond crystal are illustrated in Fig. 8 [53]. The following nucleation mechanism presented is largely adopted from their work.
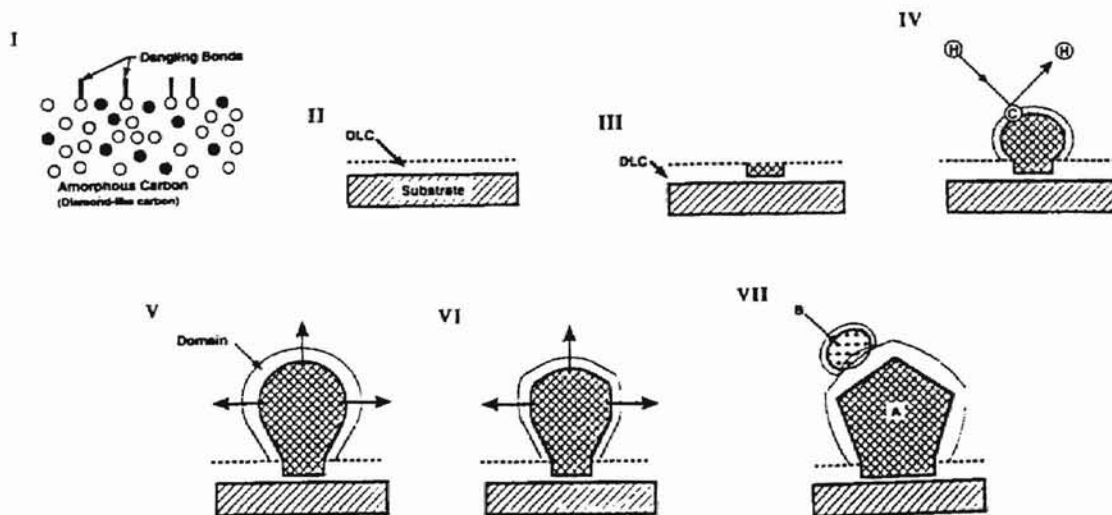
Figure 8. Schematic showing the different steps involved during the nucleation and growth of diamond crystal [53].

Step 1. Formation of carbon clusters: Clusters of carbon atoms are formed on the substrate surface in the early stages of the synthesis process. Continuos bombardment by atomic hydrogen and the local thermal conditions results in a change in the bonding structure of the carbon atoms from sp^1 to sp^2 bonding.

Step 2. Conversion of $sp^1 \rightarrow sp^2 \rightarrow sp^3$ bonding: The continuous rain of activated hydrocarbon and atomic hydrogen on to the surface of the substrate provides enough energy to convert the sp^2 bonded carbon atoms into a relatively stable network of sp^3 bonded carbon. The etching of unstable stages (sp^1 and sp^2) competes with the etching of the stable phase (sp^3). However, the unstable phase gets etched at a rate ten times faster

than that of the stable phase as a result of which there is a continuous phase transition from the sp^2 to the sp^3 carbon phase. Atomic hydrogen plays an important role in promoting this reaction and stabilizing the phase.

Step 3. Crystallization of the amorphous phase: A transition in the bonding state of the carbon network from an amorphous phase with sp^2 bonded carbon to a disordered domain with sp3 bonded carbon to diamond with sp^3 bonded carbon occurs during or before the crystallization process begins. The carbon atoms rearrange themselves to acquire minimum surface energy. They indicate a tendency to rearrange themselves so as to form the (111) crystallographic plane of the diamond crystal which possesses the lowest surface energy in the crystal. Crystallization in the amorphous layer involves the complex chemical reactions of hydrogen abstraction, dehydrogenation of adsorbed complexes, recombination of hydrogen atoms, etc. The recrystallized regions act as nuclei for the subsequent growth of diamond.

Steps 4 to 6. Growth of diamond: Clusters of carbon atoms with sp^3 bonding are deposited on the surface of the precursor layer. These carbon atoms diffuse inward by solid state diffusion. The diamond will initially be hemispherical in shape. The existence of this hemispherical shape (stage 4) has been confirmed experimentally [53]. Once the diamond reaches its critical size (stage 5), it begins to acquire a faceted crystallographic shape (stage 6).

Step 7. Secondary growth of diamond: The surface of the disordered domain varies in thickness depending on deposition conditions and concentration fluctuations on the surface of diamond. Once the thickness of the disordered domain exceeds the critical thickness of 150 °A, the carbon atoms do not have sufficient time and localized thermal energy to diffuse into the diamond crystal. As a result, an additional amorphous layer

builds up and once again recrystallizes by the proposed mechanism. The secondary recrystallization acts as a nucleation site for the growth of secondary diamond on the primary diamond crystal. An amorphous layer will always exist initially between the primary diamond and secondary diamond crystallite which may convert by atomic diffusion into diamond crystal given time and assuming a sufficient localized source of heat.

These results are in accordance with Ostwald's rule of steps which states that in the course of going from a non-equilibrium phase to a final equilibrium state, a system will pass step-wise through states of intermediate stability [53].

[iii] Nucleation mechanism of diamond on *carbide forming* substrates.

The nucleation of diamond on carbide forming substrates such as Si, Mo and Al_2O_3 proceeds with the formation of an amorphous intermediate layer formed between the diamond film deposited and the substrate surface. This amorphous layer has been analyzed and found to be a carbide crystal layer. Williams and Glass [54] reported an intermediate layer of single crystal SiC during their studies using a Si substrate. Others have reported similar findings [55].

Wang [56] proposed a model to describe the formation of a SiC buffer layer between the diamond film and the surface of the silicon substrate. They suggested the formation of three stages for the buffer layer, specifically, $Si\text{-}Si_{1-x}C_x$ / SiC / Si_yC_{1-y}-diamond. Experimentally, they used X-ray photoelectron spectroscopy and Auger electron spectroscopy to distinguish between the three separate regions within the SiC buffer layer.

Jackman et al. [57] studied the initial stages of the growth of diamond on Si(100) using a mixture of methane and hydrogen activated by heated filament. Their results indicate that C-C bond formation can occur on the Si surface through the atomic hydrogen driven addition of hydrogenated forms. Acetylenic species were seen to play a significant role in the initial formation of the carbide layer. The mechanism proposed allowed for the subsequent growth of diamond to occur via the addition of either methyl radicals or acetylenic species. The addition reactions observed were slow and may explain why the growth of diamond on smooth Si(100) is a very slow process. The surface processes occurring during the nucleation process are illustrated in Fig. 9 [57].

Step 1. Adsorption of hydrocarbon species: A complex mixture of hydrocarbon fragments is adsorbed on the substrate surface. Hydrogen, ethylene, acetylenic species and other CH_x species have been identified to be present on the surface at the onset of growth. Gas-phase kinetic studies indicate a strong possibility of acetylene molecules forming a major component of the adsorbed layer.

Step 2. Conversion of adsorbed ethylene to acetylene: The adsorbed (ads) ethylene is converted to acetylene by either one of the two processes.

(a) Abstraction of H from ethylene by the impinging atomic beam resulting in the formation of a gas-phase hydrogen molecule.

$$C_2H_4 \text{ (ads)} + 2H \text{ (g)} \rightarrow C_2H_2 \text{ (ads)} + 2H_2 \text{ (g)}$$
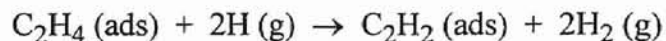
(b) Surface conversion of ethylene to acetylene.

$$C_2H_4 \text{ (ads)} \rightarrow C_2H_2 \text{ (ads)} + 2H \text{ (ads)}$$
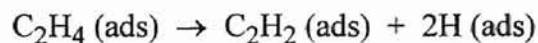
The C_1 (CH_x) species are formed during this step. Acetylene and hydrogen are left on the surface.

Step 3. C-C bond formation: Further exposure to atomic hydrogen promotes the addition of a surface methyl or methylene group and the bound acetylene resulting in the formation of C3 species. This C-C bond formation occurs only after the C concentration builds up to monolayer levels.

$$H \text{ (ads)} + C_2H_2 \text{ (ads)} + CH_x \text{ (ads)} \rightarrow C_3H_5 \text{ (ads)} + H_x \text{ (ads)}$$

$$C_3H_5 \text{ (ads)} + H \text{ (ads)} \rightarrow C_3H_6 \text{ (ads)}$$
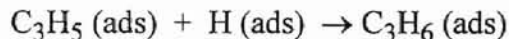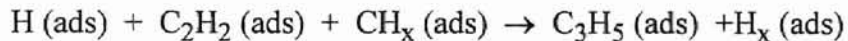
C-C bond forming reactions may also take place between hydrogenated carbon species on the surface.
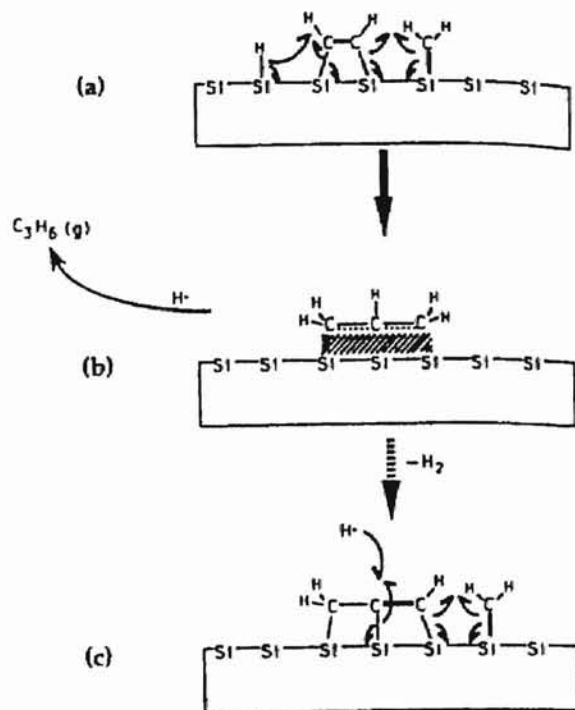
Figure 9. Schematic representation of the surface processes occurring on the surface of Si(100) to atomic hydrogen. Abstraction of the surface and subsequent addition of methyl groups takes place in step (a). Step (b) results in the thermal desorption of propene. Further hydrogen abstraction regenerates acetylenic species leading to the propagation of the carbon chain in step (c) [57].

Step 4. Propagation of sp³ hybridized carbon chain: The thermal loss of H_2 from the organic species formed during Step 3 results in the reforming of acetylenic species. The

whole cycle can then repeat itself resulting in polymerization. A self-propagating sp^3 hybridized carbon chain can form across the surface by methyl group addition, without the addition of further acetylenic species from the gas-phase.

Step 5. Growth of diamond: Diamond micro crystallites are formed on the carbide layer and act as nucleation sites for further growth. Subsequent growth of diamond may now take place via a sequence of reactions similar to those observed on non-carbide forming substrates.

Summary

While some understanding of the possible gas–phase reactions and growth mechanisms has been achieved, the nucleation of new, independent diamond crystals in the harsh growth environment of the low pressure methods remains less clear. Although the reactions preceding diamond growth apparently play a critical role in the overall diamond deposition process, sufficient attention has not been paid to the diamond surface chemistry. Detailed *in-situ* experimental studies are required before the nucleation mechanism may be established with some degree of confidence.

CHAPTER VI

SURFACE REACTION MECHANISM

Introduction

A complicated sequence of surface reactions, originating at preexisting diamond nuclei, take place during the last stage of a series of processes that ultimately results in the growth of diamond at low pressures. However, in spite of the extensive progress made in the low pressure chemical vapor deposition of diamond film, the chemistry of the processes responsible for diamond film growth on a molecular level is not entirely understood.

Studies of the gas-phase species present during typical chemical vapor deposition methods indicate that methyl radicals and acetylene are the two most likely growth species [9]. Harris et al. [58] and Goodwin and Gavillet [59] reached similar conclusions that only CH_3 or C_2H_2 could account for the measured growth rates in filament assisted systems. Martin and Hill [60], and Harris and Martin [61] demonstrated that both species are capable of contributing towards the growth of diamond depending on the details of the system. Aside from these two species, atomic carbon is suspected to contribute to the growth process under certain conditions, too [62].

Several hypothetical mechanisms have been proposed attempting to explain the surface reaction mechanism exhibited during the low pressure chemical vapor deposition

of diamond. Tsuda et al. [63, 64] proposed a growth mechanism with methyl radicals as the primary growth species. They performed semiempirical calculations to determine the lowest energy pathways for the growth of diamond via CH_3^+ intermediates. Huang et al. [65] proposed a mechanism, with acetylene assumed to be the principal growth species. Frenklach and Spear [66] proposed a similar growth mechanism for vapor deposited diamond film with acetylene as the main monomer growth species. Belton and Harris [67] criticized the mechanism proposed by Huang et al. on the basis of a thermochemical analysis and suggested an alternative pathway for the formation of diamond. In a later work, Frenklach [68] proposed a mechanism that assumes the growth of diamond via the alternate addition of methyl radicals and acetylene.

More recently, Tsuda et al. [62] proposed an elementary process for the step growth of diamond crystals in which carbon atoms are seen to play the principal role. Doty and Jesser [69] investigated the role of charged species in the hot-filament assisted chemical vapor deposition of diamond. They concluded that the primary growth reaction did not proceed entirely via a free radical mechanism. Harris and Goodwin [70] performed a thermochemical kinetic analysis for growth on the reconstructed diamond (100) surface and proposed a mechanism in which half the growth was accounted for by insertion into dimer bonds, while the other half was accounted for by addition across troughs between dimer bonds. Harris [71] used a 9-carbon model compound to describe a proposed mechanism for diamond growth from methyl radicals on a hydrogenated, electrically neutral (100) surface. For a method that contained no adjustable parameters, it was able to predict growth rates surprisingly well. Deak et al. [72] used a semiempirical quantum chemical approach to develop a sequence of energetically favorable stable surface complexes leading to diamond growth. The initial hydrogen abstraction step is a common feature of all the mechanisms developed irrespective of the growth process involved.

Numerous researchers have utilized these hypothetical surface reaction models to simulate the growth of diamond. Kim and Cappelli [73] and Matsui et al. [74] modeled the growth of diamond in flame-assisted chemical vapor deposition assuming methyl radicals as the primary growth precursors. Others have modeled diamond growth with acetylene as the primary growth precursor [75]. Meeks et al. [28] and Coltrin and Dandy [29] used the methyl addition reaction model proposed by Harris [71], and Harris and Belton [67], and the acetylene addition reaction mechanism, proposed by Frenklach [68], to successfully simulate the growth of diamond in premixed flames [28] and direct current plasma-gun reactors [29].

In another approach, researchers have studied the energetics of the surface reactions [76-79] and the stability of the various surface structures [80, 81]. Huang and Frenklach [76, 77] studied the energetics of several possible diamond (100) and (110) surface growth elementary reactions and determined the potential barriers involved. Besler et al. [78] performed similar calculations for growth mechanisms of the diamond (110) surface. Peploski et al. [79] and Chang et al. [82] determined the minimum energy paths for various elementary surface reactions in low pressure diamond film formation. In a later study, Chang et al. [83] studied the hydrogen abstraction reactions from diamond and diamond-like surfaces. Piekarczyk [84, 85] investigated the transformations of diamond crystal faces and the reactions proceeding on them during the chemical vapor deposition of diamond with the help of chemical thermodynamic methods. Harris and Belton [86] performed a thermochemical and kinetic analysis of a mechanism involving acetylene as the predominant growth species. Still others have studied the surface reaction kinetics of diamond growth aiming to determine the factors which affect growth rate and surface morphology [58, 87, 88].

Surface Reaction Mechanism

The surface reaction mechanism in this study was adopted largely from the work of Coltrin and Dandy [29], who modeled the growth of diamond in sub-atmospheric direct current arc plasma-jet reactors. They utilized the SURFACE CHEMKIN package, a general kinetic formalism developed by Coltrin et al. [89] for treating heterogeneous reactions at gas-solid interfaces. The proposed mechanism includes pathways for the incorporation of CH_3, C_2H_2, and C from the gas-phase, as well as the growth of graphite. Meeks et al. [28] used this model to successfully simulate diamond growth under combustion conditions. Others have demonstrated similar success simulating the growth of diamond using this model under conditions as diverse as those encountered in hot-filament synthesis [59].

This surface reaction mechanism includes the growth of diamond from three gas-phase precursor species. Such an approach is supported by Piekarezyk and Yarbrough [85], who felt that diamond may be deposited by many different reactions and hydrocarbon species, with the predominant species depending on the specific chemical composition of the nutrient gas-phase and/or the conditions prevalent at the time. Recent experimental evidence seems to support this view.

This mechanism allows for the growth of diamond and graphitic material. The possibility of inter-conversion between graphitic carbon and diamond under conditions of high H-atom concentration is included. Coltrin and Dandy used the methyl-addition growth sequence proposed by Harris [71] and later modified by Harris and Belton [67], as well as the acetylene addition growth sequence proposed by Frenklach [68]. The surface reaction mechanism is illustrated in Table 8 [29].

Table 8. Surface reaction mechanism[†] [29].
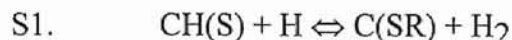
Initiation
S1. $CH(S) + H \Leftrightarrow C(SR) + H_2$

Radical recombination
S2. $C(SR) + H \Leftrightarrow CH(S)$

Methyl-radical addition
S3. $C(SR) + CH_3 \Leftrightarrow C(D) + CH_3(S)$
S4. $CH_2(S) + H \Leftrightarrow CH(SR) + H_2$
S5. $CH_3(S) + H \Leftrightarrow CH_2(SR) + H_2$
S6. $CH_2(SR) + CH(SR) \Leftrightarrow CH_2(S) + CH(S)$

Acetylene addition
S7. $C(SR) + HCCH \Leftrightarrow C(D) + HCCH(SR)$
S8. $CH(S) + HCCH(SR) \Leftrightarrow C(SR) + H_2CCH(S)$
S9. $H_2CCH(S) + C(SR) \Leftrightarrow C(D) + CH_2(S) + CH(SR)$
S10. $CH_2(S) + CH(SR) \Leftrightarrow CH_2^{*}(S) + CH(SR)$
S11. $CH(SR) + CH_2^{*}(S) + H \Leftrightarrow CH(S) + CH(S) + H_2$

Carbon-atom addition
S12. $C(SR) + C \Leftrightarrow C(D) + C(SR3)$
S13. $C(SR3) + CH_2(S) \Leftrightarrow CH(SR) + CH(S)$
S14. $CH(SR) + H \Leftrightarrow CH_2(S)$

Other radical-termination reactions
S15. $C(SR3) + H_2 \Leftrightarrow CH_2(S)$
S16. $C(SR3) + H \Leftrightarrow CH(SR2)$
S17. $CH(SR2) + H \Leftrightarrow CH_2(SR)$
S18. $CH_2(SR) + H \Leftrightarrow CH_3(S)$
S19. $CH(SR2) + H_2 \Leftrightarrow CH_3(S)$

Graphite reactions
S20. $CH(SG) + C(G) + H \Leftrightarrow CH(SR) + CH(S)$
S21. $CH(SG) + H \Leftrightarrow C(RG) + H_2$
S22. $C(RG) + H \Leftrightarrow CH(SG)$
S23. $C(RG) + CH_3 \Leftrightarrow C(G) + CH_3(S)$
S24. $C(RG) + C \Leftrightarrow C(G) + C(SR3)$
S25. $C(RG) + HCCH \Leftrightarrow C(G) HCCH(SR)$
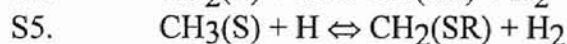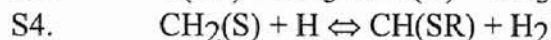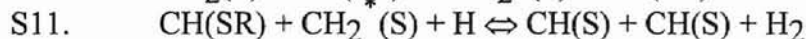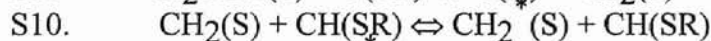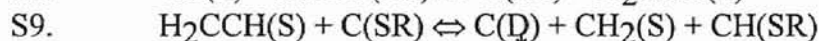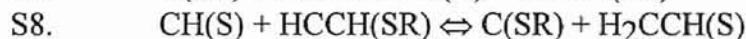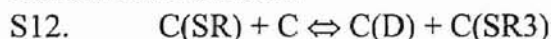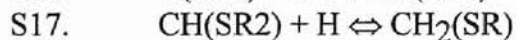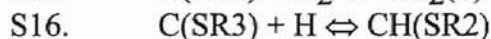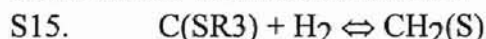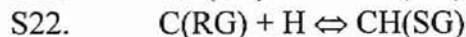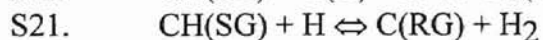
[†] Conventions, usage and formalism given in Ref. 29.

The complete surface reaction mechanism consists of 25 reversible reactions. The following is a summary of the steps involved.

Reaction S1. Initiation reaction: The growth process begins with the abstraction of a surface H atom by a gas-phase H atom. The original species CH(S) has three sp^3 C-C bonds and one sp^3 C-H bond. After abstraction a reactive radical site C(S,R) is left on the surface. A reaction probability of 0.1 was adopted for most of the H-abstraction reactions in the mechanism (S1, S4, and S11).

Reaction S2. Radical recombination resulting in the termination of surface radicals created via reaction S1: Gas-phase H-atoms may recombine with the C(S,R) surface radical formed, effectively terminating any further reaction at this site. A reaction probability of 0.3 was adopted for this reaction and all similar ones (S2, S14, S16-S18). The H-atom recombination probability of 0.16 used was within the experimental error reported by Harris and Weiner [58] in their studies.

Reactions S1 and S3 to S6. Methyl addition reactions: These reactions result in the formation of a C-C bond between the methyl group, just added to the surface, and the neighboring $CH_2(S)$ group. The reaction sequence follows the route proposed by Harris [71], and Harris and Belton [67]. The species involved in these reactions are identified in Figs. 10 and 11 [29]. The methyl addition sequence of reactions is illustrated in Figs. 12 and 13 [67, 71].

Reaction S3:   The addition of methyl takes place at the surface radical site C(S,R) created via reaction S1.

Reaction S4:   The abstraction of a second H atom occurs from the surface species, $CH_2(S)$.

Figure 10. Identification of surface species involved in reactions S1 to S5 [29].
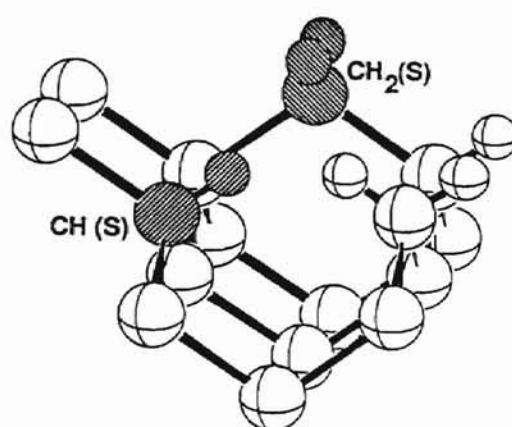
Figure 11. Identification of surface species involved in reaction S6 [29].

$$HH + H^{gas} \Leftrightarrow H^* + H_2^{gas}$$
$$H^* + H^{gas} \Leftrightarrow HH$$
$$H^* + CH_3 \Leftrightarrow HM$$
$$HM + H^{gas} \Leftrightarrow M^* + H_2^{gas}$$
$$M^* + H^{gas} \Leftrightarrow HM$$
$$HM + H^{gas} \Leftrightarrow HM^* + H_2^{gas}$$
$$HM^* + H^{gas} \Leftrightarrow HM$$
$$HM^* \Leftrightarrow M^*$$
$$HM^* + H^{gas} \Leftrightarrow H^* + CH_3^{*gas}$$
$$HM^* + CH_3^{*gas} \Leftrightarrow HE$$
$$HM^* + H^{gas} \Leftrightarrow B + H_2^{gas}$$
$$M^* + H^{gas} \Leftrightarrow B + H_2^{gas}$$
$$HH + H^{gas} \Leftrightarrow {}^*H + H_2^{gas}$$
$${}^*H + H^{gas} \Leftrightarrow HH$$
$$H^* + H^{gas} \Leftrightarrow ^{**} + H_2^{gas}$$
$$^* + H^{gas} \Leftrightarrow H^*$$
$${}^*H + H^{gas} \Leftrightarrow ^{**} + H_2^{gas}$$
$$^{**} + CH_3^{gas} \Leftrightarrow M^*$$
$$H^* \Leftrightarrow {}^*H$$

Figure 12. Methyl addition reaction mechanism proposed by Harris and Belton. Conventions, usage and formalism given in Ref. 67.

41

Reaction S5:   The sequential abstraction of H takes place resulting in the formation of a reactive radical site, $CH_2(S,R)$.

Reaction S6:   C-C bond formation occurs between the two neighboring radicals. This reaction is expected to be very rapid proceeding with no reaction barrier.
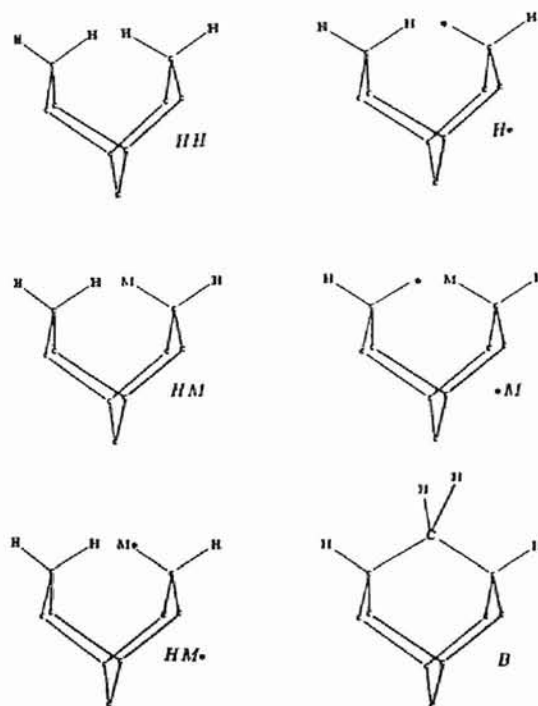
Figure 13.   Schematic of the methyl addition reaction mechanism proposed by Harris [67].

Reactions S1 and S7 to S1.   Acetylene addition reactions: The reaction sequence follows the mechanism proposed by Frenklach [68]. The species involved in these reactions are identified in Figs. 14-18 [29]. The acetylene addition sequence of reactions is illustrated in Fig. 19 [68].

Reaction S7:   Acetylene from the gas-phase reacts with a surface radical site created via reaction S1. The carbon that is covered becomes a deposited carbon C(D),

and a new radical species HCCH(S,R) is formed, as illustrated in Fig 15 [29].
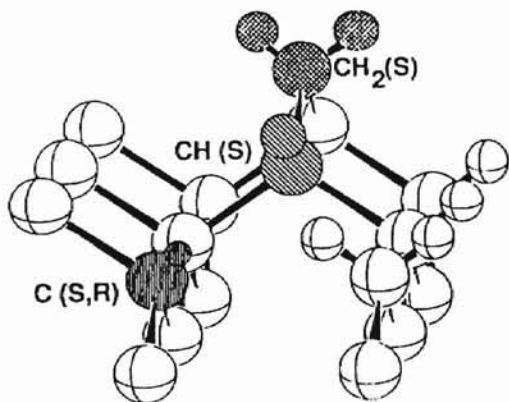
Figure 14. Identification of surface species involved in reactions S7 to S11 [29].
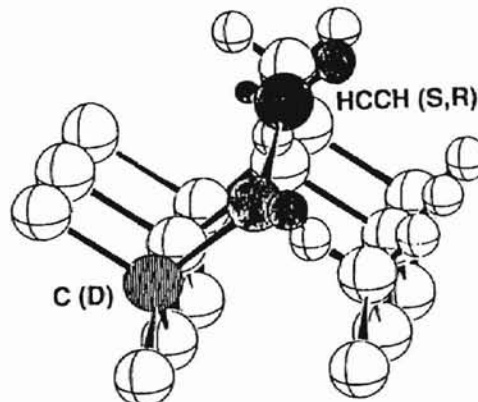
Figure 15. Identification of surface species involved in reaction S7 [29].

Reaction S8: The chemisorbed acetylene reacts with a neighboring CH(S) group. Transfer of a H-atom occurs. The adsorbed C_2 species rehybridizes from sp^1 to sp^2 bonding, and the radical site shifts to the neighboring surface carbon, as illustrated in Fig. 16 [29].
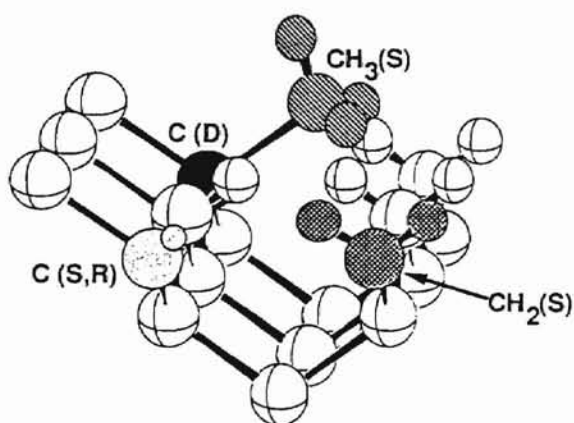

Figures 16. Identification of surface species involved in reaction S8 [29].
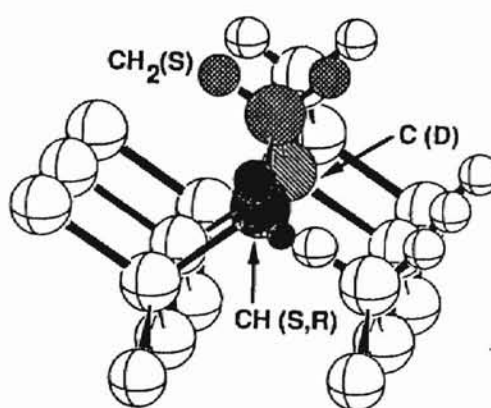
Figure 17. Identification of surface species involved in reaction S9 [29].

Reaction S9: The adsorbed C_2 species further rehybridizes from sp^2 to sp^3 forming a bond with the surface, as illustrated in Fig 17 [29].

Reactions S10 and S11: The acetylene addition sequence of reactions is completed with the extraction of a H from saturated surface CH groups by a gas-phase H atom, as illustrated in Fig. 18 [29].
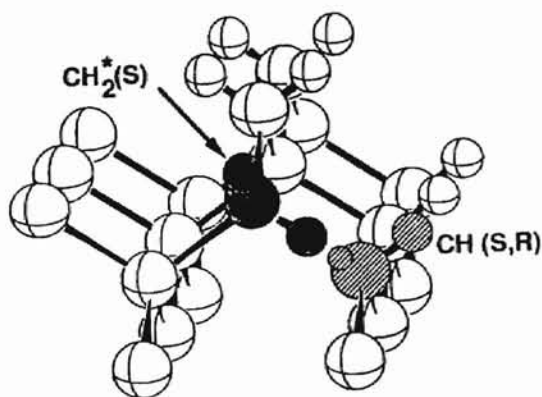
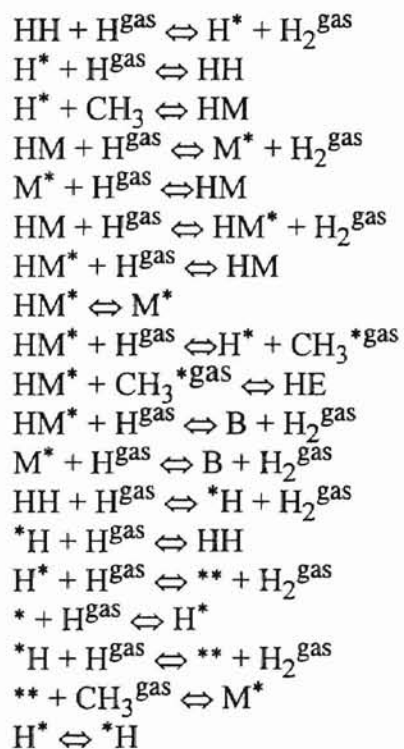**Figure 18. Identification of surface species involved in reaction S10 [29].**

Reactions S1 and S12 to S14. Deposition of bulk diamond from gas-phase C atoms:

Reaction S12: A carbon atom from the gas-phase reacts with a surface radical created via reaction S1. The carbon covered becomes a deposited carbon, C(D). A multiple surface radical site C(S,R3) is formed as a result.

Reaction S13: The surface radical site C(S,R3) created reacts with an adjacent $CH_2(S)$ group resulting in the formation of a surface radical site CH(S,R).

Reaction S14: A gas-phase H-atom is added to the surface radical site CH(S,R) formed via reaction S13.

Reactions S15 through S19: These account for additional reactions between H or H_2 atoms and surface radical species. They include the termination of radical sites. Such reactions were assigned a probability of 0.3.

44
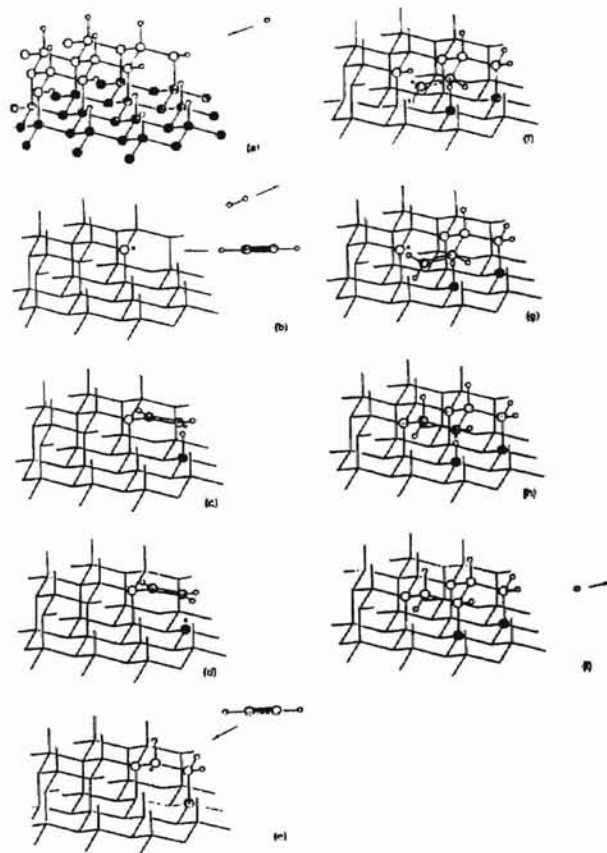
Figure 19. Acetylene addition reaction mechanism [68].

Reactions S20 to S25. Reactions of graphitic surface species: These are included in the growth mechanism with the intent of including an alternative growth pathway.

Reaction S20: This reaction is responsible for the inter conversion between diamond-type surface carbon atoms with sp^3 hybridization and graphitic surface carbon atoms with sp^2 hybridization. The species involved in this reaction are identified in Figs. 20 and 21 [29].

Reaction S21: The abstraction of a vinylic H-atom takes place via this reaction.

Reaction S22: The recombination reaction of H with a graphitic surface carbon radical $C(R,G)$ takes place.

Reaction S23: The addition reaction of a methyl radical with a graphitic surface carbon radical $C(R,G)$ takes place.

Reaction S24: A gas-phase C-atom reacts with a graphitic surface carbon radical $C(R,G)$ resulting in the deposition of a bulk graphitic carbon species $C(G)$.

45

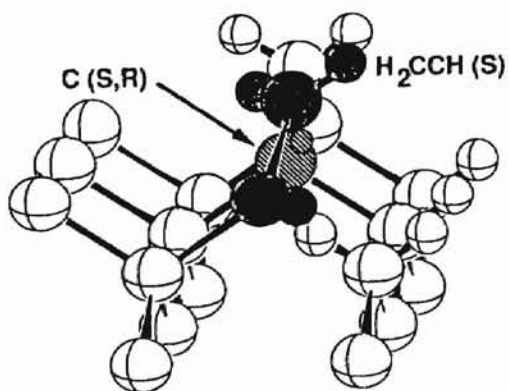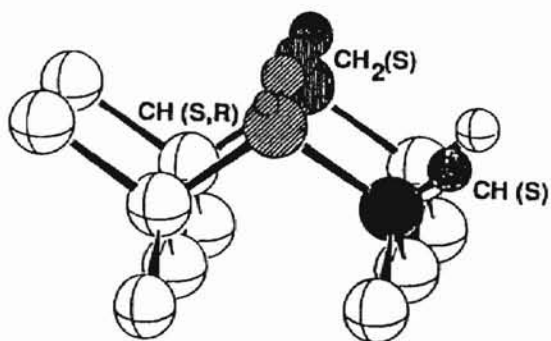**Figure 20. Identification of surface species involved in reaction S20 [29].**
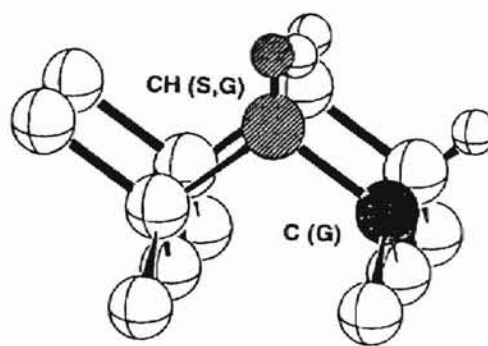
Figures 21. Identification of graphitic surface species involved in reaction S20 [29].

Reaction S25: The addition reaction of acetylene with a graphitic surface carbon radical C(R,G) takes place resulting in the formation of a bulk graphitic carbon species C(G).

Summary

Several surface reaction mechanisms have been proposed by various researchers in an effort to explain the low pressure chemical vapor deposition of diamond. However, such studies are unable to precisely portray the reactions proceeding on the surface. A lack of accurate rate data for the proposed elementary reactions further impedes the evaluation of these mechanisms. Theoretical studies of the energetics of various surface species and reactions, coupled with some '*direct* experimental observations' of the surface chemistry, would prove extremely useful.

The surface reactions mechanism illustrated in this section was utilized in the formulation of a growth model for diamond presented in a later stage of this study.

BIBLIOGRAPHY

1. J. C. Angus and C. C. Hayman, Sci., 241 (1988) 913.

2. J. C. Angus, Y. Wang, and M. Sunkara, Annu. Rev. Mater. Sci., 21 (1991) 221.

3. L. R. Martin, Am. Ceram. Soc. Bull., 71 (1992) 1419.

4. R. Komanduri (Cluster Coordinator), NSF EPSCoR Presentation on the 'Fundamental and Applied Aspects of Low Pressure CVD Diamond Synthesis,' Oklahoma State University, October 12 (1990).

5. J. T. Wang, C. Cao, and P. Zheng, J. Electrochem. Soc., 141 (1994) 278.

6. P. K. Bachmann and W. van Enckevort, Diamond Relat. Mater., 1 (1992) 1021.

7. S. J. Harris, A. M. Weiner, and T. A. Perry, Appl. Phys. Lett., 53 (1988) 24.

8. Y. Matsui, A. Yuuki, M. Sahara, and Y. Hirose, Jpn. J. Appl. Phys., 28 (1989) 1718.

9. F. G. Celii, P. E. Pehrsson, H. T. Wang, and J. E. Butler, Appl. Phys. Lett., 52 (1988) 2043.

10. F. G. Celii and J. E. Butler, Appl. Phys. Lett., 54 (1989) 1031.

11. M. A. Cappelli and P. H. Paul, J. Appl. Phys., 67 (1990) 2596

12. K. Mitsuda, Y. Kojima, T. Yoshida, and K. Akashi, J. Mater. Sci., 22 (1987) 1557.

13. T. Mitomo, T. Ohta, E. Kondah, and K. Ohtsuka, J. Appl. Phys., 70 (1991) 4532.

14. M. Frenklach, J. Appl. Phys., 65 (1989) 5142.

15. S. J. Harris, J. Appl. Phys., 65 (1989) 3044.

16. S. J. Harris and A. M. Weiner, J. Appl. Phys., 67 (1990) 6520.

17. E. Kondah, T. Ohta, T. Mitomo, and K. Ohtsuka, J. Appl. Phys., 72 (1992) 705.

18. M. Dong and D. G. Lilley, ASME Int. Computer in Engg. Conf., August 2 (1990).

19. M. P. D'Evelyn, C. J. Chu, R. H. Hange, and J. L. Margrave, J. Appl. Phys., 71 (1992) 1528.

20. S. W. Reeve, W. A. Weimer, and F. M. Cerio, J. Appl. Phys., 74 (1993) 7521.

21. P. Bou, J. C. Boettner, and L. Vandenbulcke, Jpn. J. Appl. Phys., 31 (1992) 2931.

22. Y. Genchi, T. Yasuda, and H. Komiyama, Int. Chem. Engg., 32 (1992) 560.

23. H. Shiomi, K. Tanabe, Y. Nishibayashi, and N. Fujimori, Jpn. J. Appl. Phys., 29 (1990) 34.

24. S. M. Kanetkar, G. Matera, X. Chen, S. Pramanick, P. Tiwari, and J. Narayan, J. Electron. Mater., 20 (1991) 141.

25. E. Kondoh, K. Tanaka, and T. Ohta, J. Appl. Phys., 74 (1993) 4513.

26. I. Pinter, M. Marinelli, A. Tebano, A. Paoletti, and P. Paroli, Phys. Stat. Sol. (A), 141 (1994) 397.

27. C. Wolden, K. K. Gleason, and J. B. Howard, Combust. Flame, 96 (1994) 75.

28. E. Meeks, R. J. Kee, D. S. Dandy, and M. E. Coltrin, Combust. Flame, 92 (1993) 144.

29. M. E. Coltrin and D. S. Dandy, J. Appl. Phys., 74 (1993) 5803.

30. J. A. Miller and C. F. Melius, Combust. Flame, 91 (1992) 21.

31. K. Okano, T. Iwasaki, H. Kiyota, T. Kurosu, and M. Iida, Thin Solid Films 206 (1991) 183.

32. Y. Hirose and N. Kondo, 35th Spring Meet. of the Jpn. Appl. Phys. Soc. March 29, (1988), Extended Abstracts, (1988), 434.

33. C. E. Johnson, W. A. Weimer, and F. M. Cerio, J. Mater. Res., 7 (1992) 1427.

34. L. R. Martin and M. W. Hill, J. Mater. Sci. Lett., 9 (1990) 621.

35. N. Ohtake and M. Yoshikawa, J. Electrochem. Soc., 137 (1990) 717.

36. M. Tomellini, R. Polini, and V. Sessa, J. Appl. Phys., 70 (1991) 7573.

37. M. Tomellini, J. Appl. Phys., 72 (1992) 1589.

38. N. M. Hwang, G. W. Bahng, and D. N. Yoon, Diamond Relat. Mater., 1 (1992) 191.

39. D. N. Belton and S. J. Schmieg, Thin Solid Films, 212 (1992) 68.

40. Y. Shu-Cheng, C. Hon-Sho, and G. Fon-Shu, J. Crys. Growth, 99 (1990) 1196.

41. W. A. Yarbrough, A. Inspektor, and R. Messier, Mater. Sci. Forum, 51 & 52 (1989) 151.

42. S. Iijima, Y. Aikawa, and K. Baba, J. Mater. Res., 6 (1991) 1491.

43. P. A. Dennig and D. A. Stevenson, Appl. Phys. Lett., 59 (1991) 1562.

44. R. Polini, J. Appl. Phys., 72 (1992) 2517.

45. P. E. Pehrsson and A. A. Morrish, Appl. Phys. Lett., 59 (1990) 417.

46. P. E. Pehrsson, J. Glesener, and A. Morrish, Thin Solid Films, 212 (1992) 81.

47. A. Sawabe and T. Inuzuka, Thin Solid Films, 137 (1986) 89.

48. H. Maeda, S. Masuda, K. Kusakabe, and S. Morooka, J. Crys. Growth, 121 (1992) 507.

49. J. S. Ma, H. Kawarada, T. Yonehara, J. Suzuki, Y. Yokota, and A. Hiraki, J. Crys. Growth, 99 (1990) 1206.

50. J. W. Kim, Y. J. Baik, K. Y. Eun, and D. N. Yoon, Thin Solid Films, 212 (1992) 104.

51. S. Koizumo, T. Murakami, T. Inuzuka, and K. Suzuki, Appl. Phys. Lett., 57 (1990) 536.

52. X. H. Wang, W. Zhu, J. von Windheim, and J. T. Glass, J. Crys. Growth, 129 (1990) 45.

53. J. Singh and M. Vellaikal, J. Appl. Phys., 73 (1993) 2831.

54. B. E. Williams and J. T. Glass, J. Mater. Res., 4 (1989) 373.

55. D. N. Belton, S. J. Harris, S. J. Schmieg, A. M. Weiner, and T. A. Perry, Appl. Phys. Lett., 54 (1989) 416.

56. E. G. Wang, Phys. (B), 185 (1993) 84.

57. R. B. Jackman, L. H. Chua, and J. S. Foord, Surface Sci., 292 (1993) 47.

58. S. J. Harris, A. M. Weiner, and T. A. Perry, Appl. Phys. Lett., 53 (1988) 1605.

59. D. G. Goodwin and G.G. Gavillet, J. Appl. Phys., 68 (1990) 6393.

60. L. R. Martin and M. W. Hill, Appl. Phys. Lett., 55(1989) 2248.

61. S. J. Harris and L. R. Martin, J. Mater. Res., 5 (1990) 2313.

62. M. Tsuda, S.Oikawa, S. Furukawa, C. Sekine, and M. Hata, J. Electrochem. Soc., 139 (1992) 1482.

63. M. Tsuda, M. Nakajima, and S.Oikawa, J. Am. Chem. Soc., 108 (1986) 5780.

64. M. Tsuda, M. Nakajima, and S.Oikawa, Jpn. J. Appl. Phys., 26 (1987) L527.

65. D. Huang, M. Frenklach, and M. Maroncelli, J. Appl. Phys., 92 (1988) 6379.

66. M. Frenklach and K. E. Spear, J. Mater. Res., 3 (1988) 133.

67. S. J. Harris and D. N. Belton, J. Chem. Phys., 96 (1992) 2371.

68. M. Frenklach, J. Chem. Phys., 97 (1992) 5794.

69. F. P. Doty and W. A. Jesser, J. Electronic Mater., 20 (1991) 121.

70. S. J. Harris and D. G. Goodwin, J. Phys. Chem., 97 (1993) 23.

71. S. J. Harris, Appl. Phys. Lett., 56 (1990) 2298.

72. P. Deak, J. Giber, and H. Oechsner, Surf. Sci., 250 (1991) 287.

73. J. S. Kim and M. A. Cappelli, J. Appl. Phys., 72 (1992) 5461.

74. Y. Matsui and M. Sahara, Jpn. J. Appl. Phys., 28 (1989) 1023.

75. L. R. Martin, J. Mater. Sci. Lett. 12 (1993) 246.

76. D. Huang and M. Frenklach, J. Phys. Chem., 95 (1991) 3692.

77. D. Huang and M. Frenklach, J. Phys. Chem., 96 (1992) 1868.

78. B. H. Besler, W. L. Hase,and K. C. Hass, J. Phys. Chem., 96 (1992) 9369.

79. J. Peploski, D. N. Thompson, and L. M. Raff, J. Phys. Chem., 96 (1992) 8538.

80. S. P. Mehandru and A. B. Anderson, Surface Sci., 248 (1991) 369.

81. X. M. Zheng nad P. V. Smith, Surface Sci., 262 (1992) 219.

82. X. Y. Chang, D. N. Thompson, and L. M. Raff, J. Phys. Chem., 97 (1993) 10112.

83. X. Y. Chang, M. Perry, J. Peploski, D. N. Thompson, and L. M. Raff, J. Chem. Phys., 99 (1993) 4748.

84. W. Piekarczyk, J. Crys. Growth, 119 (1992) 345.

85. W. Piekarczyk and W. A. Yarbrough, J. Crys. Growth, 108 (1991) 583.

86. S. J. Harris and D. N. Belton, Jpn. J. Appl. Phys., 30 (1991) 2615.

87. D. Kweon, J. Lee, and D. Kim, J. Appl. Phys., 69 (1991) 8329.

88. E. Kondoh, T. Ohta, T. Mitumo, and K. Ohtsuka, J. Appl. Phys., 73 (1993) 3041.

89. M. E. Coltrin, R. J. Kee, and F. M. Rupley, Int. J. Chem. Kin., 23 (1991) 1111.

90. W. A. Yarbrough, J. Am. Soc., 75 (1992) 3179.

91. C. M. Marks, H. R. Burris, J. Grun, and K. A. Snail, J. Appl. Phys., 73 (1993) 755.

92. A. R. Badzian, Mater. Res. Bull., 23 (1988) 385.

93. M. Sommer and F. W. Smith, High Temp. Sci., 27 (1990) 173.

94. A. R. Patel and K. A. Cherian, Indian J. Pure Appl. Phys., 19 (1981) 803.

95. D. V. Fedoseev, V. P. Varnin, and B.V. Deryagin, Russian Chem. Rev., 53 (1984) 435.

96. M. Sommer, K. Mui, and F. W. Smith, Sol. St. Comm., 69 (1989) 775.

97. R. Wang, M. Sommer, and F. W. Smith, J. Crys. Growth, 119 (1992) 271.

98. W. Piekarczyk, R. Roy, and R. Messier, J. Crys. Growth, 98 (1989), 765.

99. N. A. Prijaya, J. C. Angus, and P. K. Bachmann, Diamond Rel. Mater., 3 (1993) 129.

SECTION 2

CARBON GROWTH DOMAIN AND THE C-H-O PHASE DIAGRAM

CHAPTER VII

INTRODUCTION

Diamonds have long since fascinated mankind. They possess a unique combination of properties which makes them an extremely valuable commodity, sought after for their commercial value as well as in industry for optical, mechanical, thermal and electrical applications. Considerable research has been carried out, some dating as far back as World War II, in an effort to develop a simple, inexpensive method for the synthesis of diamond.

Broadly classified, there exist two major techniques of synthesizing diamond. The first involves the synthesis of diamond under conditions of very high pressure and temperature in its region of *thermodynamic stability*. The second method involves the synthesis of diamond under conditions of low pressure and high temperature in the region where diamond is *thermodynamically metastable*. This distinction on the basis of thermodynamic considerations prompted considerable interest in the structure of diamond and its relative stability with respect to the other allotropes of carbon. Both techniques have long since been developed with the high pressure method proving to be more viable. However, the substantial expenses associated with this approach, in comparison to the convenience and low costs of most low presssure methods, has lead researchers to study the low pressure methods of diamond synthesis more closely.

An understanding of the influence of the thermodynamics of carbon-hydrogen-

oxygen systems on the growth of diamond may initially seem an unlikely approach, especially in light of the fact that diamond is thermodynamically metastable under low pressure chemical vapor methods of synthesis. However, since diamond itself is an allotrope of carbon, any attempt to synthesize diamond at low pressures is restricted to those temperature and pressure ranges necessary for carbon growth. In other words, the presence of carbon is a necessary requirement, and its absence precludes the deposition of diamond altogether. Further, low pressure diamond synthesis techniques occur at high temperatures resulting in multicomponent, multiphase equilibrium mixtures. The number of variables involved is too large to adopt an experimental trial-and-error strategy. Thus, a thermodynamic analysis based on the chemical equilibria of the system would help identify the stable gas-phase species and solid phases present and other important system variables such as total pressure, temperature, and reactant ratio.

This study attempts to predict the carbon growth region and to ascertain the conditions under which carbon growth would be maximum. Such an approach assists in a preliminary estimate of the diamond growth domain. A Gibbs free energy minimization technique, incorporating the Villars Cruise Smith (VCS) stoichiometric algorithm, was used to obtain the desired carbon domain.

CHAPTER VIII

THERMODYNAMIC MODELS

Background

Problems in high temperature and high pressure were encountered with increasing regularity during the middle of this century, especially in the fields of rocketry and explosive technology. This created a greater interest in the problem of chemical equilibrium, and consequently, a considerable amount of technical literature dealing with the subject was accumulated. The first major advances in the analysis of chemical equilibrium were made during the post World War II era, largely due to the efforts of Brinkley [14]. Several approaches have been developed since then, with the range of applications having grown rapidly [15, 16, 17].

The primary focus of chemical equilibrium analyses is to determine the equilibrium composition of each species at the specified thermodynamic conditions. A commonly employed technique for studying the chemical equilibrium of reactions involves using a Gibbs free energy minimization approach. The second law of thermodynamics provides potential functions governing the direction of natural or spontaneous processes [25]. One such important potential function is the Gibbs (free energy) function, based on which a necessary criteron for chemical equilibrium may be established. The second law of thermodynamics states that the Gibbs function of a closed system at chemical equilibrium is a minimum at given conditions of temperature and

pressure. This may be expressed as follows:

$$(dG)_{T,p} = \Sigma \, \mu_i \, dn_i$$
$$\leq 0,$$

where G is the Gibbs free energy, T is the absolute temperature, p is the pressure, μ_i is the chemical potential of the ith component, and n_i is the number of moles of the ith component. Such an approach has the added advantage of being independant of stoichiometry, and does not require a prior knowledge of the chemistry of the system, nor an accurate initial guess to begin iteration.

There exist two definite approaches to the minimization problem [18]. The first approach involves the stoichiometric formulation of an unconstrained minimization problem. The second approach involves the non-stoichiometric formulation of a constrained problem. Mathematically, this approach involves the determination of a minima (or maxima) of some function, or reduces to a numerical solution of a set of non-linear simultaneous equations. The latter approach has been adopted in this study.

Some of the earliest works on chemical equilibrium analysis include that of Brinkley [25] and White et al. [25], who pioneered the initial formulations of the Gibbs free energy minization problem. Other important works include that of Eriksson and Rosen [19], who derived the general equations for the determination of the equilibrium compositions of systems containing gas phases, condensed phases and liquid and solid mixtures using a Gibbs free energy minimization technique.

In recent years, researchers have presented thermodynamic models in an effort to rationalize the low pressure deposition of diamond [28]. Some utilized thermodynamic

principles solely to model the gas-phase reactions [20, 29, 30], whereas others performed thermodynamic analyses of the growth environments with the purpose of evaluating the conditions favorable for diamond growth [23, 31-34].

Yarbrough and Stewart [20], at the Pennsylvania State University, used the work of Eriksson and Rosen [19] to determine the stable species present during the combustion synthesis of diamond. Kim et al. [29] studied the gas-phase compositions in CH_4-H_2 gas mixtures using a similar Gibbs free energy minimization method. Wang et al. [30] applied a thermodynamic quasi-equilibrium model to identify the important stable species in the C-H-O system and to determine the temperature-dependant etching and deposition rates of solid carbon (diamond and graphite).

Thermodynamic studies conducted to model the growth of the low pressure chemical vapor deposition of diamond include that of Sommer and Smith [21, 33]. They modeled the chemical vapor deposition of carbon films using the quasi-equilibrium model of Batty and Stickney, and illustrated their results in the form of a phase diagram for the carbon-hydrogen system. Wang et al. [22] developed a similar quasi-equilibrium model to perform a thermodynamic analysis of the diamond chemical vapor deposition region. Recently, Prijaya et al. [23] performed constrained chemical equilibrium calculations to examine the nature of the diamond growth domain. Three types of constrained gas phase chemical equilibrium calculations were performed in which they alternatively fixed the chemical potentials of carbon in the gas phase, solid carbon (graphite) phase, and the hydrocarbon species at various values. The resultant C-H-O phase diagram obtained showed that diamond may be grown only within a narrowly defined region.

Hwang et al. [24] performed a thermodynamic analysis of C-H and C-H-O

systems in order to evaluate the effect of the independent variables on the carbon activity in the gas phase. Their study adopted a Gibbs free energy minimization approach to obtain the gas-phase equilibrium which was used to determine the chemical potential of carbon in the gas phase and the subsequent expression for supersaturation. They obtained a 'high supersaturation region' and a 'low supersaturation region' corresponding to the non-diamond growth region and the no-growth region, respectively.

The Villars Cruise Smith (VCS) Stoichiometric Algorithm

Stoichiometric algorithms provide a convenient method for calculating the equilibrium compositions of larger systems. Such algorithms express the mole numbers of the reacting species n_i in terms of a new set of reaction extent variables, ξ. Thus, the changes in the number of moles $\delta n^{(m)}$ from any estimate $n^{(m)}$ is related to the reaction extent, ξ, by the following relationship:

$$\delta n_i^{(m)} = \sum_{i=1}^{N} V_{ij}\, \xi_j^{(m)}, \qquad i = 1, 2, 3, ..., N$$

where V_{ij} is the linearly independent non-linear solution. Consequently, the chemical equilibrium problem may be expressed as:

$$\text{minimize } G = \sum_{i=1}^{N} n_i(\xi)\, \mu_i(\xi)$$

such that,

$$n_i = n_i^* + \sum_{j=1}^{R} V_{ij}\, \xi_j \geq 0$$

where G is the Gibbs free energy, μ_i is the chemical potential of species i, N is the number of species, n_i^* is any particular solution of the elemental-abundance equations, and R is the maximum number of linearly independent chemical equations. In this formulation, the Gibbs function, considered as a function of the N-M (where M is the number of elements) reaction extent variable, is minimized. The element-abundance constraints are incorporated into the stoichiometry and only the non-negativity constraints remain. The reader is referred to Smith and Missen [25] for a more detailed derivation of the pertinent expressions.

The solution entails the introduction of an appropriate expression for the chemical potential of the various species. Assuming a pure ideal gas, μ_i may be given as:

$$\mu(T,P) = \mu^*(T) + RT \ln p$$

where μ^* is the standard chemical potential, T is the absolute temperature, R is the universal gas constant, and p is the pressure.

The VCS stoichiometric algorithm [25] was used in this work to study the chemical equilibrium of C-H-O systems in low pressure diamond-deposition environments. The algorithm is able to handle multiphase systems consisting of any number of single component phases or two multicomponent phases. It consists of the following equation:

$$\delta\xi = (dG/d\xi)_n \, (d^2G/d\xi^2)_n^{-1},$$

and involves iteratively adjusting each stoichiometric equation by the amount:

$$d\xi^{(m)} = \left(\frac{1}{n_j^{(m)} + M} + \sum \frac{V_{kj}^2}{n_k^{(m)}} - \frac{R_j^2}{n_t} \right)$$

where n_t is the total number of moles. On each iteration, the species mole number are examined to ensure that the component species are those with the largest mole numbers. If not, a new stoichiometric matrix is calculated. A flow chart of the VCS algorithm is illustrated in Fig. 22.

The computer code generated for the VCS algorithm was carefully tested in a previous study conducted by Pashupathi [36]. Various equilibrium studies reported in literature were reproduced for algorithm and code validation purposes. Predicted equilibrium mole fractions for each of the cases studied concurred well with those in the literature [36].
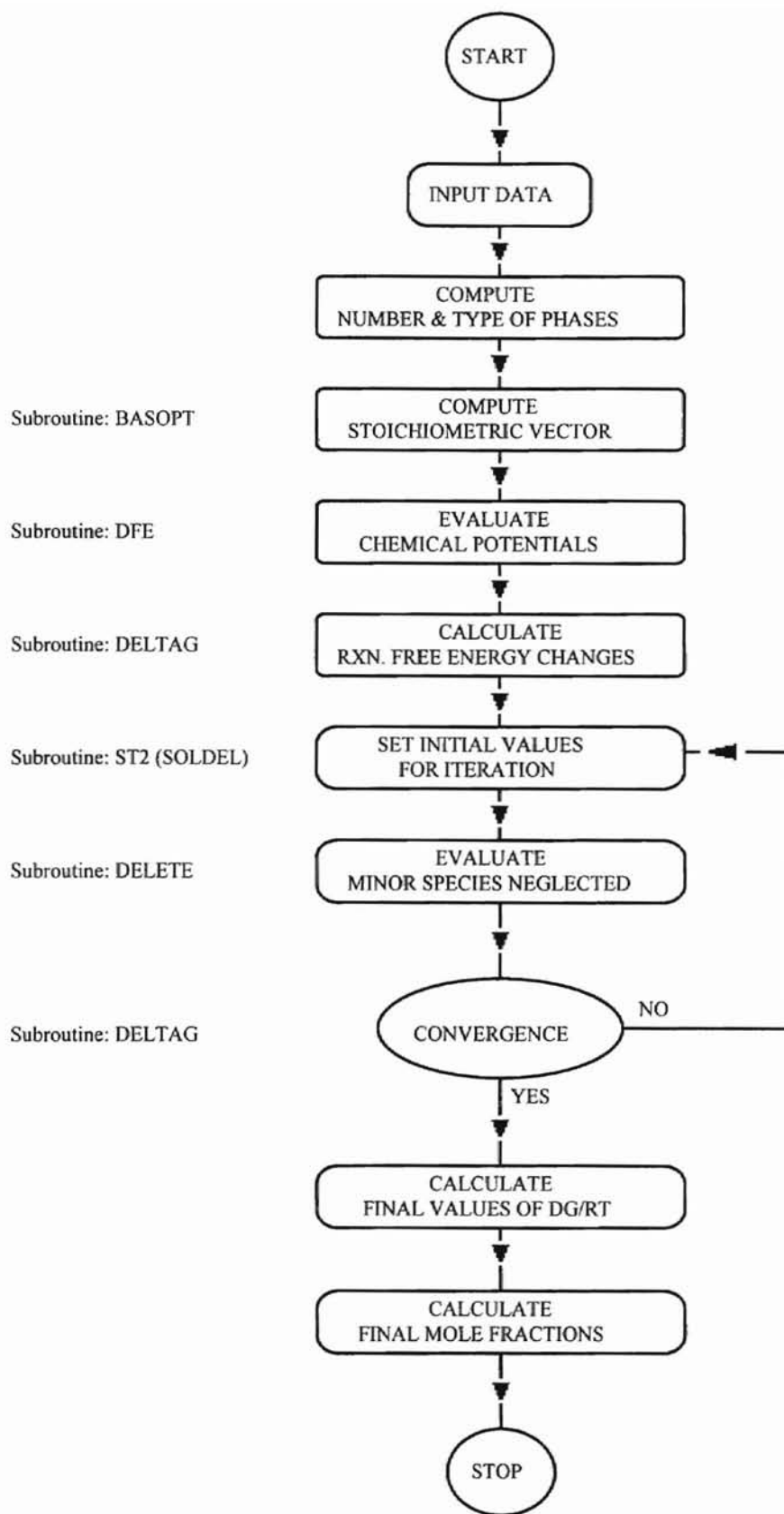
Figure 22. Flow chart of the Villars Cruise Smith algorithm.

CHAPTER IX

STUDIES IN EQUILIBRIUM ANALYSIS

This chapter presents the results of the Gibbs free energy minimization approach utilized in this study to help identify the predominant species present in $C_2H_2 + O_2$, $C_2H_4 + O_2$, and $CH_4 + O_2$ systems during the low pressure combustion synthesis of diamond. The effect of temperature, pressure, and inlet gas flow rates on the expected deposition of carbon was studied, based on which we were able to estimate the boundaries of the diamond growth domain.

Physical and Chemical Conditions

Eighteen possible chemical species, including non-diamond carbon, were assumed to be present at equilibrium. Data for the standard Gibbs free energy of formation for the 17 gas-phase species was obtained from the work of Chase et al. [26]. The method adopted in this study was flexible with regards to the possible species, since redundant species were seen to have negligible concentrations.

Equilibrium calculations were performed for three different inlet gas mixtures of $C_2H_2 + O_2$, $C_2H_4 + O_2$, and $CH_4 + O_2$. Results were obtained for substrate temperatures ranging from 400 to 1400 K for the pressures of 0.50, 0.66 and 1.0 atm. Table 9 summarizes the conditions at which this study was conducted.

Table 9. Physical and chemical conditions used for the simulation.

System	Pressure, atm	Temperature, K	Oxygen/Hydrocarbon Ratios
$C_2H_2 + O_2$ $C_2H_4 + O_2$ $CH_4 + O_2$	0.5, 0.66, 1.0	400, 500,..., 1400	0.50, 0.60, 0.72, 0.86, 1.00, 1.10, 1.20, 1.30, 1.40, 1.70, 2.00, 2.50, 5.00

Results and Discussion

The expected moles of carbon have been plotted as a function of temperature for different molar ratios of inlet gases ($C_2H_2 + O_2$, $C_2H_4 + O_2$, and $CH_4 + O_2$), at pressures of 0.50, 0.66 and 1.0 atm for each of the different systems. The results are illustrated in Figs. 23 to 31.

The results obtained clearly indicate a decrease in the amount of carbon yield with increase in temperature. The amount of carbon predicted for the three independant systems is in the order, $C_2H_4 + O_2 > C_2H_2 + O_2 > CH_4 + O_2$. Further, the amount of carbon deposited using a feed mixture of $C_2H_2 + O_2$, shown in Figs. 23 to 25, was about eight times as much as that obtained using a feed mixture of $CH_4 + O_2$, shown in Figs. 29 to 31. Similar results were obtained by Meeks et al. [35], who studied the possibility of methane-oxygen flames as an alternative to acetylene-oxygen flames for diamond synthesis. They have also observed that diamond growth rates in methane-oxygen flames appeared to be considerably lower than in acetylene-oxygen flames.

The present calculations show that carbon growth can be expected at temperatures as low as 400 K. These results have been verified experimentally by Ihara et al. [27], who were able to synthesize diamond at 408 K. They indicate on the basis of their study

that diamond growth may be possible at even lower temperatures in the lower concentration range of CH_4.

Inspite of the fact that maximum carbon growth was obtained at 400 K for all three systems ($C_2H_2 + O_2$, $C_2H_4 + O_2$, and $CH_4 + O_2$) studied, a further decrease in temperature below 400 K results in a very sharp decrease in the amount of carbon deposited (not illustrated in Figs. 23 to 31). Calculations below 400 K for the three systems over the entire range of pressures studied, and for all hydrocaron/oxygen ratios, yield no carbon growth. This sudden reduction in the amount of carbon predicted occurs over a narrow temperature range of less than 5 K. Since we were able to reproduce these results utilizing ASPEN PLUS, we believe that this may not be a computational error. In fact, the observed behavior is more likely to be the result of limitations attributable to either the thermodynamic properties used, or a result of actual variation in the deposition process itself. Experimental studies would be required to clarify this this issue.

The effect of pressure on the growth of carbon was studied by performing calculations for all three systems ($C_2H_2 + O_2$, $C_2H_4 + O_2$, and $CH_4 + O_2$) at 0.50, 0.66 and 1.0 atm. The results, illustrated in Figs. 23 to 31, indicate no substantial difference in the amount of carbon deposited over the range of pressures studied.

Carbon growth was seen to be extremely sensitive to changes in concentrations of the inlet gases and the substrate temperature. A summary of the limiting conditions for carbon growth are presented in Table 10. There is clearly *no* growth of carbon obtained for the conditions given below.

An important objective of this study was to estimate the approximate C-H-O domain for carbon growth. Based on our Gibbs free energy analysis of the $C_2H_2 + O_2$,

$C_2H_4 + O_2$, and $CH_4 + O_2$ systems, ternary C-H-O carbon deposition phase diagrams were developed for the temperatures of 800, 923, 1000, 1100 and 1200 K, as illustrated in Figs. 32 to 36.

Table 10. Limiting conditions for no carbon deposition.

System	Ratio of oxygen to hydrocarbon	Temperature, K
$C_2H_2 + O_2$	> 1.2	>1000
$C_2H_4 + O_2$	> 1.2	>1000
$CH_4 + O_2$	> 0.6	> 600

The ternary C-H-O phase diagrams developed display a well defined domain for the growth of carbon. Moreover, these phase diagrams clearly indicate a reduction in the area of the carbon growth domain with increase in temperature from 800 K to 1200 K. If one were to stack these triangular figures over each other in sequence, with each plane of the stack representing a temperature, the domain size is seen to gradually narrow.

Recently, Bachmann et al. [9] conducted a comprehensive study of all experimental work conducted in the past 30 years on the low pressure synthesis of diamond. On the basis of their study they were able to develop a C-H-O phase diagram showing the diamond growth domain. The diamond-growth limit obtained by that study, below which neither diamond nor carbon may be expected, is represented in Fig. 33. As is evident, the carbon-growth limit obtained in this study agrees well with their work. Further, they report a similar reduction in the size of the diamond growth domain with increase in temperature.
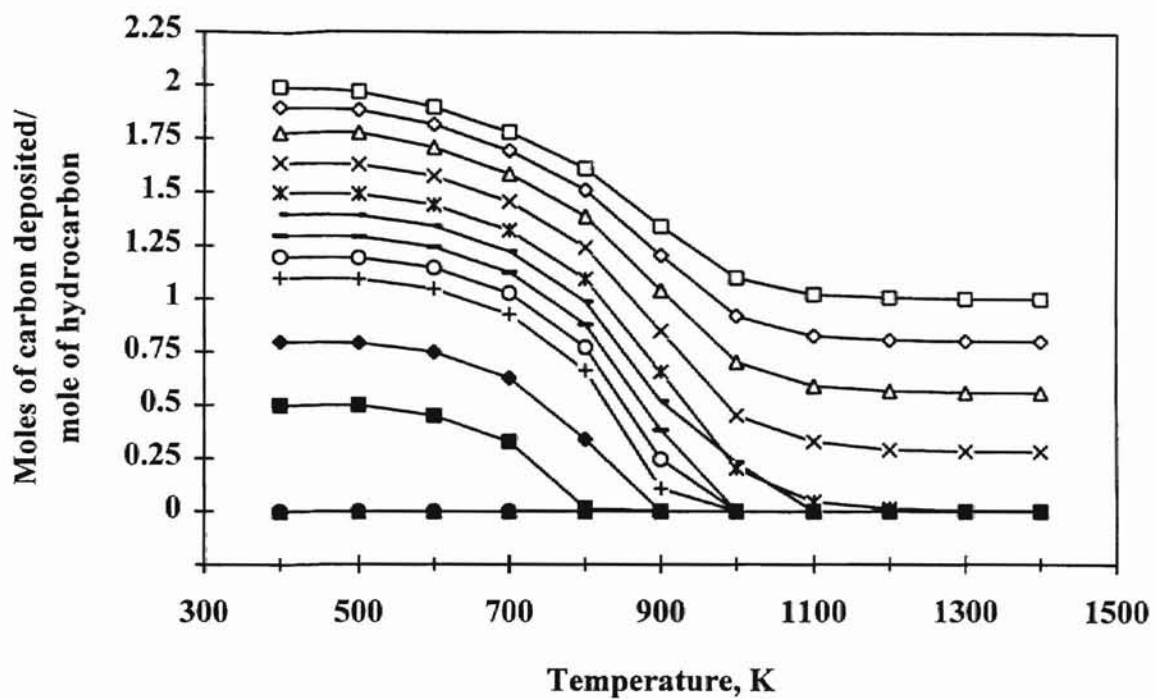
Figure 23. Carbon deposition produced by C_2H_2 and O_2 flame CVD at 0.5 atm. O_2/C_2H_2 Ratio:□, 0.5; ◇, 0.6; △, 0.72; X, 0.86; *, 1.0;− , 1.1; ▭, 1.2; o, 1.3; +, 1.4; ◆, 1.7; ■, 2.0; ▲, 2.5; •, 5.0.
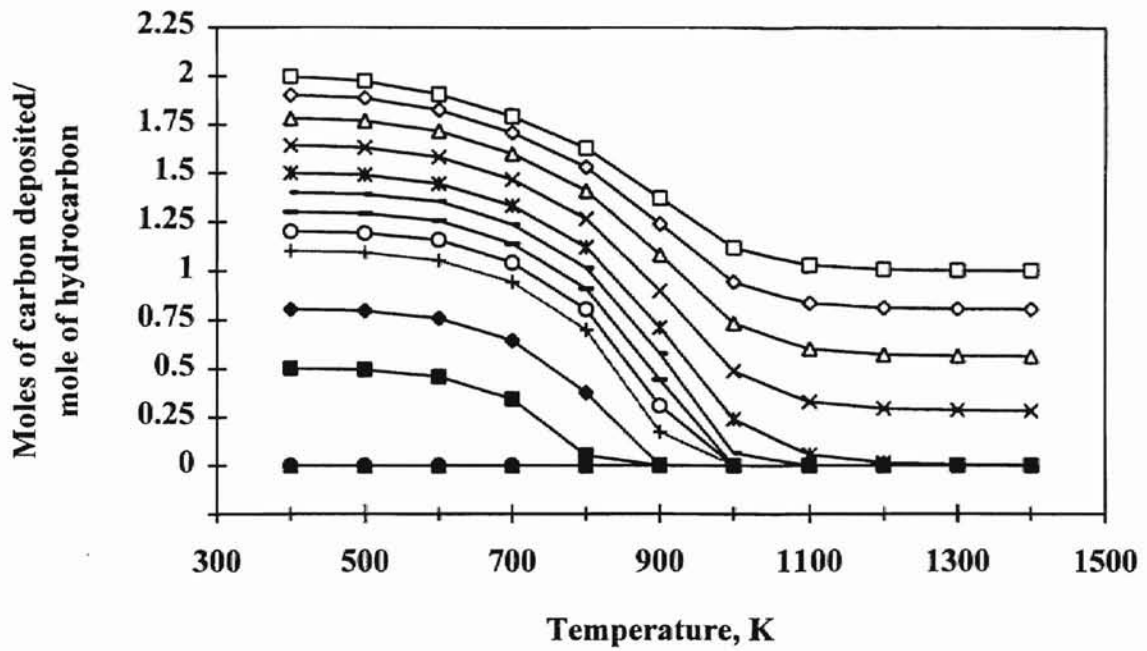
Figure 24. Carbon deposition produced by C_2H_2 and O_2 flame CVD at 0.66 atm. O_2/C_2H_2 Ratio: □, 0.5; ✧, 0.6; △, 0.72; X, 0.86; *, 1.0; −, 1.1; ▭, 1.2; o, 1.3; +, 1.4; ◆, 1.7; ■, 2.0; ▲, 2.5; •, 5.0.
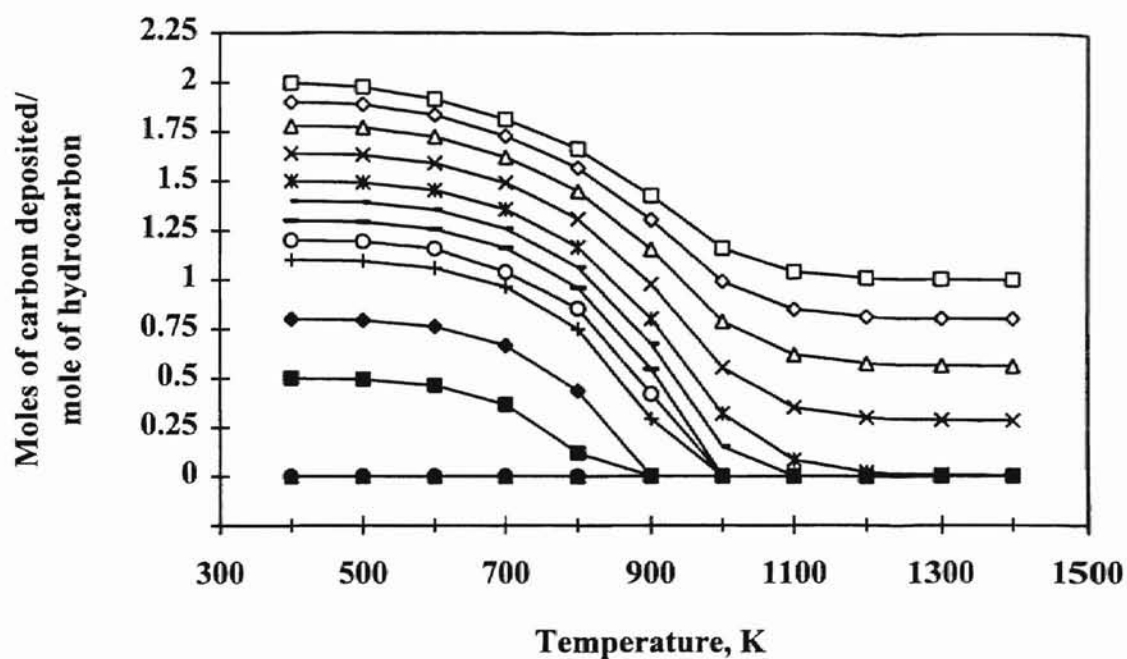
Figure 25. Carbon deposition produced by C_2H_2 and O_2 flame CVD at 1.0 atm. O_2/C_2H_2 Ratio:□, 0.5; ✧, 0.6; △, 0.72; X, 0.86; *, 1.0; −, 1.1; ▱, 1.2; o, 1.3; +, 1.4; ◆, 1.7; ■, 2.0; ▲, 2.5; •, 5.0.
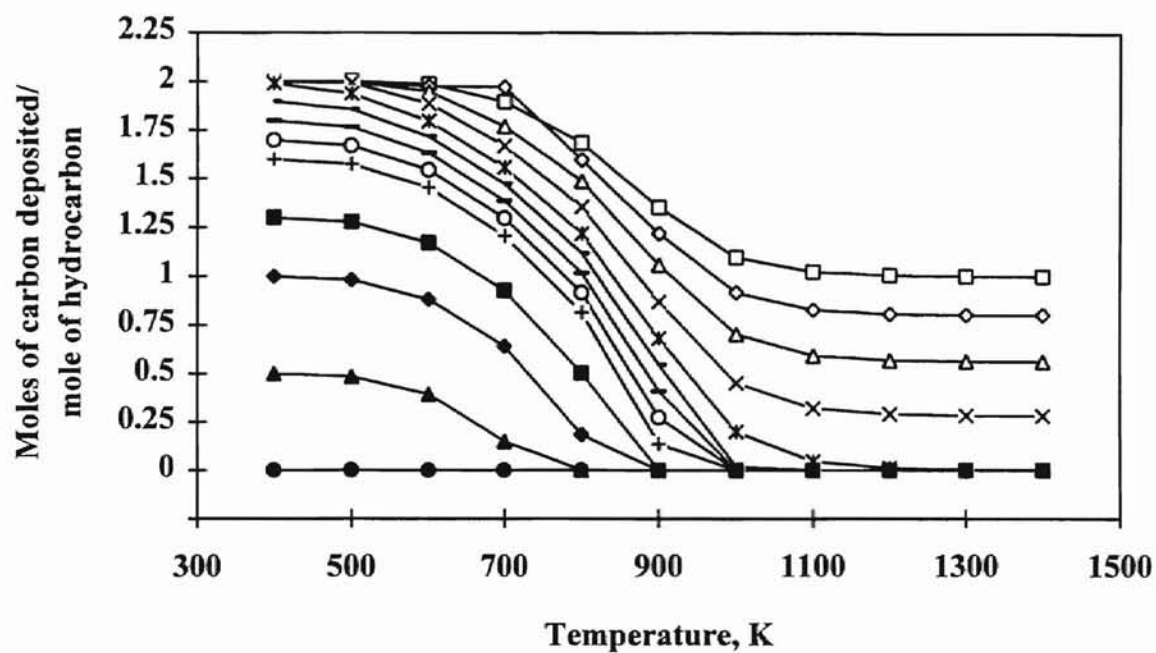
Figure 26. Carbon deposition produced by C_2H_4 and O_2 flame CVD at 0.5 atm. O_2/C_2H_2 Ratio:☐, 0.5; ✧, 0.6; Δ, 0.72; X, 0.86; *, 1.0; −, 1.1; ⌐, 1.2; o, 1.3; +, 1.4; ◆, 1.7; ■, 2.0; ▲, 2.5; •, 5.0.
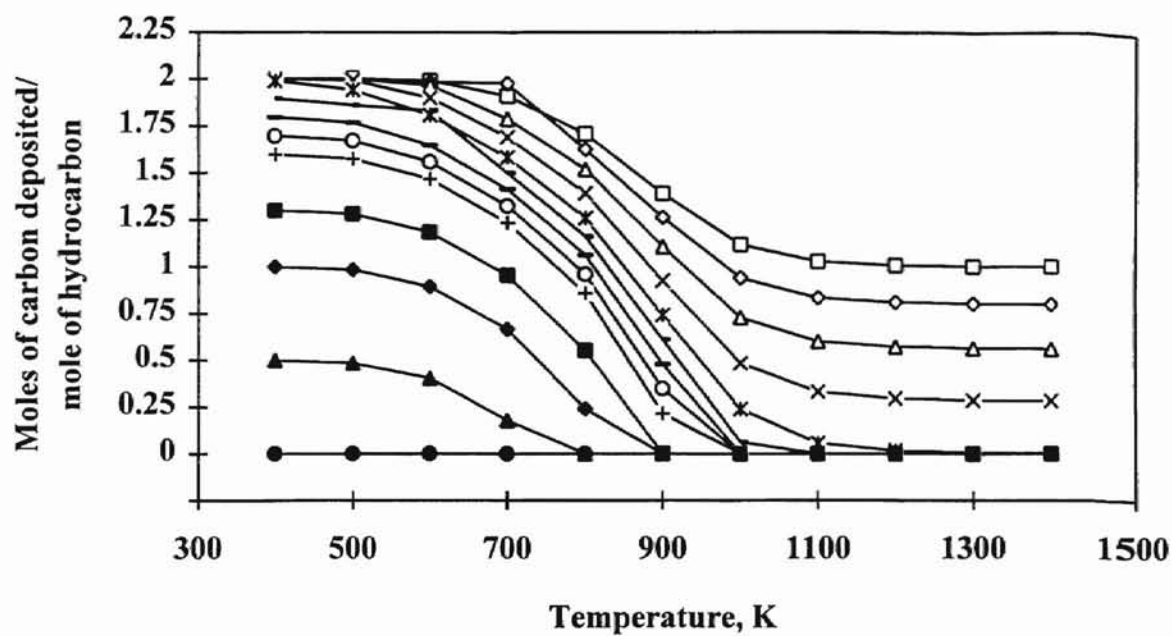
Figure 27. Carbon deposition produced by C_2H_4 and O_2 flame CVD at 0.66 atm. O_2/C_2H_2 Ratio: □, 0.5; ◇, 0.6; △, 0.72; X, 0.86; *, 1.0; –, 1.1; ▭, 1.2; o, 1.3; +, 1.4; ◆, 1.7; ■, 2.0; ▲, 2.5; •, 5.0.
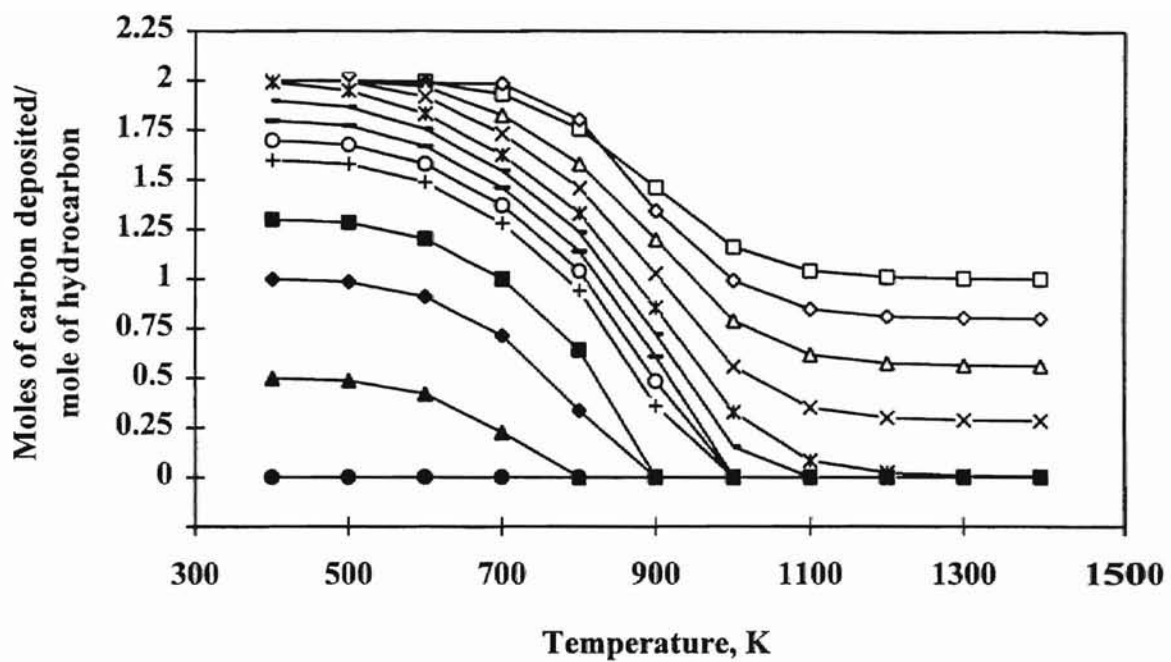
Figure 28. Carbon deposition produced by C_2H_4 and O_2 flame CVD at 1.0 atm. O_2/C_2H_2 Ratio: □, 0.5; ✧, 0.6; △, 0.72; X, 0.86; *, 1.0; −, 1.1; ▭, 1.2; o, 1.3; +, 1.4; ◆, 1.7; ■, 2.0; ▲, 2.5; •, 5.0.
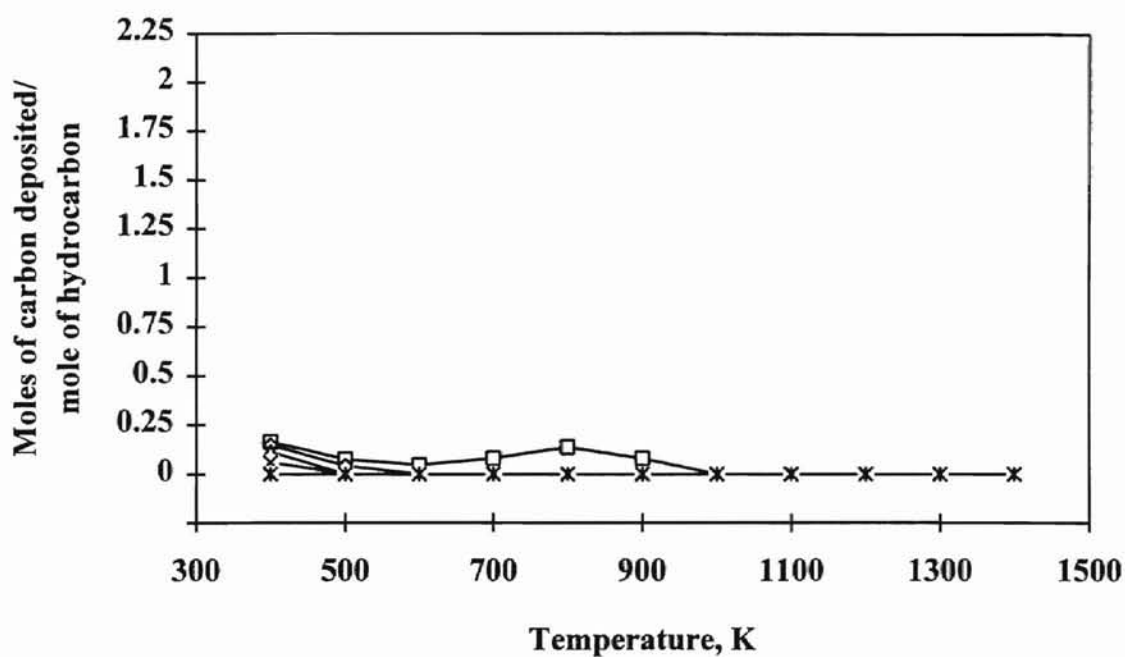
Figure 29. Carbon deposition produced by CH_4 and O_2 flame CVD at 0.5 atm. O_2/CH_4 Ratio: □, 0.5; ◇, 0.6; △, 0.72; X, 0.86; *, 1.0.
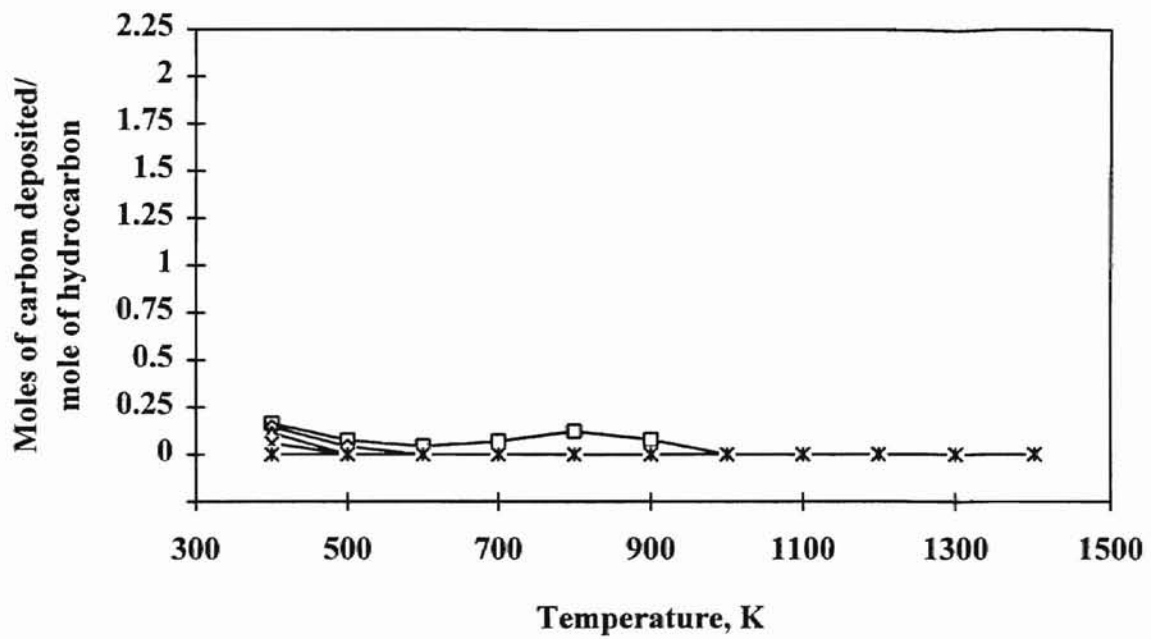
Figure 30. Carbon deposition produced by CH_4 and O_2 flame CVD at 0.66 atm. O_2/CH_4 Ratio: □, 0.5; ◇, 0.6; △, 0.72; X, 0.86; *, 1.0.
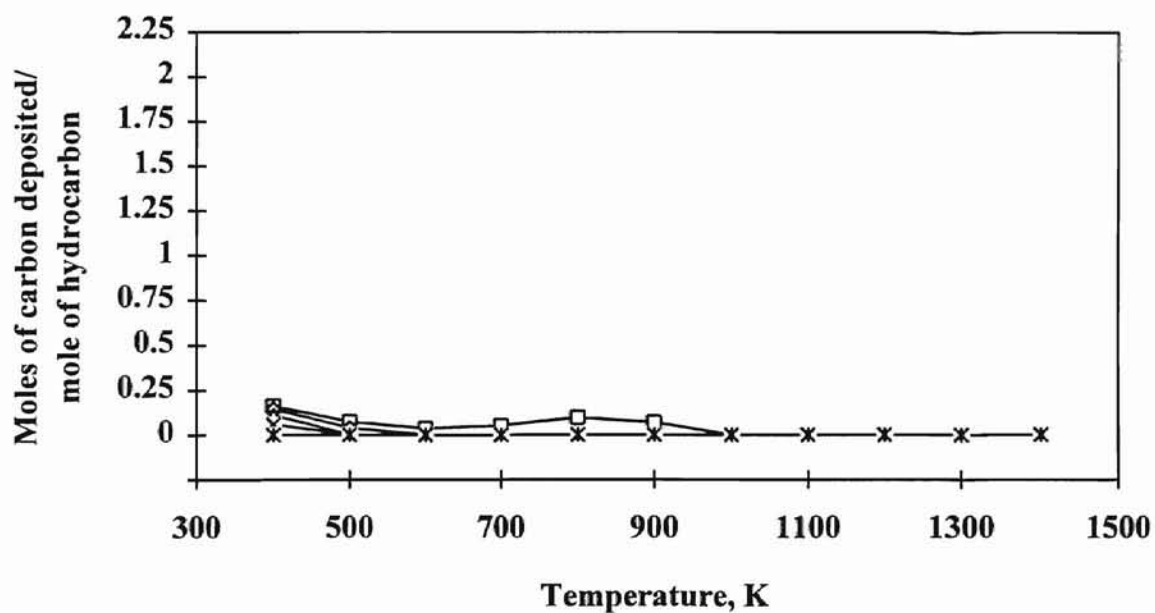
Figure 31. Carbon deposition produced by CH_4 and O_2 flame CVD at 1.0 atm. O_2/CH_4 Ratio: □, 0.5; ◇, 0.6; Δ, 0.72; X, 0.86; *, 1.0.
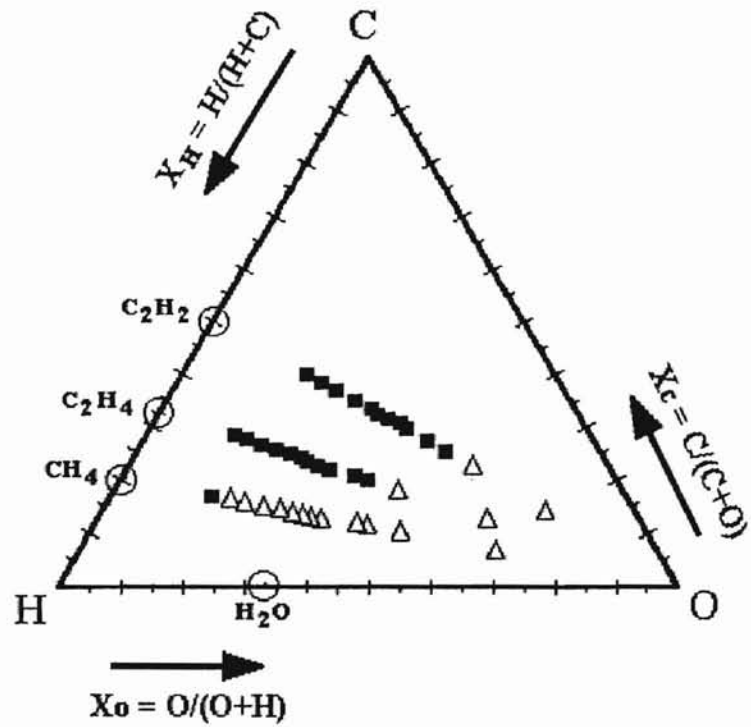
Figure. 32. C-H-O carbon deposition phase diagram obtained by using the Gibbs free energy analysis at 800K: ■, carbon growth is predicted; Δ, no growth is predicted.
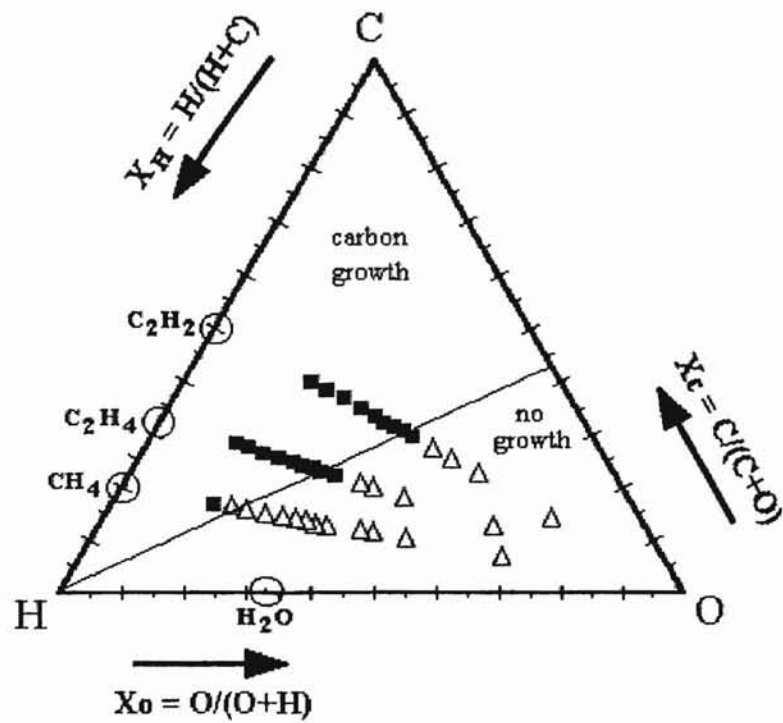
Figure 33. C-H-O carbon deposition phase diagram obtained by using the Gibbs free energy analysis at 923K: ■, carbon growth is predicted; Δ, no growth is predicted. The line indicates the diamond (carbon) growth limit as obtained by Bachmann et al [9].
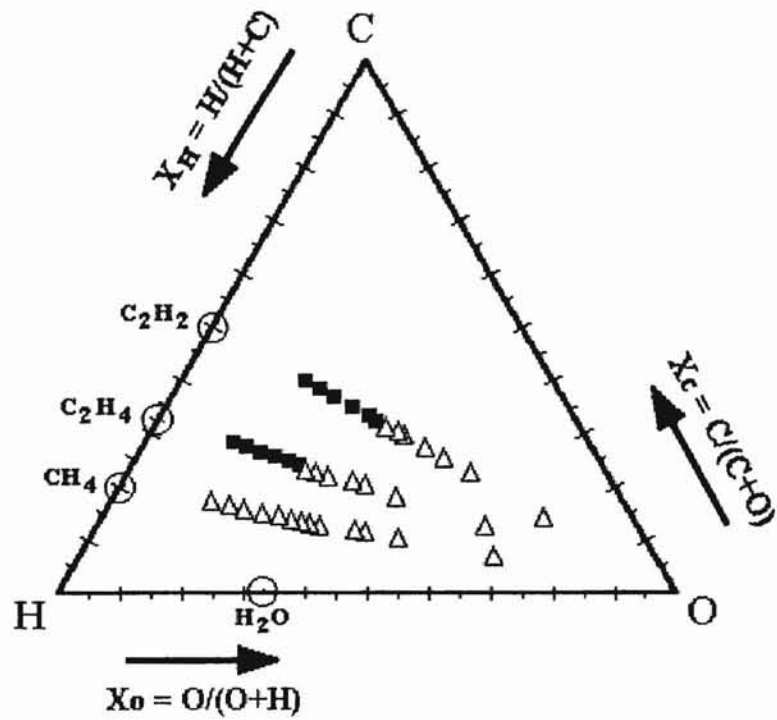
Figure 34. C-H-O carbon deposition phase diagram obtained by using the Gibbs free energy analysis at 1000K: ■, carbon growth is predicted; △, no growth is predicted.
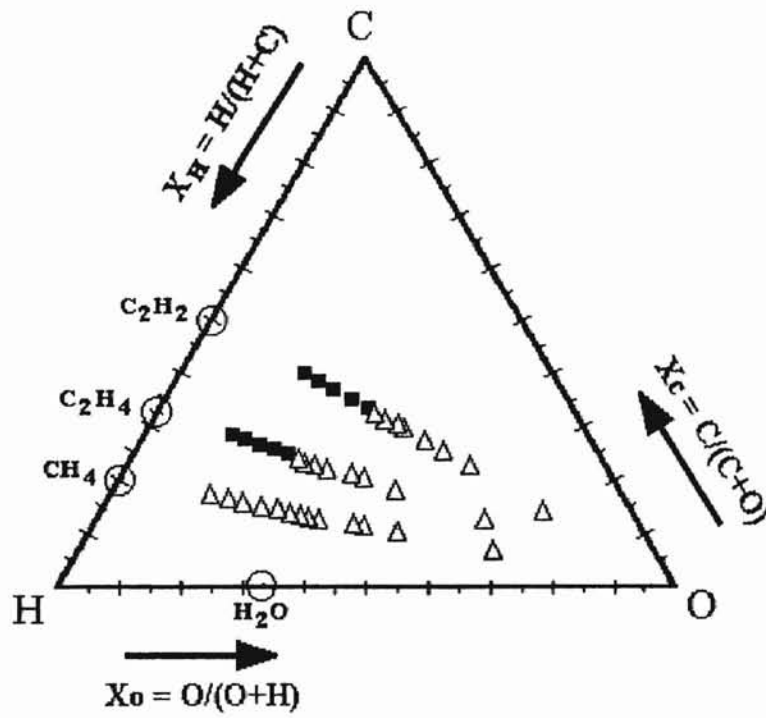
Figure 35. C-H-O carbon deposition phase diagram obtained by using the Gibbs free energy analysis at 1100K: ■, carbon growth is predicted; △, no growth is predicted.
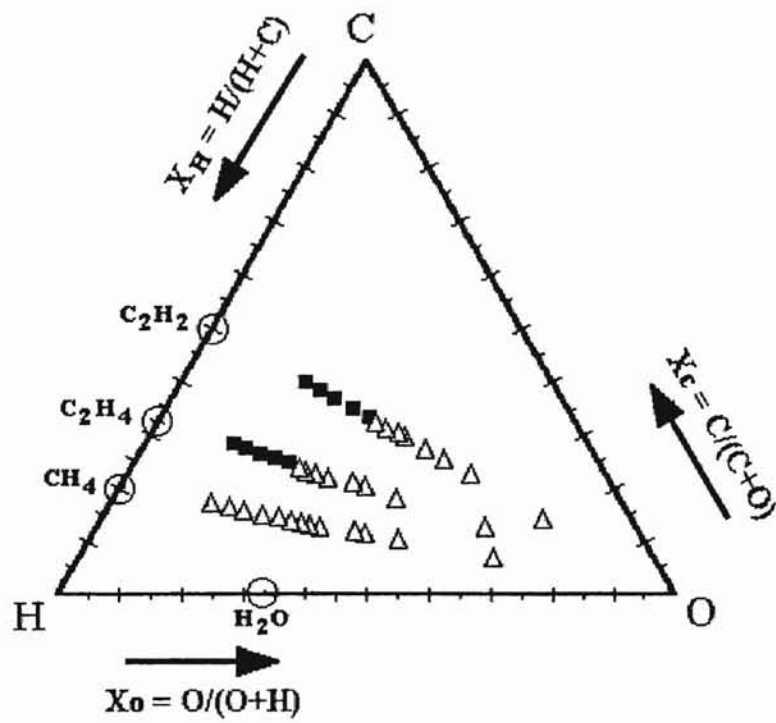
Figure. 36. C-H-O carbon deposition phase diagram obtained by using the Gibbs free energy analysis at 1200K: ■, carbon growth is predicted; Δ, no growth is predicted.

CHAPTER X

CONCLUSIONS

We were able to perform Gibbs free energy minimization calculations to model the growth of carbon in $C_2H_2 + O_2$, $C_2H_4 + O_2$, and $CH_4 + O_2$ systems. The Villars Cruise Smith stoichiometric algorithm was utilized to determine the carbon-growth domain, and to evaluate certain basic relational trends between environmental conditions and amounts of carbon deposited. The final results were represented in the form of ternary C-H-O phase diagrams.

The limits obtained for the carbon-growth domain in this study concur with similar studies conducted by Bachmann et al. [9]. A reduction in the effective area of the carbon-growth domain is predicted for an increase in temperature. Calculations performed indicate a decrease in the amounts of carbon deposited for increases in temperatures. Carbon deposition was seen to be maximum for the $C_2H_2 + O_2$ system, and unexpectedly low for the $CH_4 + O_2$ system. Contrary to popular belief, substantial deposition of carbon is predicted at temperatures as low as 400 K.

Our results appear to indicate that the total pressure of the system, between the range of 0.5 to 1.0 atm, does not play an appreciable role in the quantity of carbon deposited at atmospheric and sub-atmospheric conditions.

Although this study provides a preliminary estimate of the diamond-growth domain and the conditions favorable for the deposition of diamond, it is unable to represent the complexities of the low pressure chemical vapor synthesis of diamond with any degree of accuracy. Chemical equilibrium studies are more useful for analyzing the gas-phase reactions, and need to be augmented with detailed kinetic and transport studies if one wishes to simulate the surface processes of nucleation and subsequent deposition of diamond.

BIBLIOGRAPHY

1. W. A.Yarbrough, A. Inspektor and R. Messier, Material Science Forum, 52&53 (1989) 151.

2. P. K. Bachmann and W.van Enckevort, Diamond Relat. Mater., 1 (1992) 1021.

3. D. Huang, M. Frenklach and M. Maroncelli, J. Phys. Chem., 92 (1988) 6379.

4. D. N. Belton and S. J. Harris, J. Chem. Phys., 96 (1992) 2317.

5. M. Tsuda, M. Nakajima and S. Oikawa, J. Am. Chem. Soc., 108 (1986) 5780.

6. M. Tsuda, M. Nakajima and S. Oikawa, Jpn. J. Appl. Phys., 26 (1987) L527.

7. J. Frenklach, J. Chem. Phys., 97 (1992) 5794.

8. M. E. Coltrin and D. S. Dandy, J. Appl. Phys., 74 (1993) 5803.

9. P. K. Bachmann, D. Leers and H. Lydtin, Diamond Relat. Mater., 1 (1991) 1.

10. M. M. Szczesnlak and P. Hobza, J. Phys. Chem., 87 (1983) 2608.

11. K. T. Jacob, G. M. Kale and K. P. Abraham, J. Electrochem. Soc., 139 (1992) 517.

12. J. Dolfing and B. K. Harrison, Environ. Sci. Technol., 26 (1992) 2213.

13. B. Krishnakumari, S. Naseem and N.V.K. Dutt, The Canadian J. of Chem. Eng., 77 (1993) 489.

14. S. R. Brinkley, J. Chem. Phys., 14 (1946) 563.

15. D. S. Villars, J. Phys.Chem., 63(1950) 521.

16. W. B. White, S. M. Johnson and G. B. Dantzig, J. Chem. Phys., 28 (1958) 751.

17. R. C. Oliver, S. E. Stephanou and R. W. Baier, Chem. Eng., 69 (1962) 121.

18. F. V. Zeggerens and S. H. Storey, The Computation of Chemical Equilibria, Cambridge, London, 1970.

19. G. Erikkson and J. B. Rosen, Acta. Chem. Scand., 25 (1971).

20. W. A. Yarbrough and M. A. Stewart, Surf. Coat. Technol., 39/40 (1989) 241.

21. M. Sommer and F. W. Smith, High Temperature Science, 27 (1990) 173.

22. J. T. Wang and J. O. Carlsson, Surf. Coat. Technol., 43/44 (1990) 1.

23. N. A. Prijaya, J. C. Angus and P. K. Bachmann, Diamond Relat. Mater., 3 (1993) 129.

24. N. M. Hwang, J. H. Hahn and G. W. Bang, Diamond Relat. Mater., 3 (1993) 163.

25. W. R. Smith and R. W.Missen, Chemical Reaction Equilibrium Analysis: Theory and Algorithms, A Wiley-Interscience Publication, New York, 1982.

26. M. W. Chase, C. D. Davies, R. A. McDonald and A. N. Syverud, J. Phy. Chem. Ref. Data, 14 (1985).

27. M. Ihara, H. Maeno, K. Miyamoto and H. Komiyama, Diamond Relat. Mater., 1 (1992) 187.

28. J. T. Wang, C. Cao, and P. Zheng, J. Electrochem. Soc., 141 (1994) 278.

29. J. W. Kim, Y. Baik, K. Y. Eun, and D. N. Yoon, Thin Solid Films, 212 (1992) 104.

30. R. Wang, M. Sommer, and F. W. Smith, J. Cryst. Growth, 119 (1992) 271.

31. W. Piekarczyk, R. Roy, and R. Messier, J. Cryst. Growth, 98 (1989) 765.

32. W. Piekarczyk, J. Cryst. Growth, 119 (1992) 345.

33. M. Sommer, K Mui, and F. W. Smith, Sol. St. Comm., 69 (1989) 775.

34. W. Piekarczykand W. A. Yarbrough, J. Cryst. Growth, 108 (1991) 583.

35. E. Meeks, R. J. Kee, D. S. Dandy, and M. E. Coltrin, Combust. Flame, 92 (1993) 144.

36. K. Pashupathi, Use of Gibbs Free Energy Analysis, Parametric Analysis in Chemical Vapor Deposition Studies, (M.S. Thesis) Oklahoma State University, May 1991.

SECTION 3

SIMULATION OF DIAMOND GROWTH IN C_2H_2-O_2 & C_2H_2-O_2-H_2 FLAMES

CHAPTER XI

INTRODUCTION

The chemical vapor deposition of diamond is currently the center of much attention. Diamond has been grown in a variety of environments and under operating pressures ranging anywhere from a tenths of a Torr to an atmosphere. Recent reviews on the low pressure chemical vapor deposition of diamond only further illustrate the wide array of synthesis techniques, operating conditions, and feed stocks that may be used [1]. However, a commercially viable low pressure method for the large-scale synthesis of high quality diamond still remains elusive.

Current research includes efforts made to rationalize theoretically the diamond growth process in view of the seemingly 'impossible' thermodynamic situation whereby diamond is deposited, in spite of being the metastable phase [2]. A significant number of models have been presented to explain the phenomenon on a molecular level [3]. Some researchers have analyzed the molecular dynamics and energetics of the sequence of steps presented in such elementary models, and the stability of the various species involved [3]. Still others have performed detailed kinetic calculations of the diamond growth with the intent of determining the rate controlling parameters [4].

The chemical vapor deposition of diamond may be considered as a combination of gas-phase chemical reactions controlled by surface processes. Therefore, it is essential to account for both the chemical environment and the kinetics of diamond growth in order to

model accurately the diamond growth process. Accordingly, in recent years computational requirements have increased substantially as researchers have attempted to provide more comprehensive models for the diamond growth process. While simulation of the entire fluid dynamics with mechanisms containing well over 50 species is computationally challenging, detailed analyses are envisioned for future studies.

The purpose of this particular study is to propose a simple one-dimensional model for the low pressure chemical vapor deposition of diamond in premixed flames and to determine the optimum conditions for diamond growth. A thermodynamic approach has been employed to model the gas-phase reactions followed by a one-dimensional kinetic analysis of the subsequent surface reactions. In so doing, an effort was made to accurately represent the physical and chemical dynamics of the process without significantly increasing computational requirements. The resulting model may be extended to predict diamond growth in hot-filament reactors as well.

CHAPTER XII

MODEL FORMULATION

Background

The first few successful attempts at synthesizing diamond films at commercially viable growth rates utilized combustion as a means for activating the source hydrocarbon gases [5]. More recently, higher growth rates of diamond have been obtained using other methods. However, the combustion methods of synthesis are simple, convenient, and have demonstrated a potential for still higher growth rates of high-quality diamond. As a result they continue to be an area of much study.

The early combustion-synthesis devices commonly used oxygen-acetylene torches [6]. The torches typically ran with equal volume flow rates of acetylene and oxygen. However, these flames were found to be extremely restrictive in terms of the deposition area that could be obtained. Consequently, a variety of modifications such as using multiple torches [7], an inclined torch [8, 9], or a moving torch over the substrate [5] were employed to increase the diamond deposition area. Still others used flat premixed flames as an alternative to torch flames [9].

While considerable progress has been made since those early attempts, only an understanding of the chemistry of the processes involved would help overcome the

present difficulties being faced in commercializing the low pressure diamond synthesis methods.

Problem Description

Over the years, a substantial amount of data has been accumulated on the structure of flames and the gas phase reactions occurring within them. Combustion research has provided detailed analyses of flames, which is of utmost importance for researchers working on the low pressure chemical vapor deposition methods. Recent works include that of Miller and Melius [5], who reported a comprehensive model for the gas-phase chemistry. Kee et al. [5] developed a theoretical formulation for the prediction of flow-fields in premixed flames.

A similar study was conducted by Dong and Lilley [16], who simulated the combustion flow field of an axisymmetric acetylene-oxygen jet flame impinging normally on the surface. In another important study, Coltrin et al. [5] presented an analysis for heterogeneous chemical kinetics, and later coupled the heterogeneous surface reactions with the surrounding flow field [5].

Coltrin and Dandy [1] extended the work of Coltrin et al. [5] to predict diamond growth in a plasma-gun reactor. Goodwin and Gavillet [10] used a similar approach to model the synthesis of diamond in a hot-filament reactor. Kim and Cappelli [11] performed simulations of low pressure diamond synthesis in burner stabilized flames employing the same approach.

A schematic of the flame deposition process is illustrated in Fig. 37. This study proposes the use of a sequence of Gibbs free reactors (employing a Gibbs free energy minimization approach to calculate chemical equilibrium of species present) to model the

flame/gas-phase reactions. The subsequent surface reactions and growth of diamond were kinetically modeled using a plug-flow reactor. An overview of the entire model and the various regions under consideration is illustrated in Fig. 38.
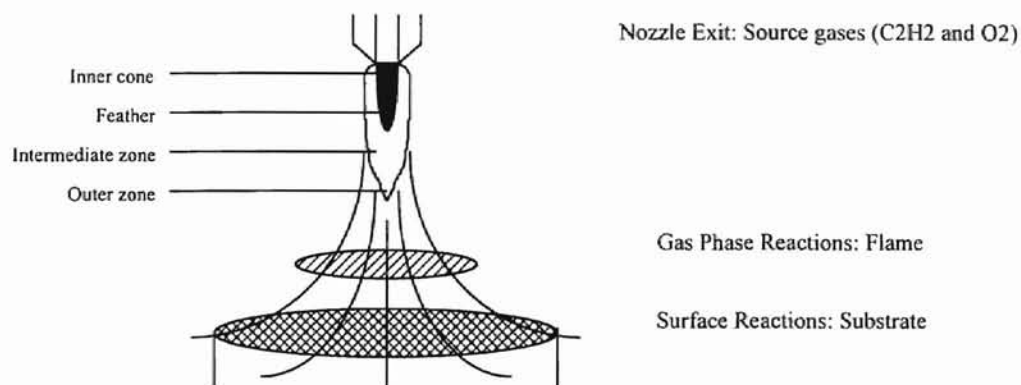
Figure 37. A simplified representation of the flame deposition process.

A simple analysis assuming a constant flame temperature would result in an inaccurate estimation of species concentrations within the flame, and more importantly, in the concentration of species reaching the substrate. Hence, a network of Gibbs reactors was used, as illustrated in Fig. 38, in an effort to replicate the variation of species concentration with flame temperature. As shown in Fig. 37, a typical oxygen-acetylene flame can be differentiated into three basic zones. Each zone is at a different temperature, as a result of which the concentrations of the various gas-phase species differ as one traverses the length and breadth of the flame.

The number of Gibbs reactors used was arrived at after preliminary studies indicated an excess of 12 reactors would be redundant, and would only increase computation; on the other hand, less than 10 Gibbs reactors would not adequately characterize the physical phenomenon. An approximate temperature profile of the flame,
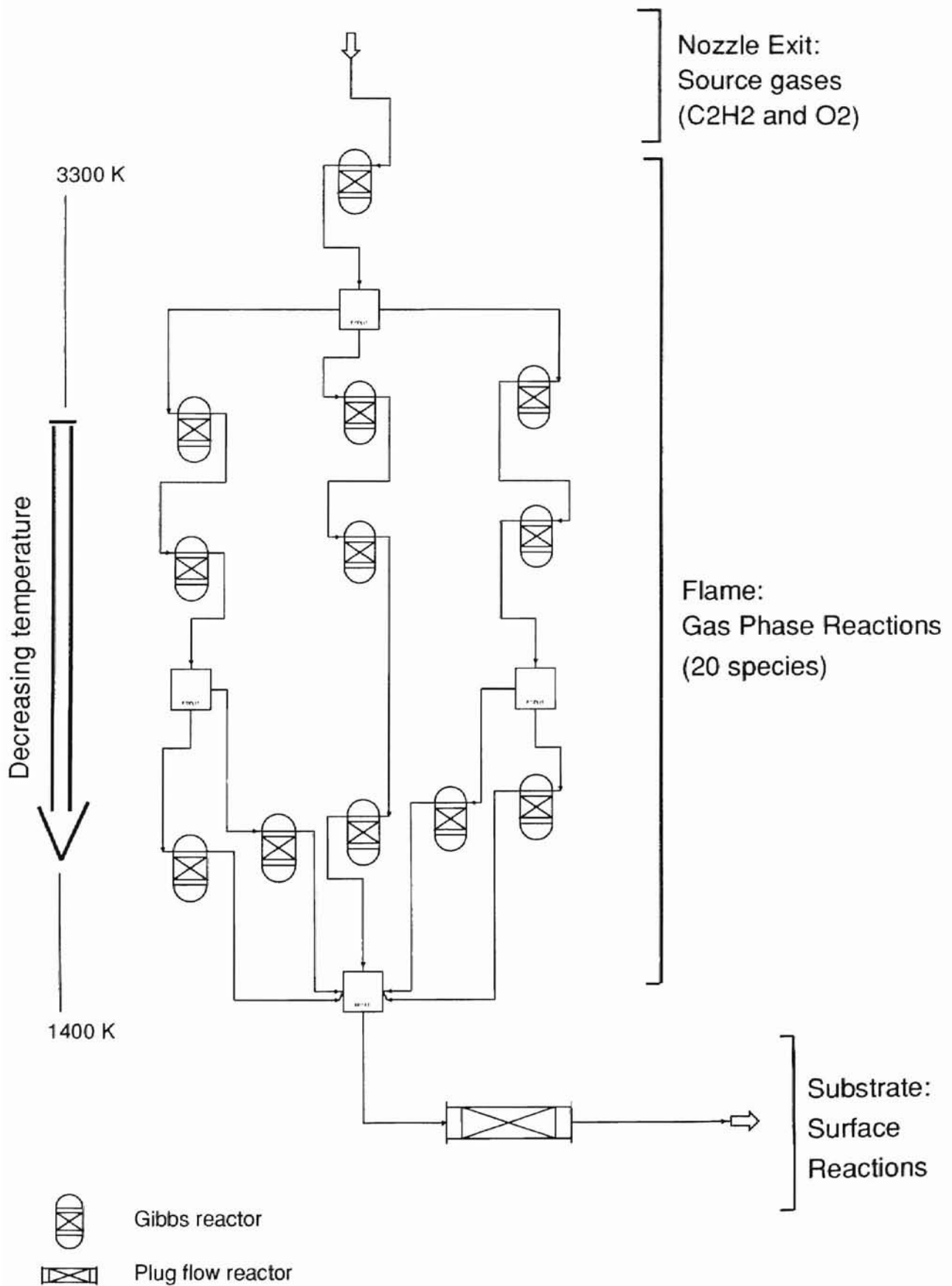
Figure 38. Schematic of the overall model.

extending from 3300 K to 1400 K, was used to set the temperatures of each of the Gibbs reactors.

The simulation involved feeding the source hydrocarbon gases to the first Gibbs reactor in the model maintained at 3300 K, as illustrated in Fig. 38. The chemical equilibrium analysis conducted on the contents of this reactor yields the equilibrium concentrations for the gas-phase species at this temperature. This gas mixture was then fed to the subsequent lower temperature Gibbs reactors in the model, and so on. Finally, the resultant species obtained from the gas-phase constituted the feed to the plug-flow reactor employed to simulate diamond growth on the surface.

Gas-phase Analysis

A sequence of Gibbs reactors was used to model the gas-phase reactions occurring in the flame. The Gibbs free reactors utilize a Gibbs free energy minimization approach to determine the composition of the gas-phase species present. All gas-phase reactions were assumed to be extremely fast with prevalent species existing at equilibrium.

Typically, the flame is configured so as to be axisymmetric in geometry. This simplifies subsequent calculations for characterization of the surface reactions. The use of the sequence of Gibbs free reactors at various positions in the flame aids in developing a profile of the concentration of the various gas-phase species along the length of the flame. Thus, the dominant species typically present in such an environment may easily be identified.

The computational simulation was performed using ASPEN PLUS. A total of 20 gas-phase species were identified, as outlined in Chapter IV of this study, to be present at

equilibrium conditions. Initial calculations were performed with a total of 44 species, including ions and some higher hydrocarbon molecules and radicals (upto C5). Based on these initial studies, the ionic species were neglected because of their minor influence. In addition, the hydrocarbon species were limited to C2 molecules and radicals, since higher species were observed to be present in negligible concentrations. Thermochemical properties for the gas-phase species were obtained from the ASPEN PLUS in-house data banks of DIPPR and COMBUST, and the JANAF combustion data banks [13].

Surface Reaction Mechanism

A one-dimensional kinetic analysis was used to model the growth of diamond on the substrate. Species obtained from the gas-phase were fed to a plug-flow reactor which was set to predict the deposition rate of diamond.

The surface reaction kinetics were adopted from the works of Coltrin and Dandy [1] and Meeks et al. [5]. The original work was written in a form compatible with the SURFACE CHEMKIN package for handling the kinetics of systems of complex reactions at gas/surface interfaces [14]. The model is for diamond growth under steady-state conditions and does not account for the induction times required for nucleation.

The complete surface reaction mechanism is presented in Table 11 [1]. The mechanism consists of 25 surface reactions, further differentiated into categories, such as the initiation step, the methyl addition step, etc. The mechanism allows for both the growth of diamond and non-diamond or graphitic material. Thus, during the growth process there will be constant competition between the two species, with the dominant species grown depending on the conditions of the reactor. The possibility of inter-conversion between graphitic carbon and diamond under high concentrations of hydrogen

Table 11. Surface reaction mechanism [29].
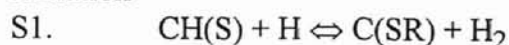
Initiation
S1.　　　　$CH(S) + H \Leftrightarrow C(SR) + H_2$

Radical recombination
S2.　　　　$C(SR) + H \Leftrightarrow CH(S)$

Methyl-radical addition
S3.　　　　$C(SR) + CH_3 \Leftrightarrow C(D) + CH_3(S)$
S4.　　　　$CH_2(S) + H \Leftrightarrow CH(SR) + H_2$
S5.　　　　$CH_3(S) + H \Leftrightarrow CH_2(SR) + H_2$
S6.　　　　$CH_2(SR) + CH(SR) \Leftrightarrow CH_2(S) + CH(S)$

Acetylene addition
S7.　　　　$C(SR) + HCCH \Leftrightarrow C(D) + HCCH(SR)$
S8.　　　　$CH(S) + HCCH(SR) \Leftrightarrow C(SR) + H_2CCH(S)$
S9.　　　　$H_2CCH(S) + C(SR) \Leftrightarrow C(D) + CH_2(S) + CH(SR)$
S10.　　　$CH_2(S) + CH(SR) \Leftrightarrow CH_2*(S) + CH(SR)$
S11.　　　$CH(SR) + CH_2*(S) + H \Leftrightarrow CH(S) + CH(S) + H_2$

Carbon-atom addition
S12.　　　$C(SR) + C \Leftrightarrow C(D) + C(SR3)$
S13.　　　$C(SR3) + CH_2(S) \Leftrightarrow CH(SR) + CH(S)$
S14.　　　$CH(SR) + H \Leftrightarrow CH_2(S)$

Other radical-termination reactions
S15.　　　$C(SR3) + H_2 \Leftrightarrow CH_2(S)$
S16.　　　$C(SR3) + H \Leftrightarrow CH(SR2)$
S17.　　　$CH(SR2) + H \Leftrightarrow CH_2(SR)$
S18.　　　$CH_2(SR) + H \Leftrightarrow CH_3(S)$
S19.　　　$CH(SR2) + H_2 \Leftrightarrow CH_3(S)$

Graphite reactions
S20.　　　$CH(SG) + C(G) + H \Leftrightarrow CH(SR) + CH(S)$
S21.　　　$CH(SG) + H \Leftrightarrow C(RG) + H_2$
S22.　　　$C(RG) + H \Leftrightarrow CH(SG)$
S23.　　　$C(RG) + CH_3 \Leftrightarrow C(G) + CH_3(S)$
S24.　　　$C(RG) + C \Leftrightarrow C(G) + C(SR3)$
S25.　　　$C(RG) + HCCH \Leftrightarrow C(G) HCCH(SR)$
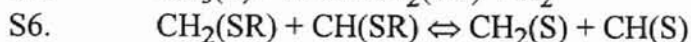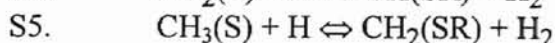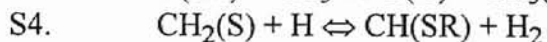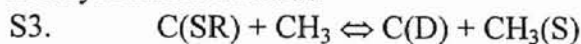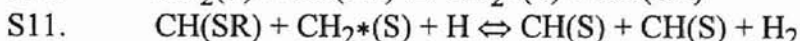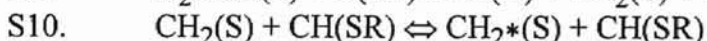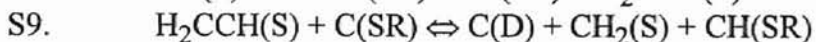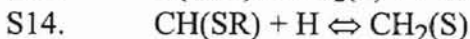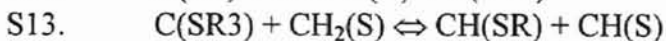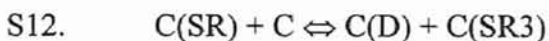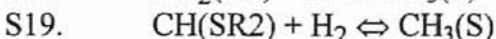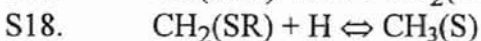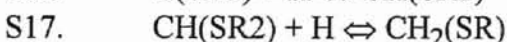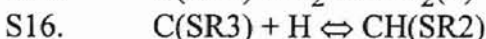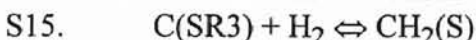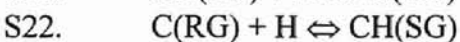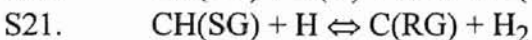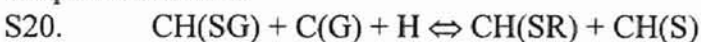
atoms is also included.

A single gas-phase growth precursor has not been identified, since the most abundant species would depend upon reactor conditions. The mechanism used provides for the growth of diamond and graphitic material from more than one precursor, with CH_3, C_2H_2, C, H. and H_2 from the gas-phase expected to play a role in the growth mechanism.

The plug-flow reactor used to model the surface reaction kinetics assumes no mixing in the axial direction, but perfect mixing in the radial direction. All reactions in the surface mechanism are assumed reversible. However, kinetic data for each reaction was entered into the ASPEN PLUS computer code in terms of separate forward and reverse reactions (as a result, the sample input file in Appendix C shows 50 reactions instead of just the 25 reversible reactions as indicated in Table 11). Data for the reaction kinetics was specified using the power law kinetics model provided by ASPEN PLUS. The general form of the power law expression is:

$$r_{ij} = k_i \, T^n \, exp(-E/RT).\pi(C_j)^{\alpha_j}$$

where r is the rate of reaction of the jth component in the ith reaction, k is the pre-exponential factor for the ith reaction, T is the absolute temperature, n is the temperature exponent, E is the activation energy, R is the universal gas constant, C is the concentration, α is the concentration exponent, and π is the product operator.

The net rate of reaction for the jth component may now be evaluated as the sum of all rates of reactions in which the species j appears. Hence,

$$r_j = \sum_{i=1}^{q} r_{ij}$$

where q is the number of reactions in which the species j is involved.

A mole balance for species, 1, 2, ...j, in the plug-flow reactor results in a set of equations of the form,

$$\frac{dF_j}{dV} = r_j$$

where F_j is the molar flow rate of the jth component, and V is the volume of the reactor (whose dimensions are fixed). Subsequently, for n species present in the system, the total molar flow rate, F_T, may be expressed as,

$$F_T = \sum_{j=1}^{n} F_j$$

Substitution of the rate expressions, r_j, for each component, into the above mentioned equations for the mole balances, results in a set of coupled first-order ordinary differential equations. These are solved for the concentrations of each component as a function of reactor volume (i.e., distance along the length of the reactor). The Newton's corrector method was used to obtain convergence using an initial step size of 0.01.

For many of the reactions in which gas-phase species react with surface species, Coltrin and Dandy [1] expressed the reaction rate constants in terms of a reaction probability, γ_j. The reaction rate expressed in this manner accounts for the probabilistic nature of a reaction occurring between a gas-phase species upon collision with a surface

completely covered by a particular surface species. The reaction probability, γ_i, may be converted to the usual mass-action kinetic rate constant (for the forward reaction) by the following expression:

$$k_{ij} = \left(\frac{\gamma_i}{1 - \gamma_i}\right) \cdot \frac{1}{\Gamma^m} \cdot \left(\frac{RT}{2\pi W}\right)^{1/2}$$

where Γ is the total surface site concentration, W is the molecular weight of the gas-phase species, and m is the sum of all the surface reactants' stoichiometric coefficients. For the diamond film, a fixed number of sites, $\Gamma = 5.22 \times 10^{-9}$ mol/cm^2, is assumed on the surface [1]. Kinetic data for all surface reactions was obtained from Coltrin and Dandy [1] and Meeks et al. [5]. Data for the forward and reverse rate constants are presented in Tables 12 and 13, respectively [1].

The ASPEN PLUS software requires complete thermochemical data for each surface component, i.e., the standard heat of formation and the standard state temperature dependent heat capacity at 298 K. Thermochemical properties of the surface reactants were obtained from Coltrin and Dandy [5], and are presented in Tables 14 and 15. The temperature dependent heat capacity of each species was represented in the following polynomial form, as required by the ASPEN PLUS program:

$$C_p = a_1 + a_2T + a_3T^2 + a_4T^3 + a_5T^4$$

The polynomial coefficients a_1 to a_5 for all surface and bulk species are presented in Table 14.

Table 12. Forward rate constants [1].

Reaction	γ_i	m	W	k_f J/kmol K	E_f Cal, gmole	n
s1	0.10	1	1.008	7.31E+07	0	0.5
s2	1.00	1	1.008	1.39E+09	0	0.5
s3	0.33	1	15.035	7.10E+07	0	0.5
s4	0.10	1	1.008	7.31E+07	0	0.5
s5	0.20	1	1.008	1.54E+08	0	0.5
s6	-	-	-	6.00E+19	0	0
s7	-	-	-	8.00E+10	7700	0
s8	-	-	-	6.00E+19	0	0
s9	-	-	-	6.00E+19	0	0
s10	-	-	-	6.00E+19	2122	0
s11	0.10	2	1.008	1.40E+15	0	0.5
s12	0.33	1	12.011	7.95E+07	0	0.5
s13	-	-	-	6.00E+19	0	0
s14	1.00	1	1.008	1.39E+09	0	0.5
s15	1.00	1	2.016	9.82E+08	0	0.5
s16	1.00	1	1.008	1.39E+09	0	0.5
s17	1.00	1	1.008	1.39E+09	0	0.5
s18	1.00	1	1.008	1.39E+09	0	0.5
s19	1.00	1	2.016	9.82E+08	0	0.5
s20	0.10	1	1.008	7.31E+07	0	0.5
s21	0.10	1	1.008	7.31E+07	0	0.5
s22	1.00	1	1.008	1.39E+09	0	0.5
s23	0.33	1	15.035	7.10E+07	0	0.5
s24	0.33	1	12.011	7.95E+07	0	0.5
s25	0.33	1	26.038	5.40E+07	0	0.5

Table 13. Reverse rate constants [1].

Reaction	k_r J/kmol K	E_r Cal, gmole
s1	1.15E+10	17620
s2	5.11E+14	96810
s3	9.21E+13	59640
s4	1.89E+10	18110
s5	2.67E+11	28470
s6	6.00E+16	94020
s7	2.64E+13	16410
s8	4.41E+16	10110
s9	1.01E+17	56300
s10	6.00E+16	0
s11	3.62E+18	83980
s12	5.87E+12	84560
s13	9.90E+16	86250
s14	3.10E+14	96320
s15	2.01E+15	79320
s16	5.11E+14	93350
s17	3.10E+14	91520
s18	5.55E+13	86380
s19	2.18E+14	72350
s20	5.99E+19	51990
s21	9.16E+07	11180
s22	4.47E+13	102900
s23	7.82E+12	89530
s24	4.99E+11	114100
s25	8.62E+13	39490

Table 14. Polynomial coefficients for heat capacities [1, 13].

Molecule	a_1	a_2	a_3	a_4	a_5
C(SR)	3.358566124	0.00219965	-2.50715E-07	-2.38398E-10	5.72549E-14
C(SR$_3$)	3.358566124	0.00219965	-2.50715E-07	-2.38398E-10	5.72549E-14
CH(S)	2.955415308	0.00655794	-5.64597E-07	-6.83278E-10	1.52339E-13
CH(SR)	2.955415308	0.00655794	-5.64597E-07	-6.83278E-10	1.52339E-13
CH(SR$_2$)	2.955415308	0.00655794	-5.64597E-07	-6.83278E-10	1.52339E-13
CH$_2$(S)	3.456629277	0.01028661	-8.37677E-07	-1.06243E-09	2.33762E-13
CH$_2$(SR)	3.456629277	0.01028661	-8.37677E-07	-1.06243E-09	2.33762E-13
CH$_2$*(S)	3.456629277	0.01028661	-8.37677E-07	-1.06243E-09	2.33762E-13
CH$_3$(S)	4.425878724	0.01288510	-1.01150E-06	-1.31678E-09	2.87060E-13
HCCH(SR)	7.231759419	0.01192724	-1.00891E-06	-1.23138E-09	2.73692E-13
H$_2$CCH(S)	7.340903994	0.01583840	-1.27924E-06	-1.62590E-09	3.57346E-13
C(RG)	3.358566323	0.00219965	-2.50713E-07	-2.38398E-10	5.72550E-14
CH(SG)	2.944572152	0.00650841	-5.52079E-07	-6.75742E-10	1.50147E-13
CD	3.358566323	0.00219965	-2.50715E-07	-2.38398E-10	5.72549E-14
CA†	20803.4	0.168416	-0.00039309	2.36518E-07	-3.13285E-11

$\dagger$ Obtained value of heat capacity in J/Kmole K

Table 15. Heat of formation of the surface species [1, 13].

Molecule	ΔH^o_f (298 K) kcal/mol
C(SR)	43.4
C(SR3)	129.1
CH(S)	0.0
CH(SR)	31.9
CH(SR2)	-11.5
CH$_2$(S)	50.7
CH$_2$(SR)	-9.4
CH$_2$*(S)	17.3
CH$_3$(S)	89.2
HCCH(SR)	87.1
H$_2$CCH(S)	33.4
C(RG)	72.5
CH(SG)	23.1
CD	0.5
CA	160.43

The spatial variation of temperature over the substrate is presented in Fig. 39. This profile is an estimate derived from the studies conducted by Butler et al. [15]. This variation in temperature was used in the plug flow reactor in an effort to characterize the actual radial temperature gradient present on the substrate during the combustion chemical vapor deposition method. A more linear variation in the radial temperature profile along the substrate was seen to have no substantial effect on the predicted growth rates of diamond.
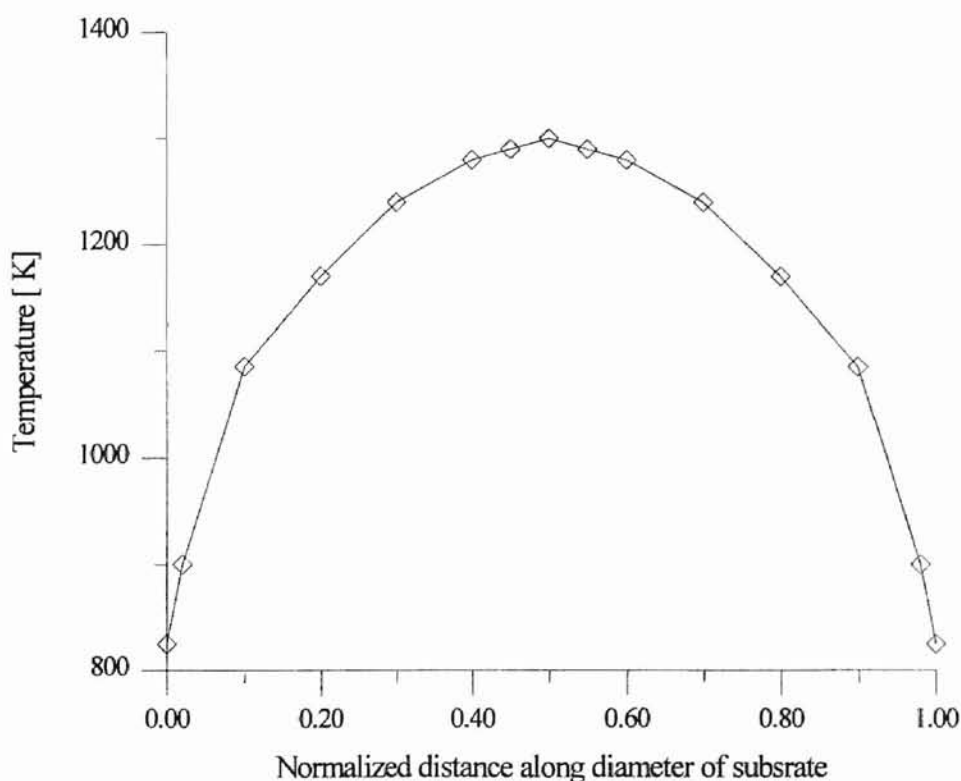
Figure 39. Temperature profile assumed along the substrate.

The reader is referred to Chapter VI of this study for identification of the various surface species involved in the reaction mechanism. The ASPEN PLUS computer codes for analysis of the gas-phase and surface reactions are included in Appendices B and C, respectively.

CHAPTER XIII

RESULTS AND DISCUSSIONS

Case Studies

The proposed model was used to simulate the low pressure chemical vapor deposition of diamond in C_2H_2-O_2 and C_2H_2-O_2-H_2 systems. The steady state growth of diamond was modeled at conditions typically prevalent in flame syntheses methods. However, the induction times required for nucleation on non-diamond substrates are not accounted for since the model is for a steady-state process.

Calculations were performed for inlet molar flow ratios of C_2H_2 to O_2 ($R=C_2H_2/O_2$) between 0.80 to 1.20 (at increments of 0.05). Results are illustrated in Fig. 40. All simulations were carried out at atmospheric pressure with inlet gases at 300 K. Further, the only gas-phase species fed to the plug flow reactor (used to model the kinetics of the surface reactions) were those incorporated in the surface reaction mechanism. This avoided unnecessary adjustments that may have had to be made to the dimensions of the plug flow reactor in order to maintain a constant residence time for all cases simulated. The mean residence time allowed for the surface reactions corresponding to the assumed reactor configuration was about 15 μs.

The deposition of diamond in C_2H_2-O_2-H_2 systems was studied as well, in an effort to illustrate the effect of hydrogen on the growth rate of diamond. The hydrogen

mole fraction in the feed mixture was varied (0.20, 0.25 and 0.30) for the same inlet flow ratios of C_2H_2/O_2 used in the previous case studies. Results are illustrated in Figs. 50-58.

Diamond Growth in Acetylene-Oxygen Flames

The results of the thermodynamic equilibrium calculations of the gas-phase component concentrations in acetylene-oxygen flames are illustrated in Figs. 41-49. The predicted species mole fractions have been plotted as a function of the flame temperature. The concentration profiles obtained in this study were in reasonable agreement with past works [9, 17].

An examination of the concentration profiles of C_2H_2 and CH_3 in Figs. 41 through 49 indicate a distinct variation in the mole fractions of the two species. At C_2H_2/O_2 ratios between 0.80 to 0.95, the amount of CH_3 reaching the substrate is almost an order in magnitude more than C_2H_2. The concentrations of both species gradually increases with decrease in temperature. However, for C_2H_2/O_2 ratios equal to and greater than 1.0, the opposite is true, with C_2H_2 being present in higher amounts. Further, the concentrations of both species reduces rapidly at temperatures below 1750 K.

The concentration of the third growth species, C, is insufficient to be able to contribute to the growth of diamond in any substantial manner. Other important species that may be expected to play a role in the growth mechanism include H, O, OH, and C_2H. The profile of the H radicals does not vary substantially with an increase in C_2H_2/O_2 ratio. However, an increase in the concentration of H in the gas medium does result in an increase in the growth rate of diamond. The results of a study on the effect of hydrogen on the growth rate of diamond have been presented later in this chapter.
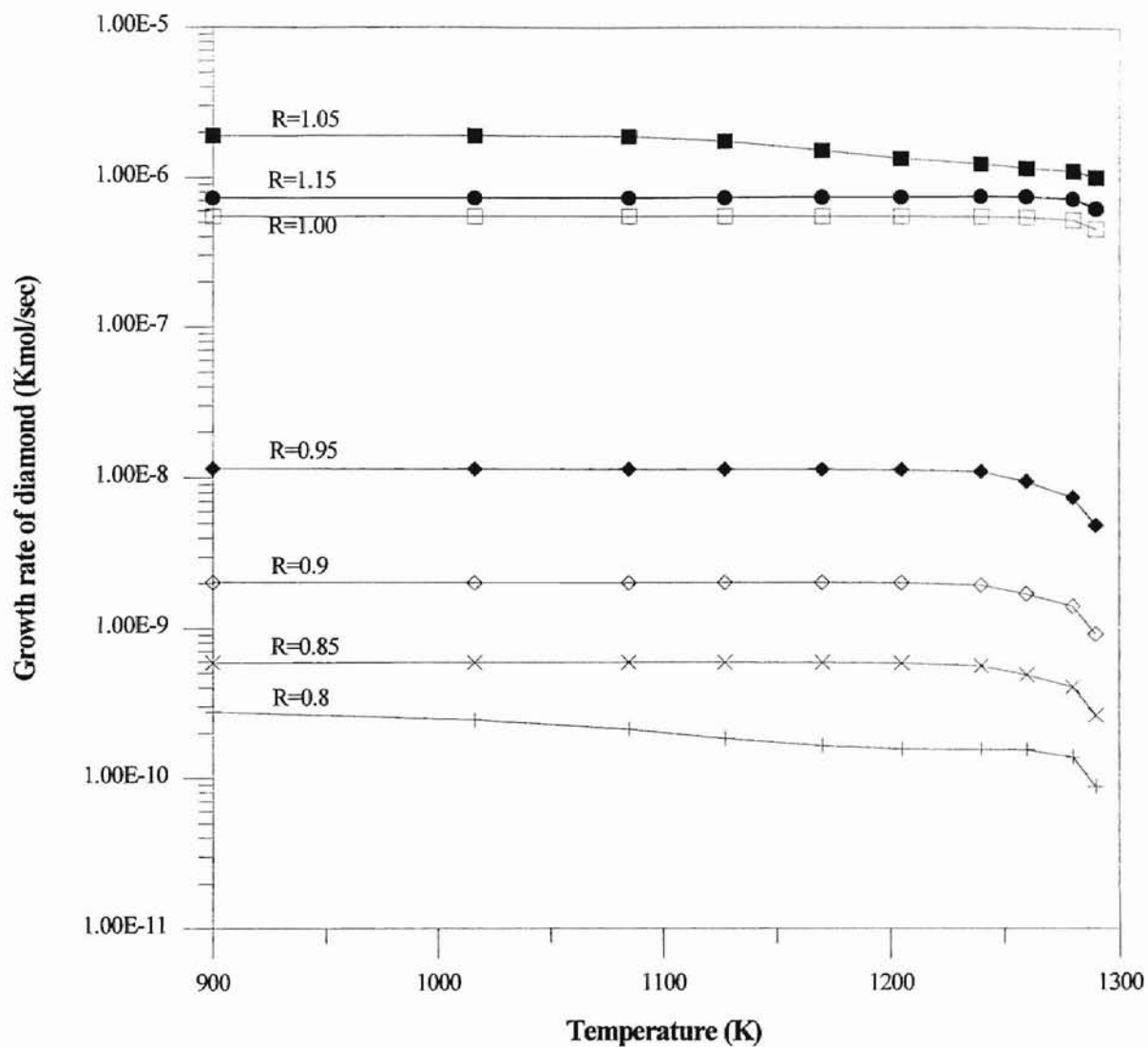
Figure 40. Predicted growth rates of diamond in C2H2-O2 flames. R=[C2H2]/[H2].
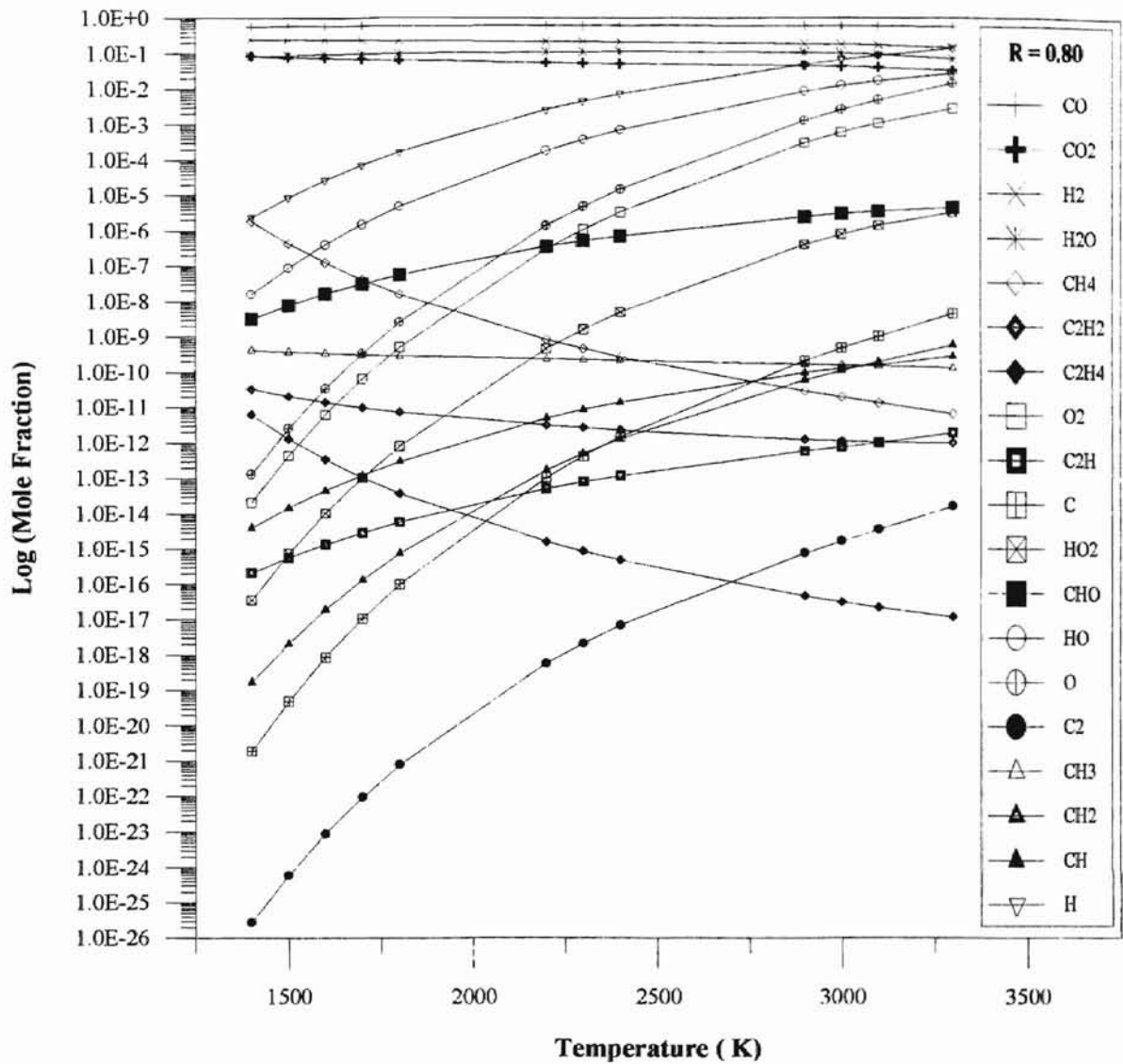
Figure 41. Profile of the gas-phase mole fractions in C_2H_2-O_2 flames. $R=[C_2H_2]/[O_2] = 0.80$.
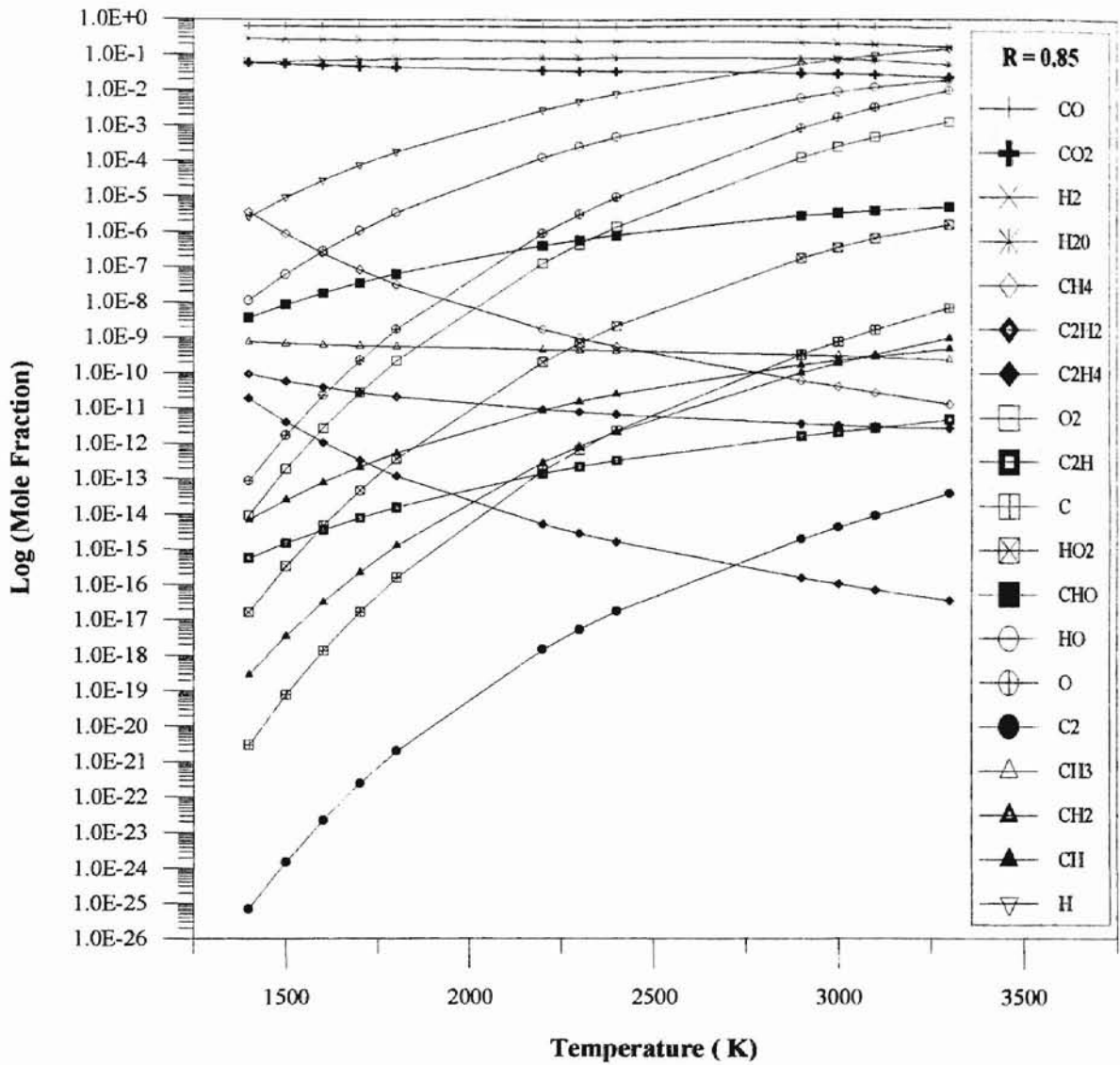
Figure 42. Profile of the gas-phase mole fractions in C_2H_2-O_2 flames. $R=[C_2H_2]/[O_2] = 0.85$
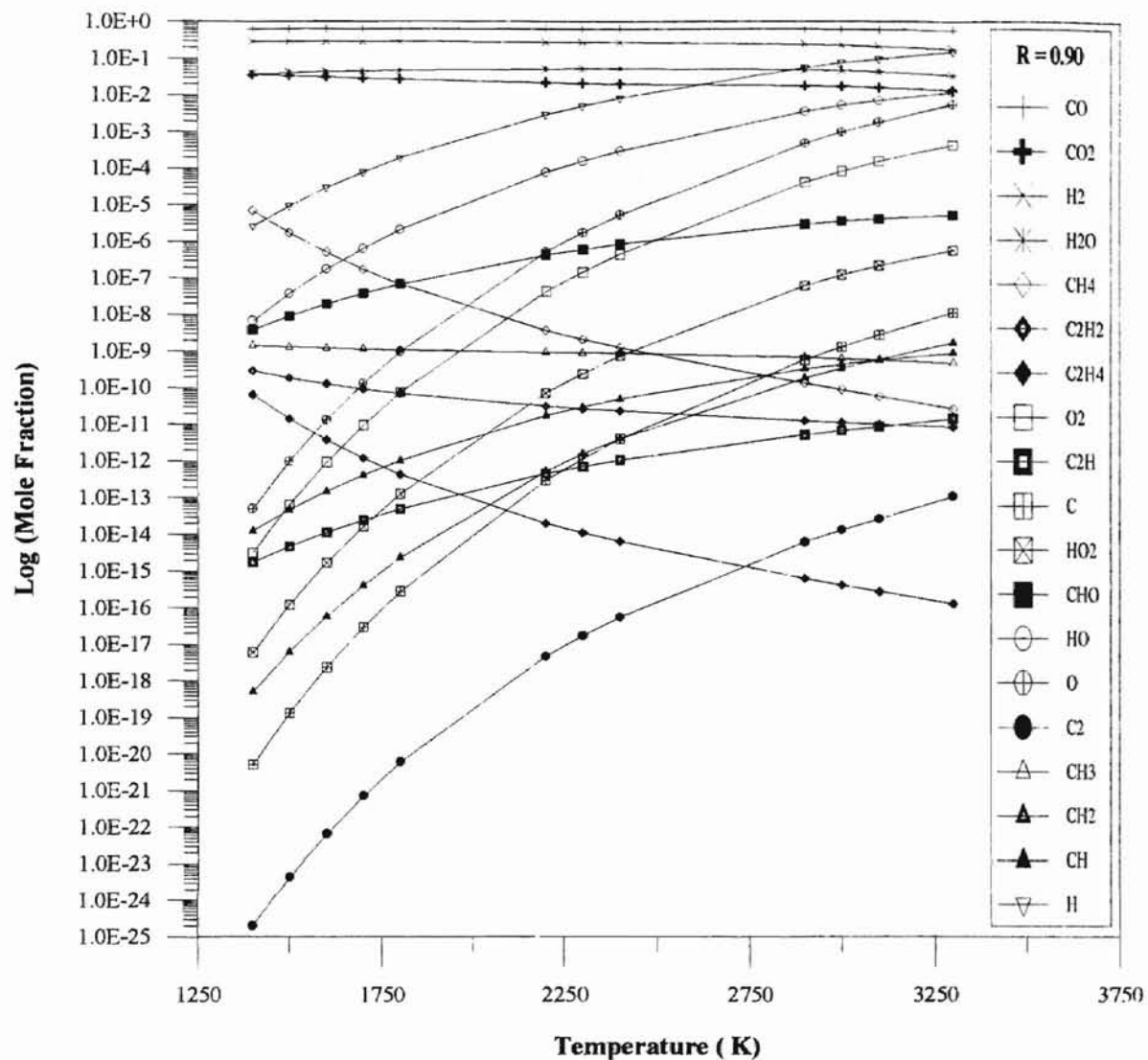
Figure 43. Profile of the gas-phase mole fractions in C_2H_2-O_2 flames. $R=[C_2H_2]/[O_2] = 0.90$
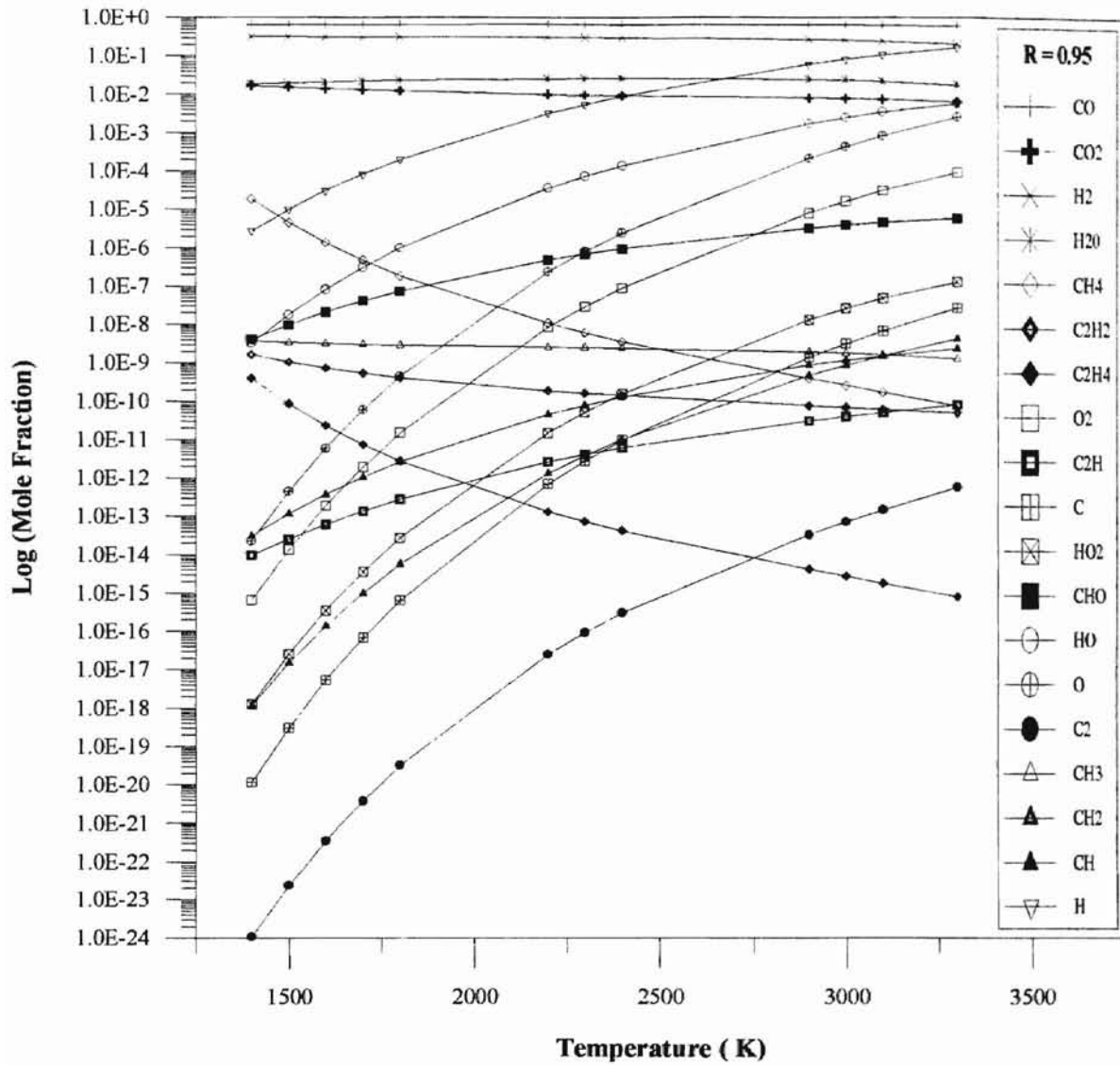
Figure 44. Profile of the gas-phase mole fractions in C_2H_2-O_2 flames. $R=[C_2H_2]/[O_2] = 0.95$
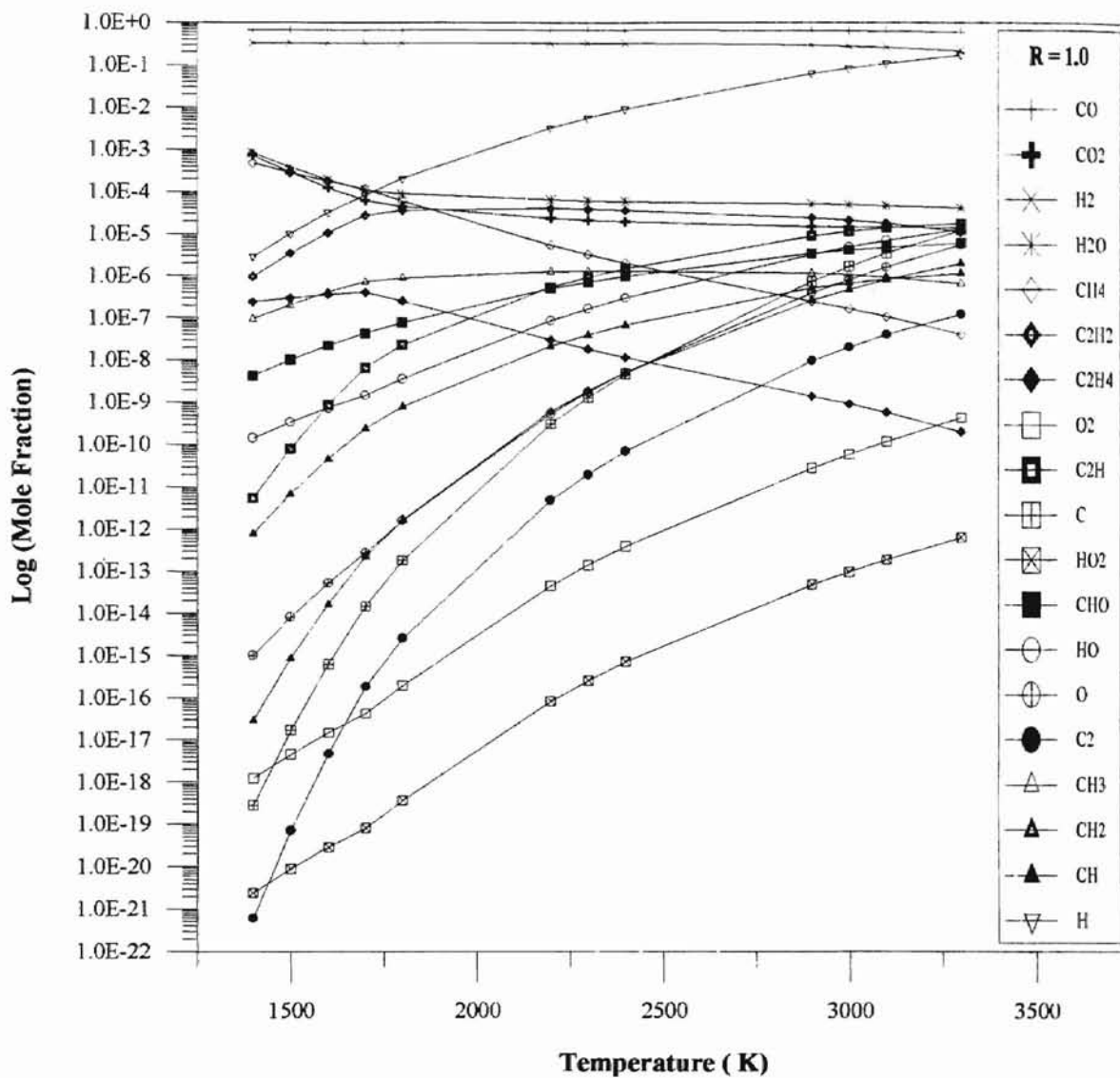
Figure 45. Profile of the gas-phase mole fractions in C_2H_2-O_2 flames. $R=[C_2H_2]/[O_2] = 1.00$
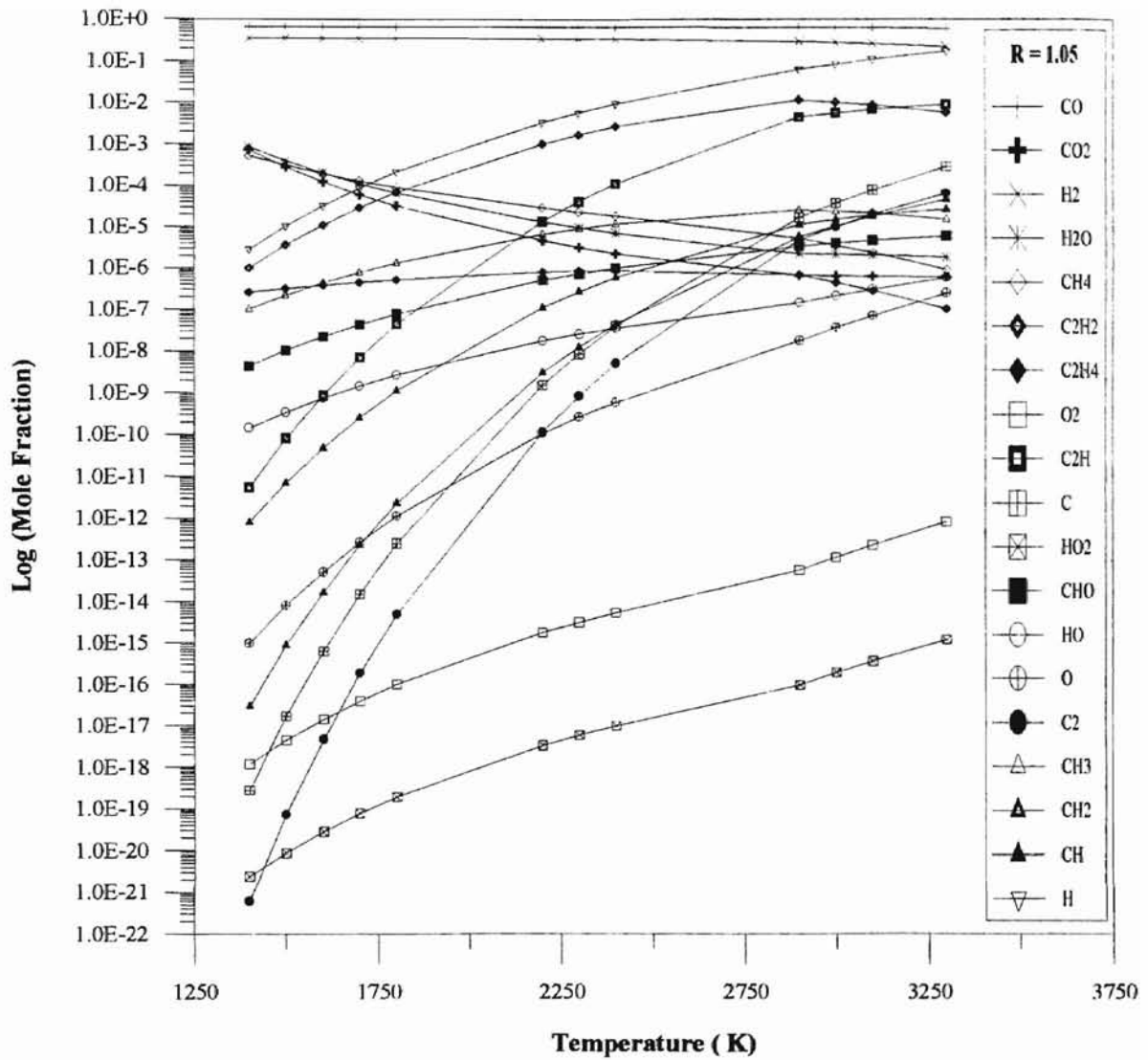
Figure 46. Profile of the gas-phase mole fractions in C_2H_2-O_2 flames. R=$[C_2H_2]/[O_2]$ = 1.05
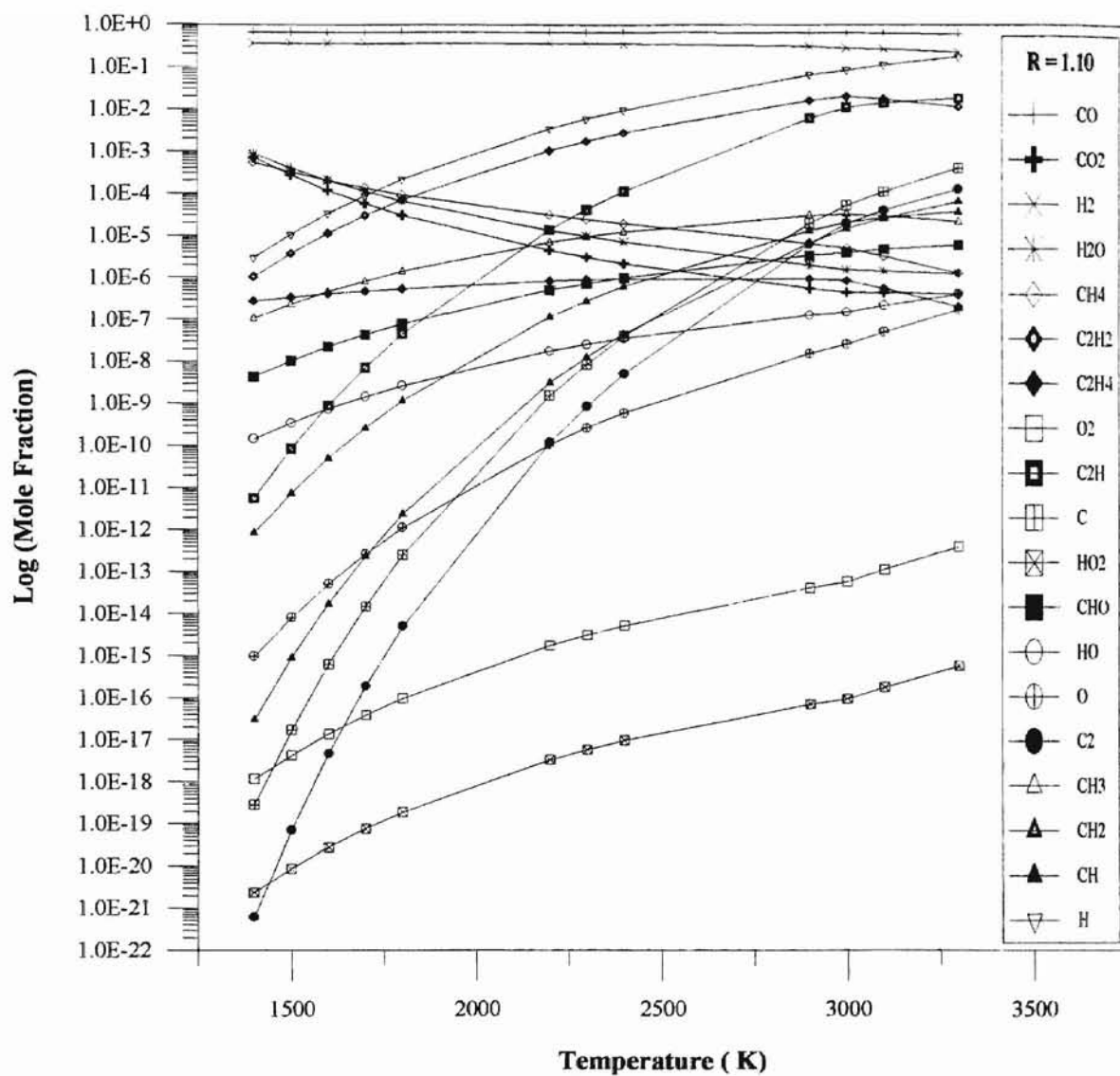
Figure 47. Profile of the gas-phase mole fractions in C_2H_2-O_2 flames. R=[C_2H_2]/[O_2] = 1.10
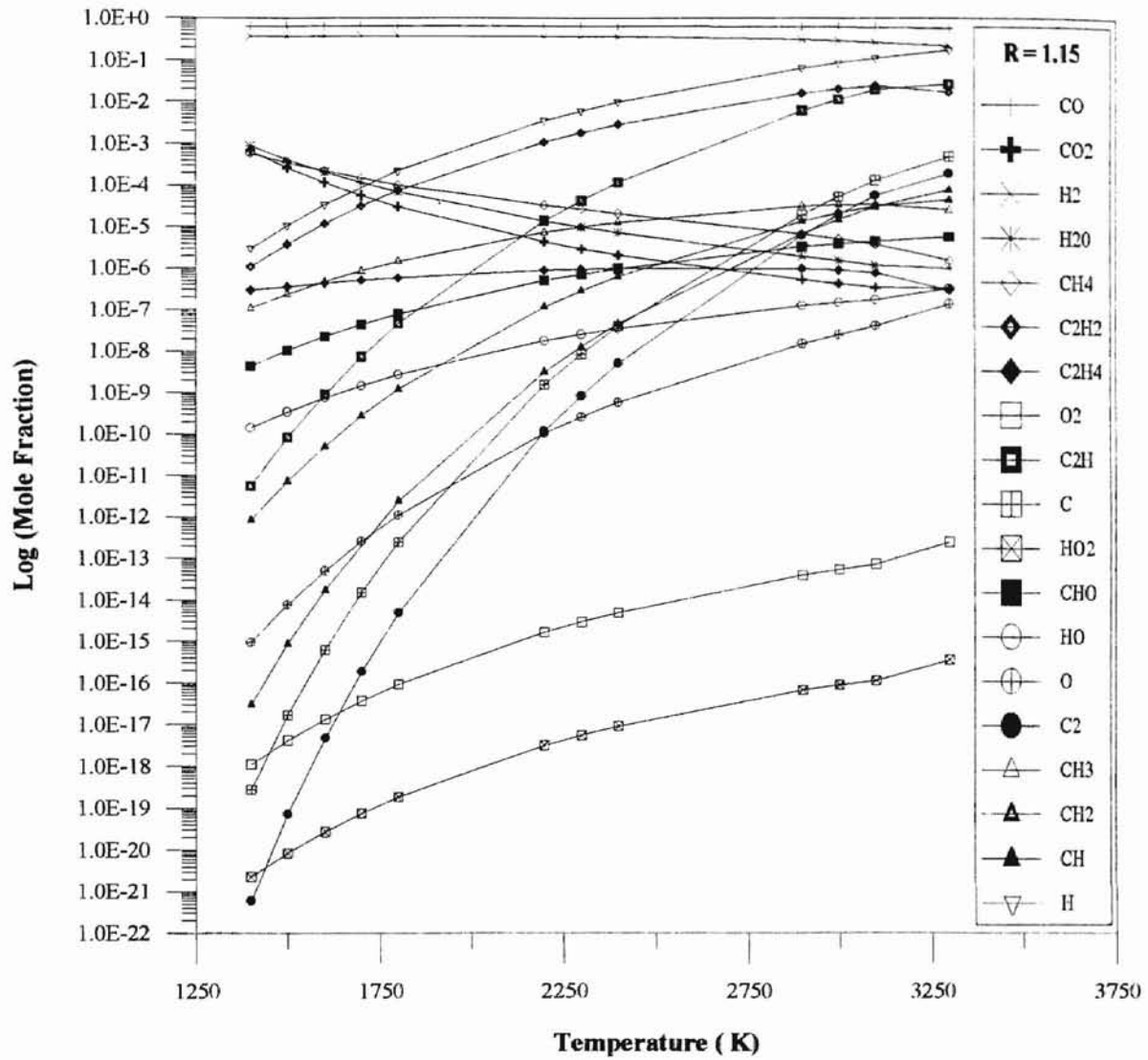
Figure 48. Profile of the gas-phase mole fractions in C_2H_2-O_2 flames. $R=[C_2H_2]/[O_2] = 1.15$
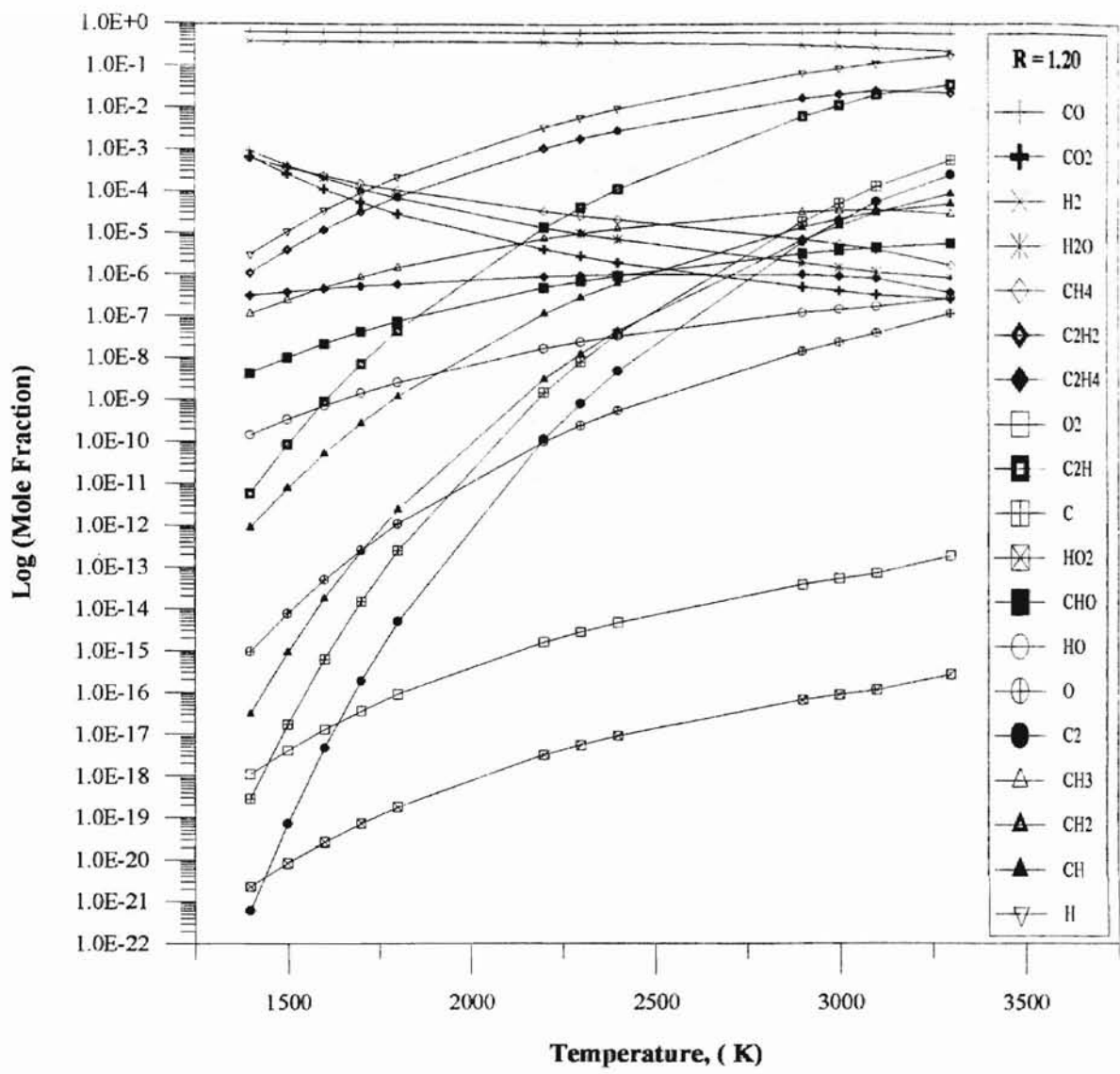
Figure 49. Profile of the gas-phase mole fractions in C_2H_2-O_2 flames. $R=[C_2H_2]/[O_2] = 1.20$

Some researchers indicate the possibility of C_2H radicals playing a role in the deposition process. The gas-phase concentration profiles indicate a substantial increase in the presence of C_2H with increase in C_2H_2/O_2 ratio. Figs. 41 and 49 clearly depict this difference. In comparison, the profiles of O and OH show a reduction in concentration as the C_2H_2/O_2 ratio increases over 1.0.

The results of the kinetic model for the surface reaction mechanism are illustrated in Fig. 40. The predicted moles of diamond for each inlet flow C_2H_2/O_2 ratio have been plotted versus temperature. The maximum steady-state growth rate of diamond was obtained for the C_2H_2/O_2 ratio of 1.05. The steady-state growth rate of diamond at 950 K was predicted to be 1.9×10^{-06} Kmol/sec. These predictions provide reasonably accurate estimates for the observed diamond deposition rates. However, while such predicted growth rates may be useful for qualitative comparisons and parametric studies, they may contain significant errors due to uncertainties and simplifications in the surface-kinetic mechanism [14, 15].

Effect of Hydrogen

Researchers have conducted a variety of studies on the possible role of atomic hydrogen in the growth mechanism of diamond [18, 19]. There is a general consensus that the presence of atomic hydrogen favors the growth of diamond. This seems to suggest that the inclusion of a more direct precursor for atomic hydrogen, such as the added presence of hydrogen gas in the feed mixture, might be a better fuel for diamond growth.

Simulations were performed using a feed of C_2H_2-O_2-H_2 in an effort to illustrate the effect of atomic hydrogen on the diamond deposition process. Feed mixtures

containing different mole fractions of hydrogen (0.20, 0.25 and 0.30), but with the same initial values for the inlet flow ratios of C_2H_2/O_2 were used in the study. Results are presented in Figs. 50-58. The predicted steady-state growth rates of diamond for the different inlet mole fractions of hydrogen have been plotted versus temperature. An increase in the mole fraction of hydrogen in the feed mixture is observed to have an unusual effect on the expected growth rate of diamond.

The plots obtained for the inlet flow ratios of C_2H_2/O_2 between 0.80 and 0.90 indicate an increase in the predicted growth rate of diamond with increase in the mole fraction of hydrogen in the feed. However, this trend is disrupted for inlet flow ratios of C_2H_2/O_2 greater than 0.95. Diamond growth seems to be inhibited by the presence of the extra hydrogen for these higher ratios. This is clearly evident in Figs. 56 to 58 where increases in the hydrogen fraction of the feed result in rather erratic variations in the steady-state growth curves for diamond. Further analyses are needed to explain this anomalous variation in behavior. Moreover, without detailed surface studies of the processes occurring at the gas-solid interface it would be difficult to fully explain the role of atomic hydrogen, and other species that are thought to play a part in the deposition mechanism.
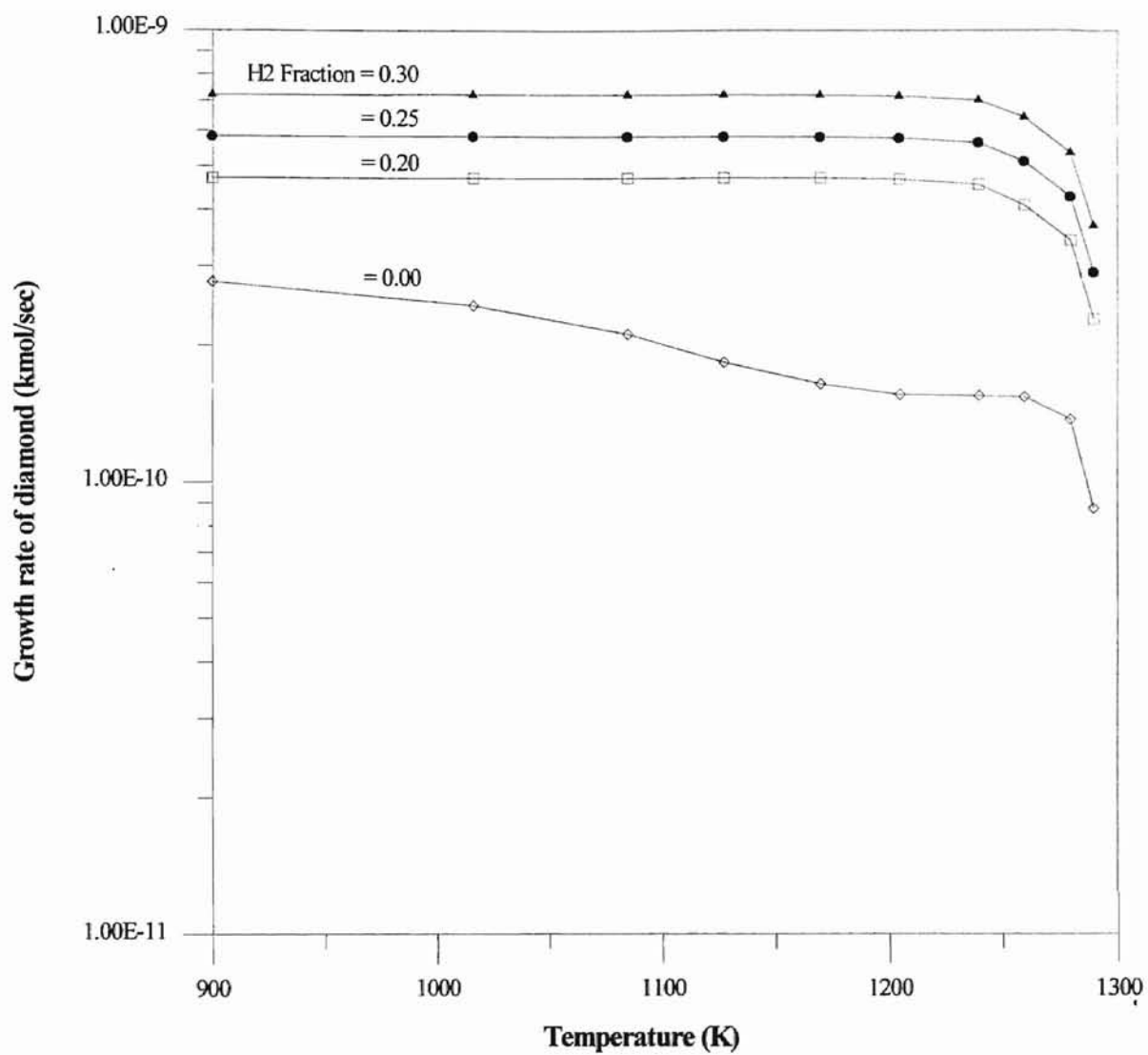
Figure 50. Effect of H_2 in the feed. R=[C2H2]/[O2]=0.80
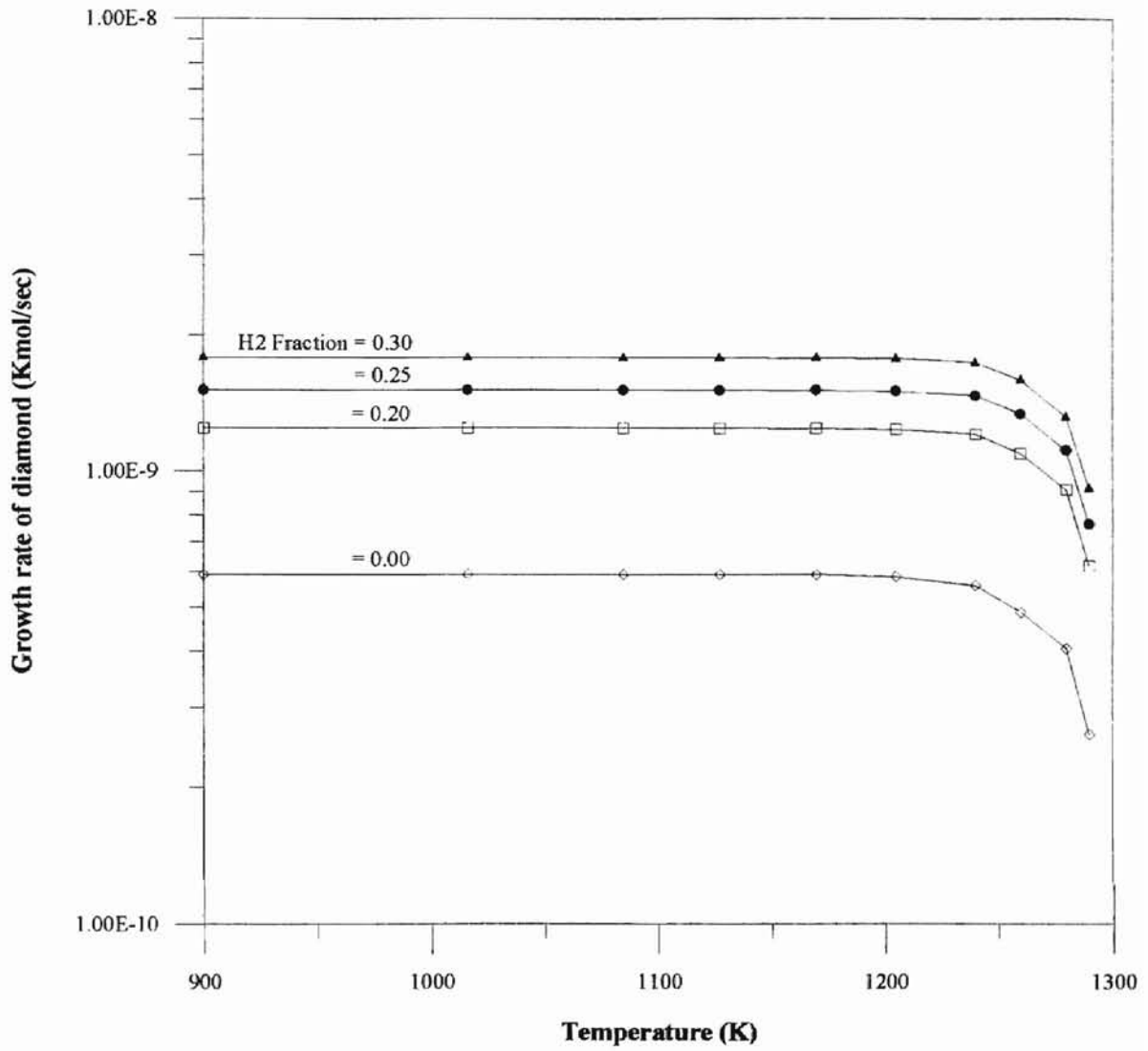
Figure 51. Effect of H_2 in the feed. R=[C2H2]/[O2]=0.85
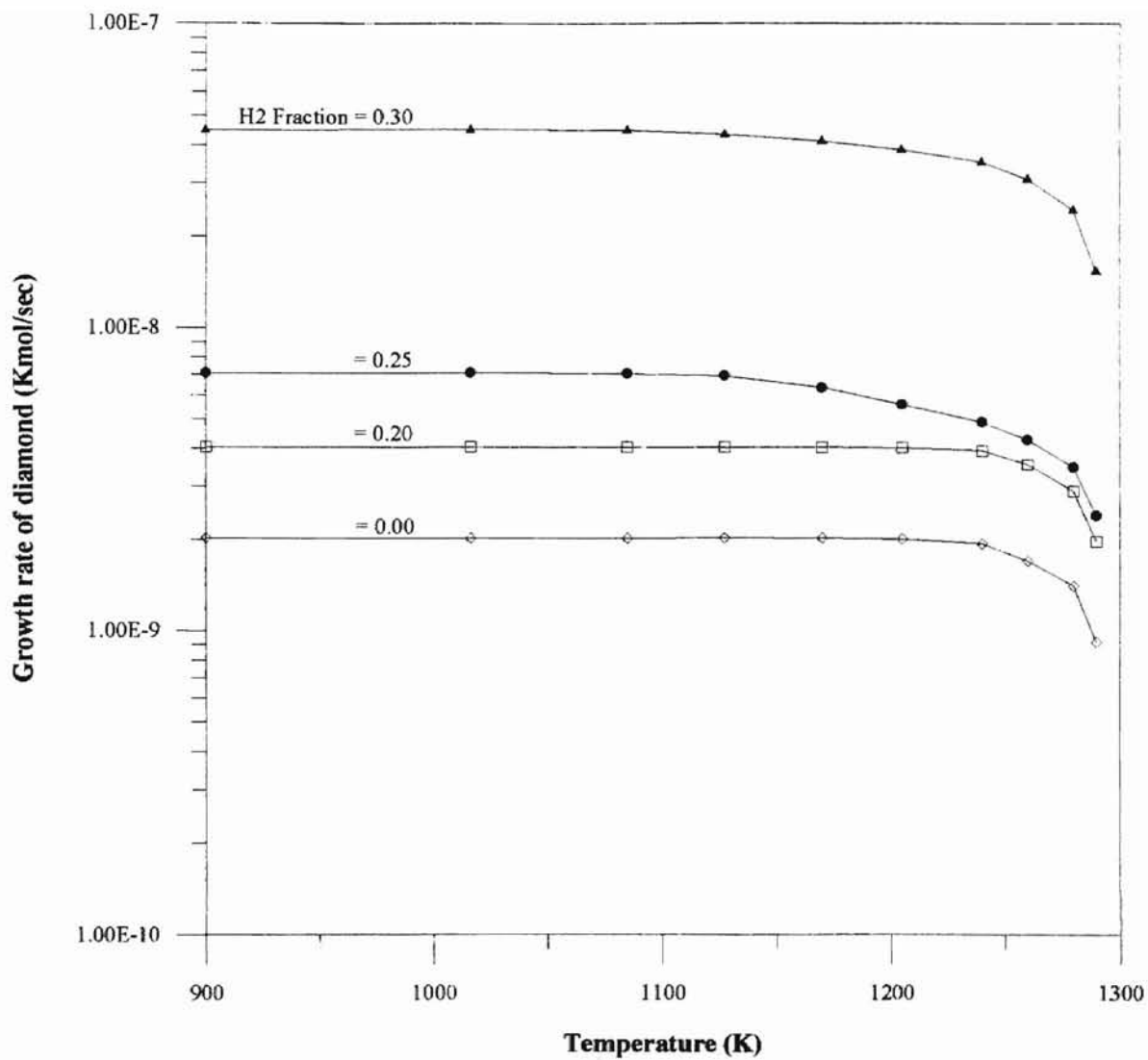
Figure 52. Effect of H$_2$ in the feed. R=[C2H2]/[O2]=0.90
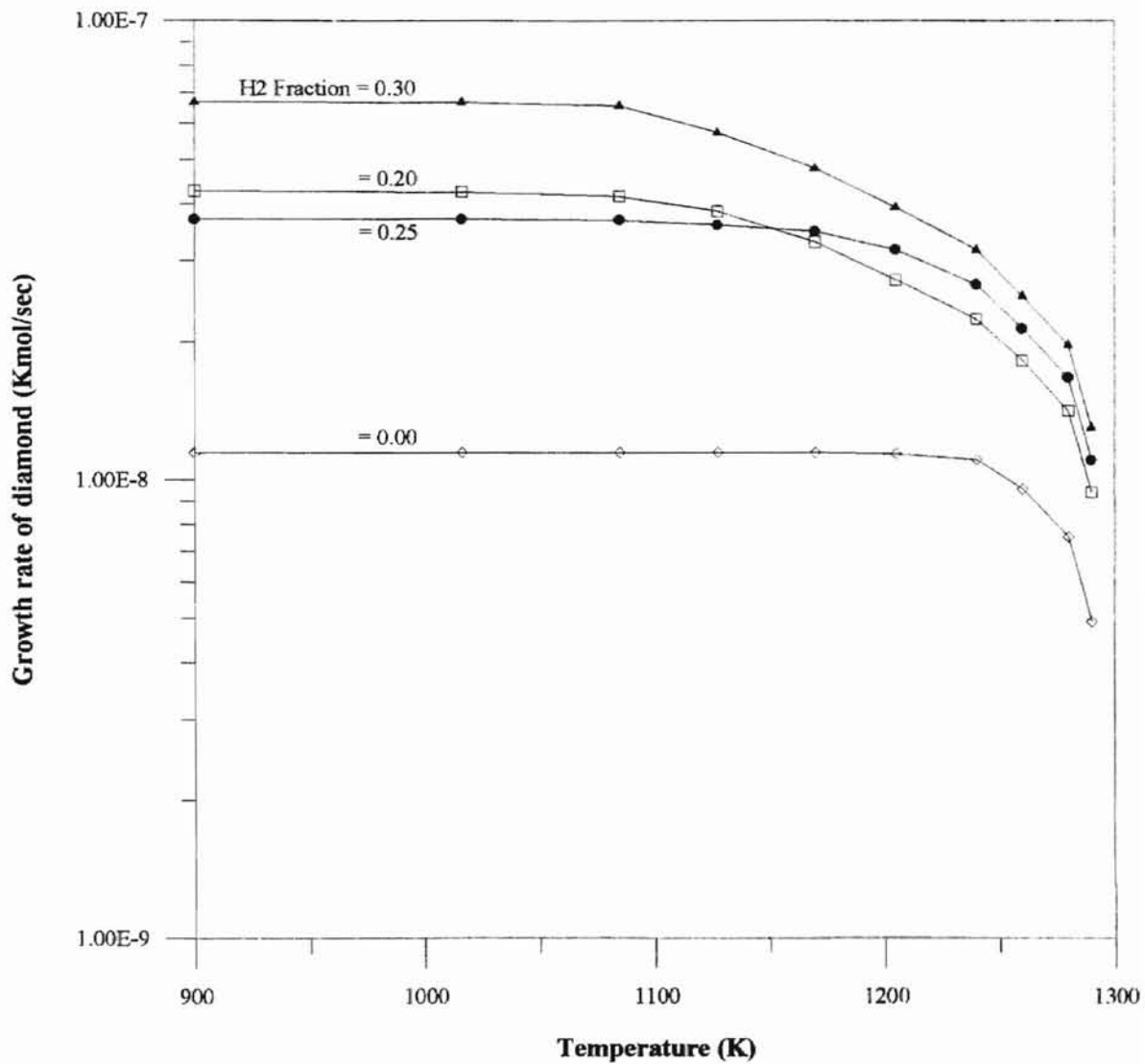
Figure 53. Effect of H$_2$ in the feed. R=[C2H2]/[O2]=0.95
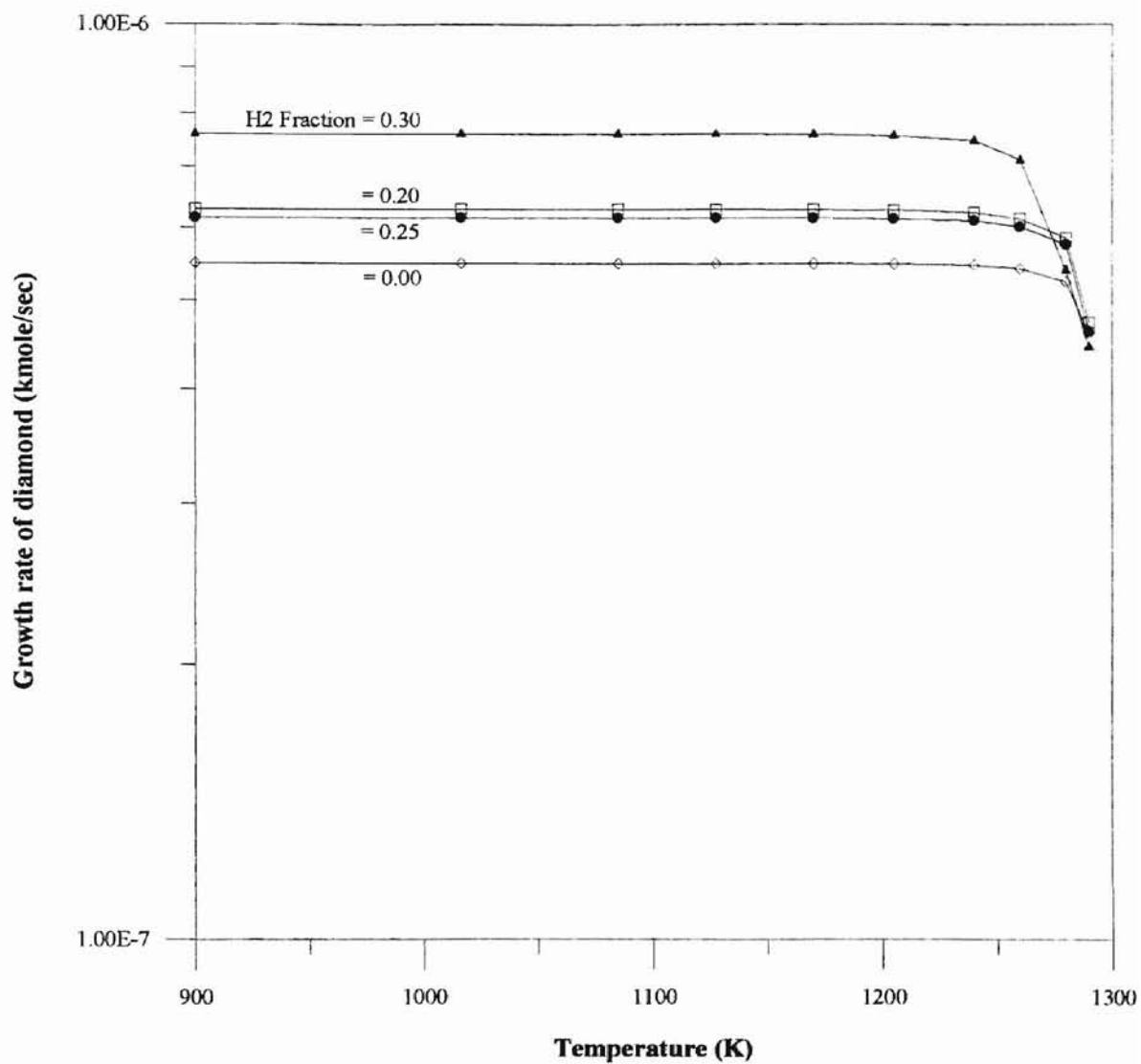
Figure 54. Effect of H_2 in the feed. R=[C2H2]/[O2]=1.00
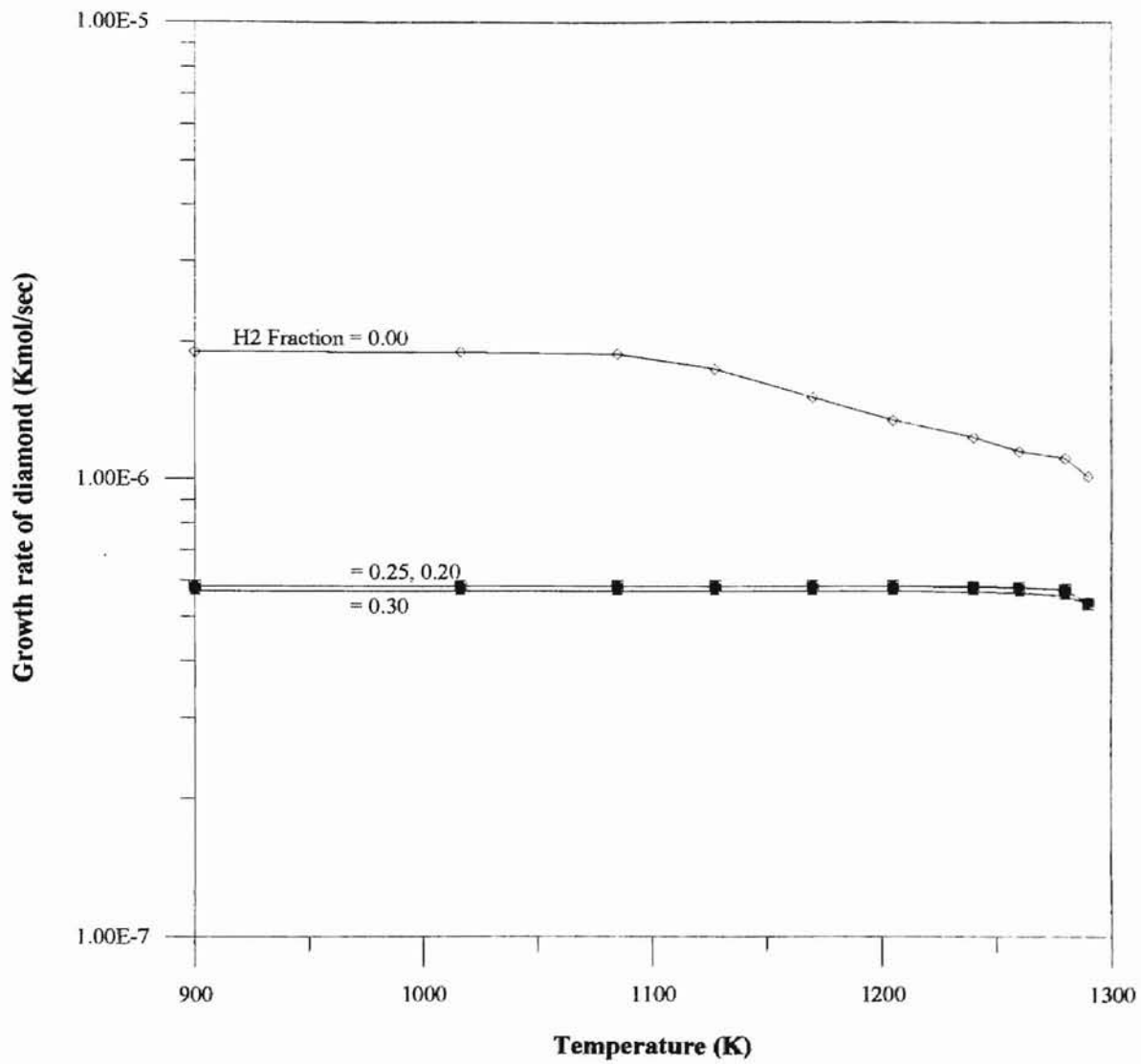
Figure 55. Effect of H$_2$ in the feed. R=[C2H2]/[O2]=1.05
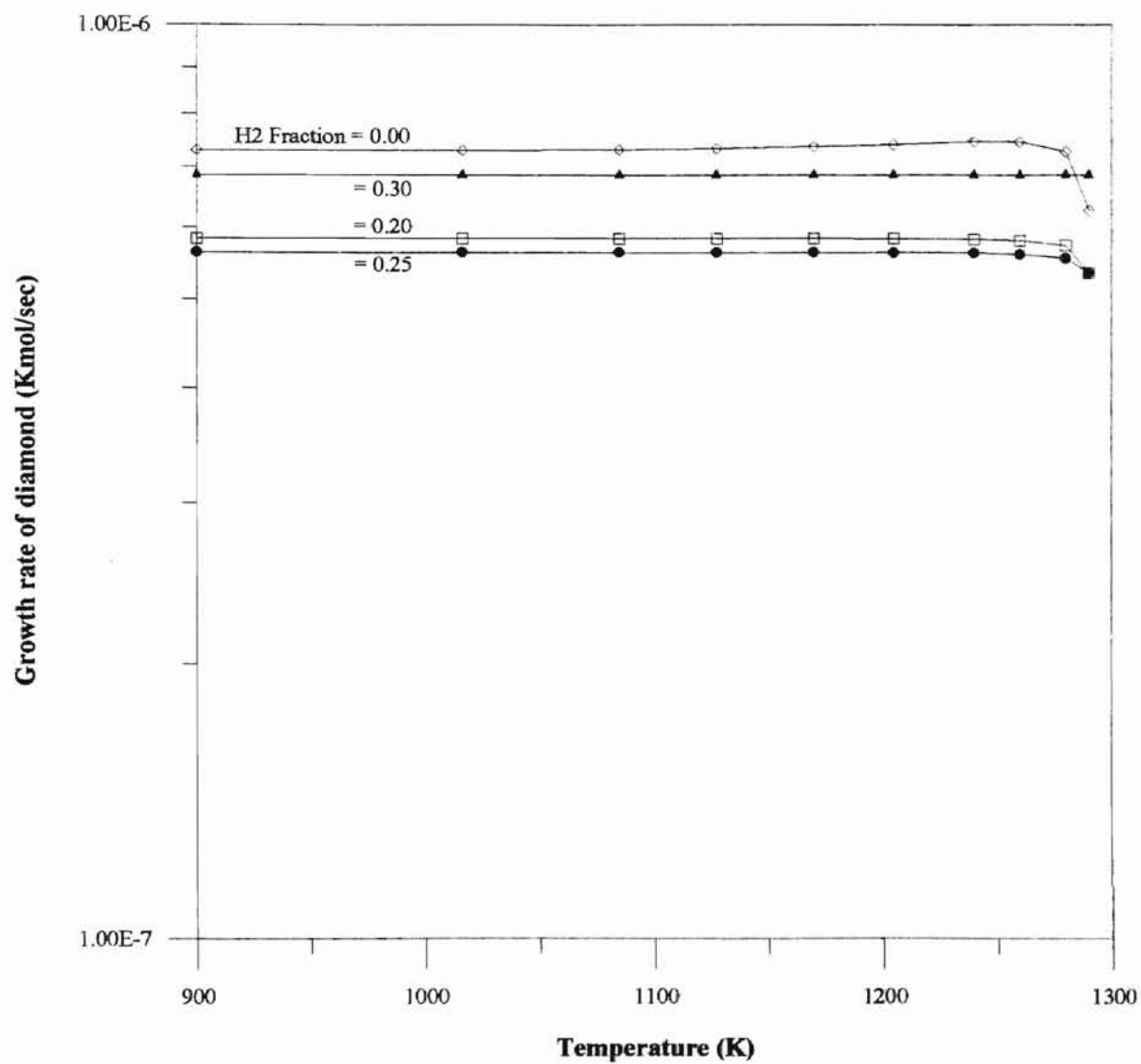
Figure 56. Effect of H$_2$ in the feed. R=[C2H2]/[O2]=1.10
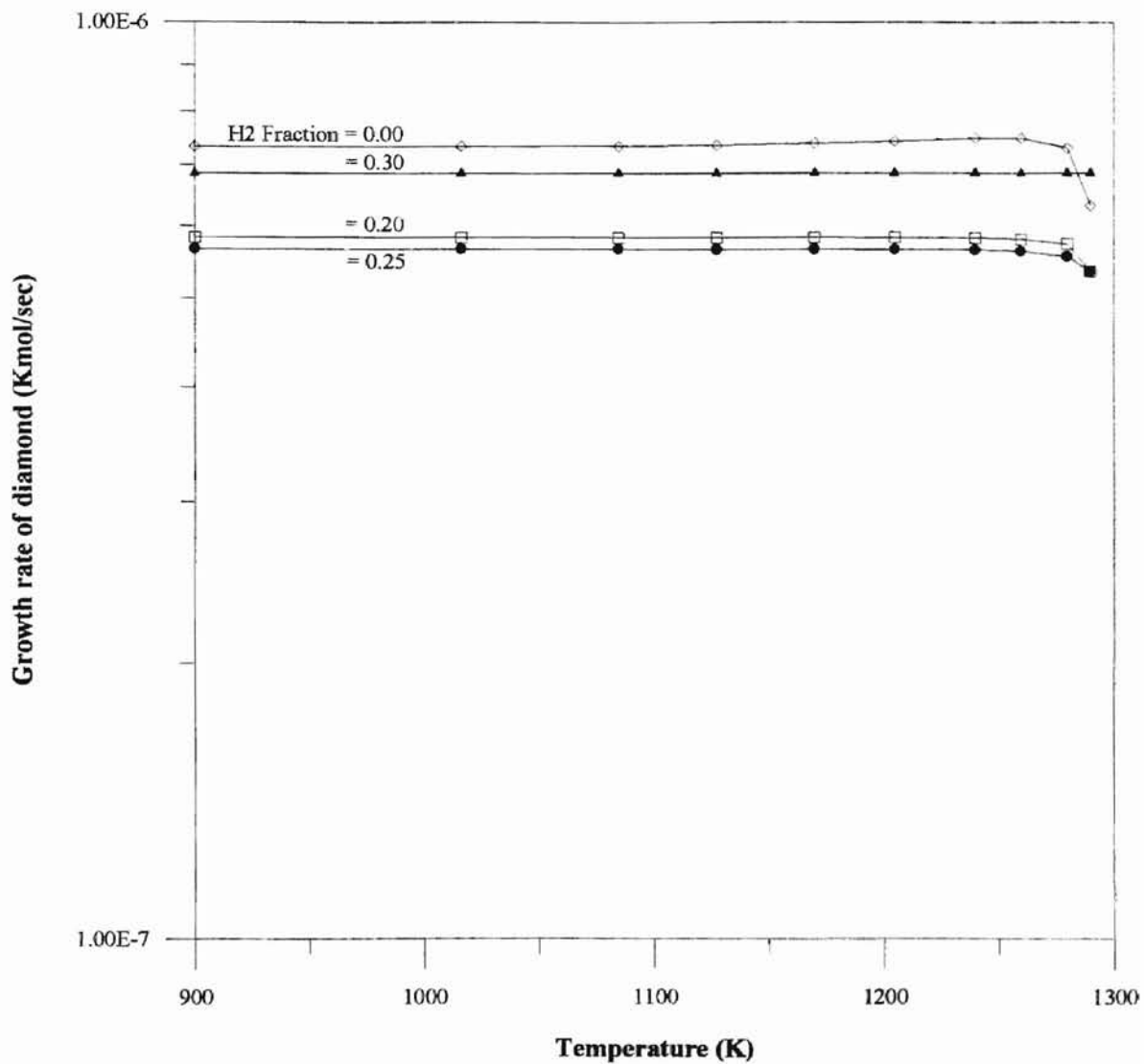
Figure 57. Effect of H$_2$ in the feed. R=[C2H2]/[O2]=1.15
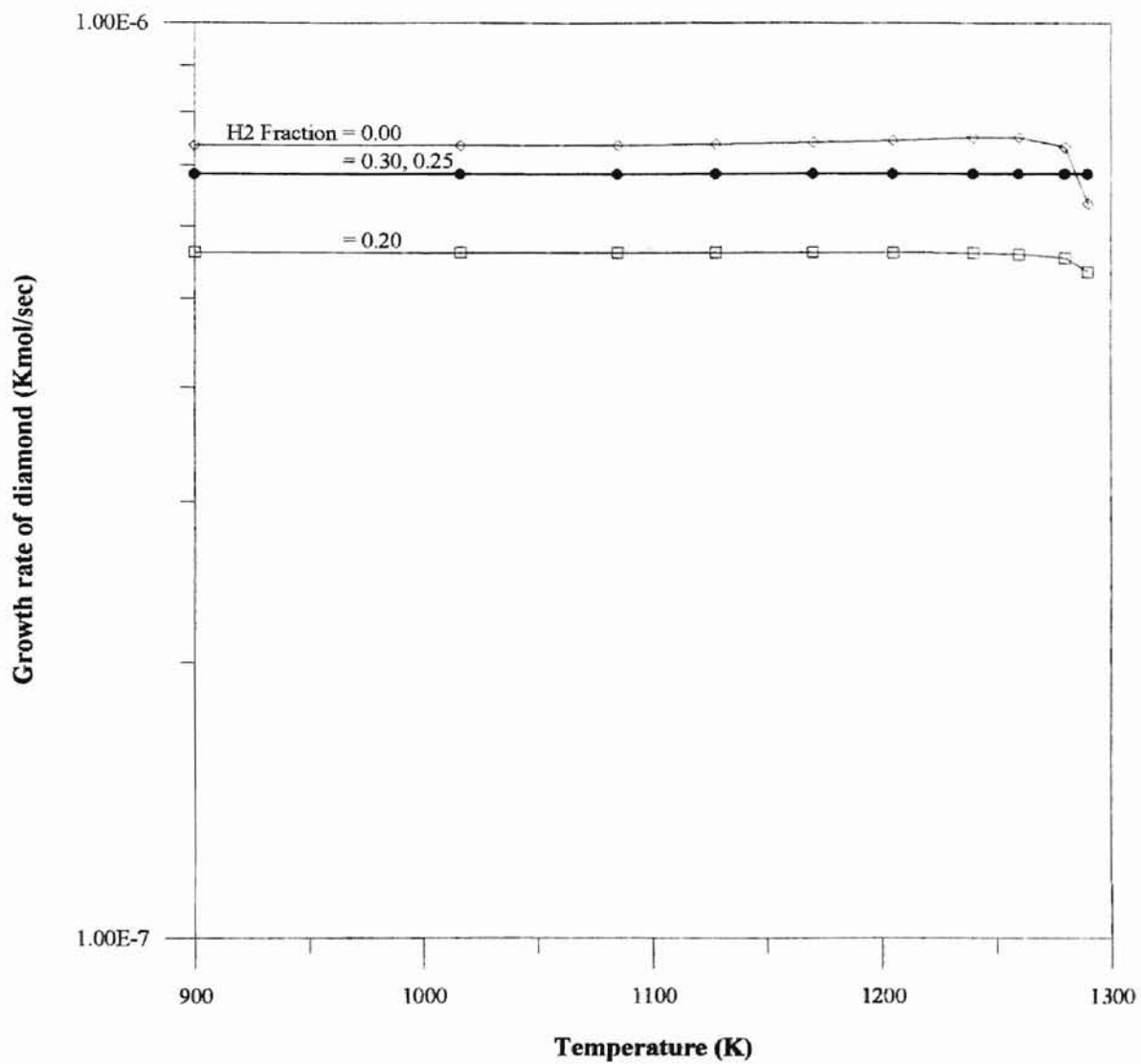
Figure 58. Effect of H$_2$ in the feed. R=[C2H2]/[O2]=1.20

CHAPTER XIV

CONCLUSIONS AND RECOMMENDATIONS

A thermodynamic-kinetic approach was utilized to study the low pressure chemical vapor deposition of diamond in atmospheric acetylene-oxygen flame systems. The high temperature gas-phase reactions involved were analyzed using a Gibbs free energy minimization chemical equilibrium method. The subsequent surface reactions were simulated using a one-dimensional kinetic model to predict for the steady-state growth of diamond.

The proposed model was employed to study the effect of temperature and inlet acetylene and oxygen concentrations on the growth rate. Calculations were performed for acetylene-oxygen inlet flow ratios between 0.80 and 1.2. The largest growth rates of diamond were predicted at 950 K, for an inlet feed ratio of acetylene to oxygen equal to 1.05. The effect of hydrogen on the growth rate of diamond was also investigated by simulating diamond growth in acetylene-oxygen-hydrogen systems. Current results indicate the possibility that an excess of atomic hydrogen could be detrimental to the growth of diamond.

The model presented in this study is still in its preliminary stages of development and requires some additional tuning. Nevertheless, it has proven to be an excellent tool for parametric studies involving low pressure combustion syntheses of diamond. Furthermore, direct application of this model for the analyses of diamond growth in other

low pressure environments is foreseen. Such a thorough assessment of the model's predictive capabilities targeting the various low pressure deposition methods would ultimately help in developing a rigorous method of analysis.

Studies (similar to the one presented in this work) involving thermodynamic analyses, coupled with kinetic reaction models, are useful for analyzing the gas-phase environment, and conducting qualitative comparisons between various process governing factors and/or parameters. However, if one is to develop a complete understanding of the low pressure chemical vapor deposition of diamond, more comprehensive, controlled *in-situ* experimental studies should be undertaken to investigate the role of the numerous factors influencing the deposition process. Such concerted experimental efforts, in conjunction with theoretical studies of the molecular dynamics at the gas-surface interface, is bound to help resolve a number of outstanding issues in diamond syntheses.

BIBLIOGRAPHY

1. M. E. Coltrin and D. S. Dandy, J. Appl. Phys., 74 (1993) 5803.

2. W. A. Yarbrough, J. Am. Soc., 75 (1992) 3179.

3. X. Y. Chang, M. Perry, J. Peploski, D. L. Thompson, and L. M. Raff, J. Chem. Phys., 99 (1993) 4748.

4. D. Kweon, J. Lee, and D. Kim, J. Appl. Phys., 69 (1991) 8329.

5. E. Meeks, R. J. Kee, D. S. Dandy, and M. E. Coltrin, Combust. Flame, 92 (1993) 144.

6. Y. Matsui, A. Yuuki, M. Sahara, and Y. Hirose, Jpn. J. Appl. Phys., 28 (1989) 1718.

7. W. Zhu, B. H. Tan, H. S. Tan, Thin Sol. Films, 236 (1993) 106.

8. Y. Hirose, S. Amanuma, N. Okada, and K. Komaki, Ext. Abstracts of Spring Meeting of Electrochem. Soc., Los Angeles, CA, (1989) 114.

9. F. C. Hong, H. Chang, J. Hsieh, J. Hwang, and J. Wu, Thin Sol. Films, 212 (1992) 127.

10. D. G. Goodwin and G. G. Gavillet, J. Appl. Phys., 68 (1990) 6393.

11. J. S. Kim and M. A. Cappelli, J. Appl. Phys. (submitted).

12. P. Bou, J. C. Boettner, and L. Vandenbulcke, Jpn. J. Appl. Phys., 31 (1992) 2931.

13. JANAF Thermochemical Tables, Dow Chemical Company, Midland, Michigan, 1979.

14. M. E. Coltrin, R. J. Kee, and F. M. Rupley, Int. J. Chem. Kinet., 23 (1991) 1111.

15. J. E. Butler, F. G. Celii, D. B. Oakes, L. M. Hanssen, W. A. Carrington, and K. A. Snail, High Temp. Sci., 27 (1990) 183.

16. M. Dong and D. G. Lilley, ASME Int. Comp. Engg. Conf., San Francisco, CA, August 1992.

17. S. J. Harris, J. Appl. Phys., 65 (1989) 3044.

18. B. Sun, X. Zhang, Q. Zhang, and Z. Lin, J. Appl. Phys., 73 (1993) 4614.

19. J. A. Mucha, D. L. Flamm, and D. E. Ibbotson, J. Appl. Phys., 65 (1989) 3448.

APPENDIX A

COMPUTER PROGRAMS FOR THE VCS ALGORITHM

APPENDIX A

The Villars Cruise Smith algorithm was used in the analysis presented in Section 2 of this study. Included here is a sample input and output file. The reader is requested to refer to the work of W. R. Smith and R. W. Missen, 'Chemical Reaction Equilibrium Analysis: Theory and Algorithms', Wiley-Interscience Publication (1982), for the entire FORTRAN computer code for the VCS algorithm and detailed explanation.

Sample input file for the VCS algorithm.

```
11
018003001001 -1  0
CO              0 1 1                              1 -34.975
CH4             4 1 0                              1 -10.051
C(D)            0 1 0                              0   0.783
CO2             0 1 2                              1 -94.327
H2O             2 0 1                              1 -53.512
H2              2 0 0                              1   0.000
O2              0 0 2                              1   0.000
C2              0 2 0                              1 182.170
H               1 0 0                              1  47.358
CH              1 1 0                              1 131.274
C2H4            4 2 0                              1  17.772
HO2             1 0 2                              1   4.488
CHO             1 1 1                              1   5.539
O               0 0 1                              1  53.935
CH2             2 1 0                              1  86.863
OH              1 0 1                              1   7.806
CH3             3 1 0                              1  35.595
C2H2            2 2 0                              1  61.117
0.0000001 0.0000001 0.0000001 0.0000001 0.0000001 0.0000001 1.0000000
0.0000001
0.0000001 0.0000001 0.0000001 0.0000001 0.0000001 0.0000001 0.0000001
0.0000001
0.0000001 1.0000000
2.000000  2.0000000 2.0000000
400.0     1.0000000
H C O
FLAME ANALYSIS
```

Sample output file for the VCS alogorithm.

```
1VCS CALCULATION METHOD


FLAME ANALYSIS
NUMBER OF PHASE2 SPECIES DOES NOT COMPUTE ***


   18 SPECIES           3 ELEMENTS          3 COMPONENTS
   17 PHASE1 SPECIES    0 PHASE2 SPECIES    1 SINGLE SPECIES PHASES

PRESSURE                    1.000 ATM
TEMPERATURE              400.000 K
PHASE1 INERTS               .000

USER ESTIMATE OF EQUILIBRIUM
STAN. CHEM. POT. IN KCAL./MOLE

SPECIES         FORMULA VECTOR      STAN. CHEM. POT.    EQUILIBRIUM EST.

O2              0  0  2  1           0.00000D+00        1.00000D+00
C2H2            2  2  0  1           6.11170D+01        1.00000D+00
C(D)            0  1  0  0           7.83000D-01        1.00000D-07
CO2             0  1  2  1          -9.43270D+01        1.00000D-07
H2O             2  0  1  1          -5.35120D+01        1.00000D-07
H2              2  0  0  1           0.00000D+00        1.00000D-07
CO              0  1  1  1          -3.49750D+01        1.00000D-07
C2              0  2  0  1           1.82170D+02        1.00000D-07
H               1  0  0  1           4.73580D+01        1.00000D-07
CH              1  1  0  1           1.31274D+02        1.00000D-07
C2H4            4  2  0  1           1.77720D+01        1.00000D-07
HO2             1  0  2  1           4.48800D+00        1.00000D-07
CHO             1  1  1  1           5.53900D+00        1.00000D-07
O               0  0  1  1           5.39350D+01        1.00000D-07
CH2             2  1  0  1           8.68630D+01        1.00000D-07
OH              1  0  1  1           7.80600D+00        1.00000D-07
CH3             3  1  0  1           3.55950D+01        1.00000D-07
CH4             4  1  0  1          -1.00510D+01        1.00000D-07


ITERATIONS =      14
EVALUATIONS OF STOICHIOMETRY =       4

SPECIES          EQUILIBRIUM MOLES      MOLE FRACTION      DG/RT REACTION

C(D)             1.1626044D+00          1.0000000D+00
CO2              6.6883547D-01          4.4580826D-01
H2O              6.6232871D-01          4.4147121D-01
CH4              1.6855973D-01          1.1235248D-01      -3.8085D-12
H2               5.5182782D-04          3.6781751D-04      -1.3732D-06
CO               3.5915305D-07          2.3939131D-07       7.0875D-07
C2H4             2.8382270D-16          1.8918031D-16      -3.4746D-06
CH3              1.0105712D-24          6.7359015D-25      -2.4239D-06
H                3.8392075D-28          2.5590006D-28      -3.2244D-07
CHO              5.0427866D-31          3.3612390D-31      -3.4198D-07
```

127

OH   1.0870708D-32   7.2458050D-33   -3.4198D-07

G/RT =   -1.2639896D+02
TOTAL PHASE1MOLES =   1.5003D+00

LESS THAN 1.E-32 MOLES

HO2
C2H2
O2
CH2
O
CH
C2

ELEMENTAL ABUNDANCES   H   2.000000000000D+00
                          C   2.000000000000D+00
                          O   2.000000000000D+00

APPENDIX B

The ASPEN PLUS computer code used in Section 3 of this study to simulate the gas phase reaction mechanism during the flame chemical vapor deposition of diamond is included in this appendix.

Sample input file for the gas phase reaction mechanism.

```
;Input file created by ModelManager Rel. 3.3-4 on Mon Jul 18 16:32:59
1994
;Directory /u/rbandor/rs6000   Runid TRIAL


TITLE "CVD of DIAMOND"

IN-UNITS SI

DEF-STREAMS MIXCISLD ALL

DESCRIPTION "A sequence of Gibbs free reactors have been used to
characterize the gas phase reactions occurring during the combustion
chemical vapor deposition of diamond."

DATABANKS COMBUST / SOLIDS

PROP-SOURCES COMBUST / SOLIDS

COMPONENTS
      C     C     C     /
      CO    CO    CO    /
      CO2   CO2   CO2   /
      H     H     H     /
      H2    H2    H2    /
      H2O   H2O   H2O   /
      CH    CH    CH    /
      CH2   CH2   CH2   /
      CH3   CH3   CH3   /
      CH4   CH4   CH4   /
      C2    C2    C2    /
      AC    C2H2  AC    /
      C2H4  C2H4  C2H4  /
      H     H     H     /
```

```
        H2      H2      H2      /
        H2O     H2O     H2O     /
        CH      CH      CH      /
        CH2     CH2     CH2     /
        CA      *       CA      /
        C2H     *       C2H

FLOWSHEET
    BLOCK B1    IN=FEED OUT=2
    BLOCK B2    IN=2    OUT=3 4 5
    BLOCK B3    IN=3    OUT=6
    BLOCK B4    IN=4    OUT=7
    BLOCK B5    IN=5    OUT=8
    BLOCK B6    IN=6    OUT=9
    BLOCK B7    IN=7    OUT=10
    BLOCK B8    IN=8    OUT=11
    BLOCK B9    IN=10   OUT=18
    BLOCK B10   IN=12   OUT=16
    BLOCK B11   IN=9    OUT=12 13
    BLOCK B12   IN=11   OUT=14 15
    BLOCK B13   IN=13   OUT=17
    BLOCK B14   IN=14   OUT=19
    BLOCK B15   IN=15   OUT=20

FORMULA
    FORMULA  CA C / C2H C2H

PROP-DATA
    IN-UNITS   SI   MOLE-ENTHALPY='J/KMOL'
    PROP-LIST  MW           / DHFORM    / DGFORM
    PVAL   CA   12.01100 / 716670000 / 671244000
    PVAL   C2H  25.02994 / 476976000 / 438031000

PROP-DATA
    IN-UNITS SI  MOLE-HEAT-CAPACITY='J/KMOL-K'
    PROP-LIST  CPIG
    PVAL   CA   20803.4 0.168416 -0.00039309 2.36518E-07 -3.13285E-11
    PVAL   C2H  27088.1 40.80340 -0.02275120 6.62917E-06 -7.34742E-10

PROPERTIES SYSOP0

STREAM FEED
    SUBSTREAM MIXED TEMP=300 PRES=1 <ATM>
    MOLE-FLOW AC 0.80 / O2 1.00
    SUBSTREAM CISOLID TEMP=300 PRES=1 <ATM>

BLOCK B1 RGIBBS
    PARAM TEMP=3300 PRES=1 <ATM> NATOM=3 SOLIDS=2
    ATOM     C          1    1 / 0 / 0 /
             CO         1    1 / 1 / 0 /
             CO2        1    1 / 2 / 0 /
             H          1    0 / 0 / 1 /
             H2         1    0 / 0 / 2 /
             H2O        1    0 / 1 / 2 /
             CH         1    1 / 0 / 1 /
             CH2        1    1 / 0 / 2 /
             CH3        1    1 / 0 / 3 /
             CH4        1    1 / 0 / 4 /
             C2         1    2 / 0 / 0 /
             AC         1    2 / 0 / 2 /
```

130

```
                         C2H4          1    2 / 0 / 4 /
                         O             1    0 / 1 / 0 /
                         O2            1    0 / 2 / 0 /
                         CA            1    1 / 0 / 0 /
                         HO            1    0 / 1 / 1 /
                         CHO           1    1 / 1 / 1 /
                         HO2           1    0 / 2 / 1 /
                         C2H           1    2 / 0 / 1

BLOCK B2 FSPLIT
     FRAC 3 0.33
     FRAC 4 0.34

BLOCK B3 RGIBBS
     PARAM TEMP=2900 PRES=1 <ATM> NATOM=3 SOLIDS=6
     ATOM    C             1    1 / 0 / 0 /
                         CO            1    1 / 1 / 0 /
                         CO2           1    1 / 2 / 0 /
                         H             1    0 / 0 / 1 /
                         H2            1    0 / 0 / 2 /
                         H2O           1    0 / 1 / 2 /
                         CH            1    1 / 0 / 1 /
                         CH2           1    1 / 0 / 2 /
                         CH3           1    1 / 0 / 3 /
                         CH4           1    1 / 0 / 4 /
                         C2            1    2 / 0 / 0 /
                         AC            1    2 / 0 / 2 /
                         C2H4          1    2 / 0 / 4 /
                         O             1    0 / 1 / 0 /
                         O2            1    0 / 2 / 0 /
                         CA            1    1 / 0 / 0 /
                         HO            1    0 / 1 / 1 /
                         CHO           1    1 / 1 / 1 /
                         HO2           1    0 / 2 / 1 /
                         C2H           1    2 / 0 / 1

BLOCK B4 RGIBBS
     PARAM TEMP=3000 PRES=1 <ATM> NATOM=3 SOLIDS=7
     ATOM    C             1    1 / 0 / 0 /
                         CO            1    1 / 1 / 0 /
                         CO2           1    1 / 2 / 0 /
                         H             1    0 / 0 / 1 /
                         H2            1    0 / 0 / 2 /
                         H2O           1    0 / 1 / 2 /
                         CH            1    1 / 0 / 1 /
                         CH2           1    1 / 0 / 2 /
                         CH3           1    1 / 0 / 3 /
                         CH4           1    1 / 0 / 4 /
                         C2            1    2 / 0 / 0 /
                         AC            1    2 / 0 / 2 /
                         C2H4          1    2 / 0 / 4 /
                         O             1    0 / 1 / 0 /
                         O2            1    0 / 2 / 0 /
                         CA            1    1 / 0 / 0 /
                         HO            1    0 / 1 / 1 /
                         CHO           1    1 / 1 / 1 /
                         HO2           1    0 / 2 / 1 /
                         C2H           1    2 / 0 / 1

BLOCK B4 RGIBBS
```

```
PARAM TEMP=3000 PRES=1 <ATM> NATOM=3 SOLIDS=7
ATOM      C         1    1 / 0 / 0 /
          CO        1    1 / 1 / 0 /
          CO2       1    1 / 2 / 0 /
          H         1    0 / 0 / 1 /
          H2        1    0 / 0 / 2 /
          H2O       1    0 / 1 / 2 /
          CH        1    1 / 0 / 1 /
          CH2       1    1 / 0 / 2 /
          CH3       1    1 / 0 / 3 /
          CH4       1    1 / 0 / 4 /
          C2        1    2 / 0 / 0 /
          AC        1    2 / 0 / 2 /
          C2H4      1    2 / 0 / 4 /
          O         1    0 / 1 / 0 /
          O2        1    0 / 2 / 0 /
          CA        1    1 / 0 / 0 /
          HO        1    0 / 1 / 1 /
          CHO       1    1 / 1 / 1 /
          HO2       1    0 / 2 / 1 /
          C2H       1    2 / 0 / 1

BLOCK B5 RGIBBS
    PARAM TEMP=3100 PRES=1 <ATM> NATOM=3 SOLIDS=8
    ATOM      C         1    1 / 0 / 0 /
              CO        1    1 / 1 / 0 /
              CO2       1    1 / 2 / 0 /
              H         1    0 / 0 / 1 /
              H2        1    0 / 0 / 2 /
              H2O       1    0 / 1 / 2 /
              CH        1    1 / 0 / 1 /
              CH2       1    1 / 0 / 2 /
              CH3       1    1 / 0 / 3 /
              CH4       1    1 / 0 / 4 /
              C2        1    2 / 0 / 0 /
              AC        1    2 / 0 / 2 /
              C2H4      1    2 / 0 / 4 /
              O         1    0 / 1 / 0 /
              O2        1    0 / 2 / 0 /
              CA        1    1 / 0 / 0 /
              HO        1    0 / 1 / 1 /
              CHO       1    1 / 1 / 1 /
              HO2       1    0 / 2 / 1 /
              C2H       1    2 / 0 / 1

BLOCK B6 RGIBBS
    PARAM TEMP=2200 PRES=1 <ATM> NATOM=3 SOLIDS=9
    ATOM      C         1    1 / 0 / 0 /
              CO        1    1 / 1 / 0 /
              CO2       1    1 / 2 / 0 /
              H         1    0 / 0 / 1 /
              H2        1    0 / 0 / 2 /
              H2O       1    0 / 1 / 2 /
              CH        1    1 / 0 / 1 /
              CH2       1    1 / 0 / 2 /
              CH3       1    1 / 0 / 3 /
              CH4       1    1 / 0 / 4 /
              C2        1    2 / 0 / 0 /
              AC        1    2 / 0 / 2 /
              C2H4      1    2 / 0 / 4 /
```

```
                        O            1    0 / 1 / 0 /
                        O2           1    0 / 2 / 0 /
                        CA           1    1 / 0 / 0 /
                        HO           1    0 / 1 / 1 /
                        CHO          1    1 / 1 / 1 /
                        HO2          1    0 / 2 / 1 /
                        C2H          1    2 / 0 / 1

BLOCK B7 RGIBBS
    PARAM TEMP=2300 PRES=1 <ATM> NATOM=3 SOLIDS=10
        ATOM    C            1    1 / 0 / 0 /
                        CO           1    1 / 1 / 0 /
                        CO2          1    1 / 2 / 0 /
                        H            1    0 / 0 / 1 /
                        H2           1    0 / 0 / 2 /
                        H2O          1    0 / 1 / 2 /
                        CH           1    1 / 0 / 1 /
                        CH2          1    1 / 0 / 2 /
                        CH3          1    1 / 0 / 3 /
      .                 CH4          1    1 / 0 / 4 /
                        C2           1    2 / 0 / 0 /
                        AC           1    2 / 0 / 2 /
                        C2H4         1    2 / 0 / 4 /
                        O            1    0 / 1 / 0 /
                        O2           1    0 / 2 / 0 /
                        CA           1    1 / 0 / 0 /
                        HO           1    0 / 1 / 1 /
                        CHO          1    1 / 1 / 1 /
                        HO2          1    0 / 2 / 1 /
                        C2H          1    2 / 0 / 1

BLOCK B8 RGIBBS
    PARAM TEMP=2400 PRES=1 <ATM> NATOM=3 SOLIDS=11
        ATOM    C            1    1 / 0 / 0 /
                        CO           1    1 / 1 / 0 /
                        CO2          1    1 / 2 / 0 /
                        H            1    0 / 0 / 1 /
                        H2           1    0 / 0 / 2 /
                        H2O          1    0 / 1 / 2 /
                        CH           1    1 / 0 / 1 /
                        CH2          1    1 / 0 / 2 /
                        CH3          1    1 / 0 / 3 /
                        CH4          1    1 / 0 / 4 /
                        C2           1    2 / 0 / 0 /
                        AC           1    2 / 0 / 2 /
                        C2H4         1    2 / 0 / 4 /
                        O            1    0 / 1 / 0 /
                        O2           1    0 / 2 / 0 /
                        CA           1    1 / 0 / 0 /
                        HO           1    0 / 1 / 1 /
                        CHO          1    1 / 1 / 1 /
                        HO2          1    0 / 2 / 1 /
                        C2H          1    2 / 0 / 1

BLOCK B9 RGIBBS
    PARAM TEMP=1600 PRES=1 <ATM> NATOM=3 SOLIDS=18
        ATOM    C            1    1 / 0 / 0 /
                        CO           1    1 / 1 / 0 /
                        CO2          1    1 / 2 / 0 /
                        H            1    0 / 0 / 1 /
```

```
              H2          1    0 / 0 / 2 /
              H2O         1    0 / 1 / 2 /
              CH          1    1 / 0 / 1 /
              CH2         1    1 / 0 / 2 /
              CH3         1    1 / 0 / 3 /
              CH4         1    1 / 0 / 4 /
              C2          1    2 / 0 / 0 /
              AC          1    2 / 0 / 2 /
              C2H4        1    2 / 0 / 4 /
              O           1    0 / 1 / 0 /
              O2          1    0 / 2 / 0 /
              CA          1    1 / 0 / 0 /
              HO          1    0 / 1 / 1 /
              CHO         1    1 / 1 / 1 /
              HO2         1    0 / 2 / 1 /
              C2H         1    2 / 0 / 1

BLOCK B10 RGIBBS
      PARAM TEMP=1400 PRES=1 <ATM> NATOM=3 SOLIDS=16
      ATOM    C           1    1 / 0 / 0 /
              CO          1    1 / 1 / 0 /
              CO2         1    1 / 2 / 0 /
              H           1    0 / 0 / 1 /
              H2          1    0 / 0 / 2 /
              H2O         1    0 / 1 / 2 /
              CH          1    1 / 0 / 1 /
              CH2         1    1 / 0 / 2 /
              CH3         1    1 / 0 / 3 /
              CH4         1    1 / 0 / 4 /
              C2          1    2 / 0 / 0 /
              AC          1    2 / 0 / 2 /
              C2H4        1    2 / 0 / 4 /
              O           1    0 / 1 / 0 /
              O2          1    0 / 2 / 0 /
              CA          1    1 / 0 / 0 /
              HO          1    0 / 1 / 1 /
              CHO         1    1 / 1 / 1 /
              HO2         1    0 / 2 / 1 /
              C2H         1    2 / 0 / 1

BLOCK B11 FSPLIT
      FRAC 12 0.5

BLOCK B12 FSPLIT
      FRAC 14 0.5

BLOCK B13 RGIBBS
      PARAM TEMP=1500 PRES=1 <ATM> NATOM=3 SOLIDS=17
      ATOM    C           1    1 / 0 / 0 /
              CO          1    1 / 1 / 0 /
              CO2         1    1 / 2 / 0 /
              H           1    0 / 0 / 1 /
              H2          1    0 / 0 / 2 /
              H2O         1    0 / 1 / 2 /
              CH          1    1 / 0 / 1 /
              CH2         1    1 / 0 / 2 /
              CH3         1    1 / 0 / 3 /
              CH4         1    1 / 0 / 4 /
              C2          1    2 / 0 / 0 /
              AC          1    2 / 0 / 2 /
```

```
                        C2H4          1    2 / 0 / 4 /
                        O             1    0 / 1 / 0 /
                        O2            1    0 / 2 / 0 /
                        CA            1    1 / 0 / 0 /
                        HO            1    0 / 1 / 1 /
                        CHO           1    1 / 1 / 1 /
                        HO2           1    0 / 2 / 1 /
                        C2H           1    2 / 0 / 1

BLOCK B14 RGIBBS
    PARAM TEMP=1700 PRES=1 <ATM> NATOM=3 SOLIDS=19
        ATOM    C             1    1 / 0 / 0 /
                CO            1    1 / 1 / 0 /
                CO2           1    1 / 2 / 0 /
                H             1    0 / 0 / 1 /
                H2            1    0 / 0 / 2 /
                H2O           1    0 / 1 / 2 /
                CH            1    1 / 0 / 1 /
                CH2           1    1 / 0 / 2 /
                CH3           1    1 / 0 / 3 /
                CH4           1    1 / 0 / 4 /
                C2            1    2 / 0 / 0 /
                AC            1    2 / 0 / 2 /
                C2H4          1    2 / 0 / 4 /
                O             1    0 / 1 / 0 /
                O2            1    0 / 2 / 0 /
                CA            1    1 / 0 / 0 /
                HO            1    0 / 1 / 1 /
                CHO           1    1 / 1 / 1 /
                HO2           1    0 / 2 / 1 /
                C2H           1    2 / 0 / 1

BLOCK B15 RGIBBS
    PARAM TEMP=1800 PRES=1 <ATM> NATOM=3 SOLIDS=20
        ATOM    C             1    1 / 0 / 0 /
                CO            1    1 / 1 / 0 /
                CO2           1    1 / 2 / 0 /
                H             1    0 / 0 / 1 /
                H2            1    0 / 0 / 2 /
                H2O           1    0 / 1 / 2 /
                CH            1    1 / 0 / 1 /
                CH2           1    1 / 0 / 2 /
                CH3           1    1 / 0 / 3 /
                CH4           1    1 / 0 / 4 /
                C2            1    2 / 0 / 0 /
                AC            1    2 / 0 / 2 /
                C2H4          1    2 / 0 / 4 /
                O             1    0 / 1 / 0 /
                O2            1    0 / 2 / 0 /
                CA            1    1 / 0 / 0 /
                HO            1    0 / 1 / 1 /
                CHO           1    1 / 1 / 1 /
                HO2           1    0 / 2 / 1 /
                C2H           1    2 / 0 / 1

CASE-STUDY
    VARY  MOLE-FLOW  STREAM=FEED  COMPONENT=AC
    CASE  1   0.85   REINIT-BLOCKS=ALL    REINIT-STREAMS=ALL
    CASE  2   0.90   REINIT-BLOCKS=ALL    REINIT-STREAMS=ALL
    CASE  3   0.95   REINIT-BLOCKS=ALL    REINIT-STREAMS=ALL
```

135

```
CASE  4  1.00  REINIT-BLOCKS=ALL  REINIT-STREAMS=ALL
CASE  5  1.05  REINIT-BLOCKS=ALL  REINIT-STREAMS=ALL
CASE  6  1.10  REINIT-BLOCKS=ALL  REINIT-STREAMS=ALL
CASE  7  1.15  REINIT-BLOCKS=ALL  REINIT-STREAMS=ALL
CASE  8  1.20  REINIT-BLOCKS=ALL  REINIT-STREAMS=ALL
```

APPENDIX C

ASPEN PLUS CODE FOR THE SURFACE REACTION MODEL

APPENDIX C

The ASPEN PLUS code used in Section 3 of this study to model the surface reaction mechanisms occuring during the flame chemical vapor deposition of diamond is included in this appendix.

Sample input file for the surface reaction mechanism.

```
;Input file created by ModelManager Rel. 3.3-4 on Mon Oct 24 18:03:33
1994
;Directory /u/rbandor/rs6000  Runid SURF
;

TITLE "CVD of DIAMOND"

IN-UNITS SI

DEF-STREAMS MIXCISLD ALL

DESCRIPTION "A plug flow reactor has been used to kinetically model
the surface reactions occuring during the combustion chemical vapor
deposition of diamond in combustion flame."

DATABANKS COMBUST / SOLIDS

PROP-SOURCES COMBUST / SOLIDS

COMPONENTS
    CH3    CH3   CH3   /
    H      H     H     /
    H2     H2    H2    /
    CHS    *     CHS   /
    CSR    *     CSR   /
    CD     *     CD    /
    1CH2S  *     1CH2S /
    1CHSR  *     1CHSR /
    CH2SR  *     CH2SR /
    CH3S   *     CH3S  /
    AC     C2H2  AC    /
    ACSR   *     ACSR  /

    HACS   *     HACS  /
    2CH2S  *     2CH2S /
```

```
      2CHSR  *      2CHSR /
      CSR3   *      CSR3  /
      CG     C      CG    /
      CA     *      CA    /
      CHSR2  *      CHSR2 /
      CHSG   *      CHSG  /
      CRG    *      CRG

FORMULA
      FORMULA  CHS CH      / CSR C      / CD C      / 1CH2S CH2 /
               1CHSR CH  / CH2SR CH2 / CH3S CH3 / ACSR C2H2 /
               HACS C2H3 / 2CH2S CH2 / 2CHSR CH / CSR3  C    /
               CHSR2 CH  / CHSG CH   / CRG C     / CA C

FLOWSHEET
      BLOCK B18 IN=18 OUT=PRODUCT

PROPERTIES SYSOP0

PROP-DATA
      IN-UNITS SI MOLE-ENTHALPY='J/KMOL'
      PROP-LIST    MW        / DHFORM
      PVAL CHS     13.01894 / 0
      PVAL CSR     12.011   / 181585600
      PVAL CD      12.011   / 2092000
      PVAL 1CH2S   14.02688 / -48116000
      PVAL 1CHSR   13.01894 / 133469600
      PVAL CH2SR   14.02688 / 212128800
      PVAL CH3S    15.03482 / 72383200
      PVAL ACSR    26.0379  / 364426400
      PVAL HACS    27.04582 / 139745600
      PVAL 2CH2S   14.02688 / -39329600
      PVAL 2CHSR   13.01894 / 133469600
      PVAL CSR3    12.011   / 540154400
      PVAL CA      12.011   / 716670000
      PVAL CHSR2   13.01894 / 373212800
      PVAL CHSG    13.01894 / 96650400
      PVAL CRG     12.011   / 303340000

PROP-DATA
      IN-UNITS MET MOLE-HEAT-CAPACITY='CAL/MOL-K'
      PROP-LIST CPIG
      PVAL     CSR     3.358566124  0.00219965  -2.50715E-07  -2.38398E-10
5.72549E-14
      PVAL     CSR3    3.358566124  0.00219965  -2.50715E-07  -2.38398E-10
5.72549E-14
      PVAL     CHS     2.955415308  0.00655794  -5.64597E-07  -6.83278E-10
1.52339E-13
      PVAL     1CHSR   2.955415308  0.00655794  -5.64597E-07  -6.83278E-10
1.52339E-13
      PVAL     2CHSR   2.955415308  0.00655794  -5.64597E-07  -6.83278E-10
1.52339E-13
      PVAL     CHSR2   2.955415308  0.00655794  -5.64597E-07  -6.83278E-10
1.52339E-13
      PVAL     1CH2S   3.456629277  0.01028661  -8.37677E-07  -1.06243E-09
2.33762E-13
      PVAL     CH2SR   3.456629277  0.01028661  -8.37677E-07  -1.06243E-09
2.33762E-13
      PVAL     2CH2S   3.456629277  0.01028661  -8.37677E-07  -1.06243E-09
2.33762E-13
```

```
      PVAL    CH3S    4.425878724  0.01288510  -1.01150E-06  -1.31678E-09
2.87060E-13
      PVAL    ACSR    7.231759419  0.01192724  -1.00891E-06  -1.23138E-09
2.73692E-13
      PVAL    HACS    7.340903994  0.01583840  -1.27924E-06  -1.62590E-09
3.57346E-13
      PVAL    CRG     3.358566323  0.00219965  -2.50713E-07  -2.38398E-10
5.72550E-14
      PVAL    CHSG    2.944572152  0.00650841  -5.52079E-07  -6.75742E-10
1.50147E-13
      PVAL    CD      3.358566323  0.00219965  -2.50715E-07  -2.38398E-10
5.72549E-14

PROP-DATA
    IN-UNITS SI  MOLE-HEAT-CAPACITY='J/KMOL-K'
    PROP-LIST  CPIG
    PVAL   CA    20803.4 0.168416 -0.00039309 2.36518E-07 -3.13285E-11

STREAM 18  TEMP=1320  PRES=1 <ATM> NPHASE=1
    MOLE-FLOW  CH3 2.6E-04 / H2 0.65 /  CG 1.1E-03 /
               H 1.8E-02 / AC 7.12E-05 / CA 9.31E-9 /
               CHS 2.3E-08 / 1CH2S 2.3E-08 / CHSG 3.11E-08

BLOCK B18 RPLUG
    PARAM TYPE=T-SPEC LENGTH=0.50 DIAM=0.04  NPHASE=1 PHASE=V
    T-SPEC  0.0 1300 / 0.1 1290 / 0.2 1280 / 0.4 1240 /
            0.6 1170 / 0.8 1085 / 0.96 900 / 1.0 825
    STOIC 1   MIXED H -1 / CHS -1 / CSR 1 / H2 1
    STOIC 2   MIXED H 1 /  CHS 1 / CSR -1 / H2 -1
    STOIC 3   MIXED CSR -1 / H -1 / CHS 1
    STOIC 4   MIXED CSR 1 /  H 1 / CHS -1
    STOIC 5   MIXED CSR -1 / CH3 -1 / CD 1 / CH3S 1
    STOIC 6   MIXED CSR 1 / CH3 1 / CD -1 / CH3S -1
    STOIC 7   MIXED 1CH2S -1 / H -1 / 1CHSR 1 / H2 1
    STOIC 8   MIXED 1CH2S 1 / H 1 / 1CHSR -1 / H2 -1
    STOIC 9   MIXED CH3S -1 / H -1 / CH2SR 1 / H2 1
    STOIC 10  MIXED CH3S 1 / H 1 / CH2SR -1 / H2 -1
    STOIC 11  MIXED CH2SR -1 / 1CHSR -1 / 1CH2S 1 / CHS 1
    STOIC 12  MIXED CH2SR 1 / 1CHSR 1 / 1CH2S -1 / CHS -1
    STOIC 13  MIXED CSR -1 / AC -1 / CD 1 / ACSR 1
    STOIC 14  MIXED CD -1 / ACSR -1 / CSR 1 / AC 1
    STOIC 15  MIXED CHS -1 / ACSR -1 / CSR 1 / HACS 1
    STOIC 16  MIXED CSR -1 / HACS -1 / ACSR 1 / CHS 1
    STOIC 17  MIXED HACS -1 / CSR -1 / CD 1 / 1CH2S 1 / 1CHSR 1
    STOIC 18  MIXED 1CHSR -1 / 1CH2S -1 / CD -1 / HACS 1 / CSR 1
    STOIC 19  MIXED 1CH2S -1 / 1CHSR -1 / 2CH2S 1 / 2CHSR 1
    STOIC 20  MIXED 2CHSR -1 / 2CH2S -1 / 1CHSR 1 / 1CH2S 1
    STOIC 21  MIXED 2CHSR -1 / 2CH2S -1 / H -1 / CHS 2 /  H2 1
    STOIC 22  MIXED CHS -2 / H2 -1 / 2CHSR 1 / 2CH2S 1 / H 1
    STOIC 23  MIXED CSR -1 / CA -1 / CD 1 / CSR3 1
    STOIC 24  MIXED CSR3 -1 / CD -1 / CA 1 / CSR 1
    STOIC 25  MIXED CSR3 -1 / 1CH2S -1 / 1CHSR 1 / CHS 1
    STOIC 26  MIXED CHS -1 / 1CHSR -1 / 1CH2S 1 / CSR3 1
    STOIC 27  MIXED 1CHSR -1 / H -1 / 1CH2S 1
    STOIC 28  MIXED 1CH2S -1 / H 1 / 1CHSR 1
    STOIC 29  MIXED CSR3 -1 / H2 -1 / 1CH2S 1
    STOIC 30  MIXED 1CH2S -1 / CSR3 1 / H2 1
    STOIC 31  MIXED CSR3 -1 / H -1 / CHSR2 1
    STOIC 32  MIXED CHSR2 -1 / CSR3 1 / H 1
    STOIC 33  MIXED CHSR2 -1 / H -1 / CH2SR 1
```

```
STOIC 34 MIXED CH2SR -1 / H 1 / CHSR2 1
STOIC 35 MIXED CH2SR -1 / H -1 / CH3S 1
STOIC 36 MIXED CH3S -1 / H 1 / CH2SR 1
STOIC 37 MIXED CHSR2 -1 / H2 -1 / CH3S 1
STOIC 38 MIXED CH3S -1 / CHSR2 1 / H2 1
STOIC 39 MIXED CHSG -1 / CG -1 / H -1 / 1CHSR 1 / CHS 1
STOIC 40 MIXED 1CHSR -1 / CHS -1 / CG 1 / H 1 / CHSG  1
STOIC 41 MIXED CHSG -1 / H -1 / CRG 1 / H2 1
STOIC 42 MIXED CRG -1 / H2 -1 / CHSG 1 / H 1
STOIC 43 MIXED CRG -1 / H -1 / CHSG 1
STOIC 44 MIXED CHSG -1 / CRG 1 / H 1
STOIC 45 MIXED CRG -1 / CH3 -1 / CH3S 1 / CG 1
STOIC 46 MIXED CH3S -1 / CG -1 / CH3 1 / CRG 1
STOIC 47 MIXED CRG -1 / CA -1 / CG 1 / CSR3 1
STOIC 48 MIXED CA -1 / CSR3 -1 / CG -1 / CRG 1
STOIC 49 MIXED CRG -1 / AC -1 / CG 1 / ACSR 1
STOIC 50 MIXED ACSR -1 / CG -1 / CRG 1 / AC 1
RATE-CON 1   73065379.8      0 0.5
RATE-CON 2   1.15E+10        17620   <CAL/MOL>
RATE-CON 3   1388242216      0 0.5
RATE-CON 4   5.11E+14        96810   <CAL/MOL>
RATE-CON 5   71028221.37     0 0.5
RATE-CON 6   9.21E+13        59640   <CAL/MOL>
RATE-CON 7   73065379.8      0 0.5
RATE-CON 8   1.89E+10        18110   <CAL/MOL>
RATE-CON 9   154249135.1     0 0.5
RATE-CON 10  2.67E+11        28470   <CAL/MOL>
RATE-CON 11  6.00E+19        0
RATE-CON 12  6.00E+16        94020   <CAL/MOL>
RATE-CON 13  8.00E+10        7700    <CAL/MOL>
RATE-CON 14  2.64E+13        16410   <CAL/MOL>
RATE-CON 15  6.00E+19        0
RATE-CON 16  4.41E+16        10110   <CAL/MOL>
RATE-CON 17  6.00E+19        0
RATE-CON 18  1.01E+17        56300   <CAL/MOL>
RATE-CON 19  6.00E+19        2122    <CAL/MOL>
RATE-CON 20  6.00E+16        0
RATE-CON 21  1.39972E+15     0 0.5
RATE-CON 22  3.62E+18        83980   <CAL/MOL>
RATE-CON 23  79467668.7      0 0.5
RATE-CON 24  5.87E12         4560    <CAL/MOL>
RATE-CON 25  6.00E+19        0
RATE-CON 26  9.9E+16         86250   <CAL/MOL>
RATE-CON 27  1388242216      0 0.5
RATE-CON 28  3.1E+14         96320   <CAL/MOL>
RATE-CON 29  981635485       0 0.5
RATE-CON 30  2.01E+15        79320   <CAL/MOL>
RATE-CON 31  1388242216      0 0.5
RATE-CON 32  5.11E+14        93350   <CAL/MOL>
RATE-CON 33  1388242216      0 0.5
RATE-CON 34  3.1E+14         91520   <CAL/MOL>
RATE-CON 35  1388242216      0 0.5
RATE-CON 36  5.55E+13        86380   <CAL/MOL>
RATE-CON 37  981635485       0 0.5
RATE-CON 38  2.18E+14        72350   <CAL/MOL>
RATE-CON 39  73065379.8      0 0.5
RATE-CON 40  5.99E+19        51990   <CAL/MOL>
RATE-CON 41  73065379.8      0 0.5
RATE-CON 42  91600000        11180   <CAL/MOL>
RATE-CON 43  1388242216      0 0.5
```

```
RATE-CON 44 4.47E+13      102900 <CAL/MOL>
RATE-CON 45 71028221.37   0 0.5
RATE-CON 46 7.82E+12      89530  <CAL/MOL>
RATE-CON 47 79467668.7    0 0.5
RATE-CON 48 4.99E+11      114100 <CAL/MOL>
RATE-CON 49 53973085.4    0 0.5
RATE-CON 50 8.62E+13      39490  <CAL/MOL>
POWLAW-EXP 1  CHS 1 / H 1
POWLAW-EXP 2  H2 1 / CSR 1
POWLAW-EXP 3  CSR 1 / H 1
POWLAW-EXP 4  CHS 1
POWLAW-EXP 5  CSR 1 / CH3 1
POWLAW-EXP 6  CD 1 / CH3S 1
POWLAW-EXP 7  1CH2S 1 / H 1
POWLAW-EXP 8  1CHSR 1 / H2 1
POWLAW-EXP 9  CH3S 1 / H 1
POWLAW-EXP 10 CH2SR 1 / H2 1
POWLAW-EXP 11 CH2SR 1 / 1CHSR 1
POWLAW-EXP 12 1CH2S 1 / CHS 1
POWLAW-EXP 13 CSR 1 / AC 1
POWLAW-EXP 14 CD 1 / ACSR 1
POWLAW-EXP 15 CHS 1 / ACSR 1
POWLAW-EXP 16 CSR 1 / HACS 1
POWLAW-EXP 17 HACS 1 / CSR 1
POWLAW-EXP 18 CD 1 / 1CH2S 0.5 / 1CHSR 0.5
POWLAW-EXP 19 1CH2S 1 / 1CHSR 1
POWLAW-EXP 20 2CH2S 1 / 2CHSR 1
POWLAW-EXP 21 2CHSR 1 / 2CH2S 1 / H 1
POWLAW-EXP 22 CHS 1 / H2 1
POWLAW-EXP 23 CA 1 / CSR 1
POWLAW-EXP 24 CD 1 / CSR3 1
POWLAW-EXP 25 1CH2S 1 / CSR3 1
POWLAW-EXP 26 1CHSR 1 / CHS 1
POWLAW-EXP 27 H 1 / 1CHSR 1
POWLAW-EXP 28 1CH2S 1
POWLAW-EXP 29 CSR3 1 / H2 1
POWLAW-EXP 30 1CH2S 1
POWLAW-EXP 31 CSR3 1 / H 1
POWLAW-EXP 32 CHSR2 1
POWLAW-EXP 33 CHSR2 1 / H 1
POWLAW-EXP 34 CH2SR 1
POWLAW-EXP 35 CH2SR 1 / H 1
POWLAW-EXP 36 CH3S 1
POWLAW-EXP 37 CHSR2 1 / H2 1
POWLAW-EXP 38 CH3S 1
POWLAW-EXP 39 CHSG 0.5 / CG 1 / H 0.5
POWLAW-EXP 40 1CHSR 1 / CHS 1
POWLAW-EXP 41 CHSG 1 / H 1
POWLAW-EXP 42 CRG 1 / H2 1
POWLAW-EXP 43 CRG 1 / H 1
POWLAW-EXP 44 CHSG 1
POWLAW-EXP 45 CRG 1 / CH3 1
POWLAW-EXP 46 CG 1 / CH3S 1
POWLAW-EXP 47 CRG 1 / CA 1
POWLAW-EXP 48 CG 1 / CSR3 1
POWLAW-EXP 49 CRG 1 / AC 1
POWLAW-EXP 50 CG 1 / ACSR 1
```

γ

VITA

Rustom J Bandorawalla

Candidate for the Degree of

Master of Science

Thesis: MODELING THE CHEMICAL VAPOR DEPOSITION OF DIAMOND

Major Field: Chemical Engineering

Biographical:

     Personal Data: Born in Bombay, Maharashtra, India, April 12, 1971, the son of Jamshed S. Bandorawalla and Katayune S. Bandorawalla.

     Education: Graduated from Greenlawns High School, Bombay, Maharashtra, India, in March 1987 (Std X); attended Jai Hind Junior College (Std X + II), graduated in March 1989; received Bachelor of Chemical Engineering Degree from the Manipal Institute of Technology, Manglore University, Manipal, India, in June 1993. Completed the requirements for the Master of Science Degree with a major in Chemical Engineering at Oklahoma State University, Stillwater, in July 1995.

     Professional Experience: Research Assistant, School of Chemical Engineering, Oklahoma State University, August 1993 to June 1994; Teaching Assistant, School of Chemical Engineering, Oklahoma State University, August 1994 to December 1994.